PREDICTIVE MODELING OF NEAR DRY MACHINING: MECHANICAL PERFORMANCE AND ENVIRONMENTAL IMPACT

A Dissertation
Presented to
The Academic Faculty

by

Kuan-Ming Li

In Partial Fulfillment
of the Requirements for the Degree
Doctor of Philosophy in the
School of Mechanical Engineering

Georgia Institute of Technology
August 2006

PREDICTIVE MODELING OF NEAR DRY MACHINING: MECHANICAL PERFORMANCE AND ENVIRONMENTAL IMPACT

Approved by:

Dr. Steven Y. Liang, Advisor
School of Mechanical Engineering
Georgia Institute of Technology

Dr. Chen Zhou
School of Industrial and Systems Engineering
Georgia Institute of Technology

Dr. Shreyes N. Melkote
School of Mechanical Engineering
Georgia Institute of Technology

Dr. Roshan Joseph Vengazhiyil
School of Industrial and Systems Engineering
Georgia Institute of Technology

Dr. Min Zhou
School of Mechanical Engineering
Georgia Institute of Technology

Date Approved: April 10, 2006

ACKNOWLEDGEMENTS

I would like to thank my advisor, Dr. Steven Y. Liang, for his guidance, encouragement and support during my studies at Georgia Institute of Technology. Also I would like to thank the thesis committee, Dr. Shreyes N. Melkote, Dr. Min Zhou, Dr. Chen Zhou and Dr. Roshan Joseph Vengazhiyil for their advice. Thanks to the faculty, staff, and students of the Precision Machining Research Consortium for their help and support to this research. I appreciate the partial financial support from the National Science Foundation under Grant Number DMI-0225688.

Most importantly, I would like to thank my parents, Cheng-Hsin Lee and Kuang-Hui Chen, for their sacrifices and continuous support during my research. I truly could not have done it without them.

TABLE OF CONTENTS

LIST OF TABLES

LIST OF FIGURES

LIST OF SYMBOLS

A_b	Adsorbed lubricant film contact area
A_m	Metallic contact area
a_{ch}	Thermal diffusivity of the chip
a_s	Approach of two surfaces
a_{wk}	Thermal diffusivity of the workpiece
B_1	Fraction of the secondary heat source transferred into the chip
B_2	Fraction of the rubbing heat source transferred into the workpiece
C	The condensation coefficient
C_a	The coefficient in Equation (6-7)
C_s^*	Equivalent side cutting angle
D	Inclination of distribution function in Chapter 4
	Droplet diameter in Chapter 6
D_{32}	Sauter mean diameter
D_{AB}	The diffusion coefficient
D_j	Diameter of jet nozzle

d	Depth of cut
d_{avg}	Average nozzle diameter
E	The evaporation coefficient
F_c	Cutting force
F_{cw}	Cutting force in the cutting direction due to tool flank wear
F_r	The force normal to F_c and F_t in Oxley's machining theory
F_t	Thrust force
F_{tw}	Cutting force in the thrust direction due to tool flank wear
f	Feed per revolution
$H_{\max}$	Distribution height of asperities
$\overline{h}$	Average heat transfer coefficient
$\overline{h}_{eff}$	Effective heat transfer coefficient for the air-oil mixture flow in the tool flank face
i^*	Equivalent inclination angle
K	Constant in Equation (6-6)
K_0	Modified Bessel function of the second kind of order zero
$K_{abrasion}$	Abrasive wear coefficient
$K_{adhesion}$	Adhesive wear coefficient

$K_{diffusion}$	Diffusive wear coefficient
K_Q	Constant related to activation energy for diffusion
k_{air}	Thermal conductivity of the air
k_{ch}	Thermal conductivity of the chip
k_t	Thermal conductivity of the tool insert
k_{wk}	Thermal conductivity of the workpiece
L	Length of the shear plane in Chapter 3 ~ 5
	The characteristic length of surface in Chapter 6
L_c	Contact length
L_{eff}	Effective length for calculating Nusselt number
L_t	Length of the effective cooling area
L_{VB}	Flank wear length
L_{VB}^*	Critical tool flank wear length
M	The molecular weight of cutting fluid
Ma	Mach number
m_a	Mass of air
m_l	Mass of liquid
N	Normal load in Chapter 4

	Number of drops in Chapter 6
n	Constant in Equation (6-6)
n_0	Total asperity number
P_1	Force in the cutting velocity direction
P_2	Force in the feed direction
P_3	Force in the radial direction
Pr	Prandtl number
p_{atm}	The vapor pressure in the ambient environment
p_b	Mean contact pressure at the adsorbed lubricant film contact area
p_m	Yield pressure of the metallic contact area
p_{stg}	Stagnation air pressure
p_{tr}	The vapor pressure at the temperature T_{tr}
$Q_{a,0}$	The aerosol concentration
Q_{flux}	The aerosol generation flux at the distance S
q	Distribution parameter in Rosin-Rammler equation
q_f	Heat intensity of the secondary heat source
q_{hl}	Heat intensity of the heat loss due to the air-oil mixture flow
q_r	Heat intensity of the rubbing heat source

q_s	Heat intensity of the primary heat source
R	The gas constant in Equation (3-11)
	Radius of asperity tip in Chapter 4
r	Cylindrical coordinate for correlation of contours of constant Nu
SMR	Spray momentum rate
s_b	Shear strength at the adsorbed lubricant film contact area
s_m	Shear strength at the metallic contact area
T_0	Ambient temperature
T_{flank}	Average tool flank face temperature
T_{mod}	Modified temperature in Oxley's machining theory
T_{stg}	Stagnation air temperature
T_{tr}	The cutting fluid surface temperature
T_v	The ambient temperature
T_∞	The ambient temperature
TE	Transfer efficiency
t_0	Undeformed chip thickness
t_b	Effective adsorbed lubricant film thickness
t_{ch}	Deformed chip thickness

t^*	Equivalent undeformed chip thickness
U_∞	Velocity of air jet
V	Velocity of a moving heat source
V_c	Cutting velocity
V_{ch}	Chip velocity
v_a	Velocity of air
v_l	Velocity of liquid
w	Width of cut
w^*	Equivalent width of cut
X	Sliding distance in Chapter 5
	Characteristic diameter in Rosin-Rammler equation in Chapter 6
X_i	The projection of the distance R in the direction of velocity V
α	Tool rake angle in Chapter 3 ~ 5
	The coefficient in equation in Equation (6-10)
α_n^*	Equivalent cutting edge normal rake angle
β	Friction angle in 2D force cutting model
ϕ	Shear angle
γ	Clearance angle

$\dot{\gamma}$	Shear strain rate of the lubricant
η_c^*	Equivalent chip flow angle
μ	Friction coefficient between tool and workpiece in Chapter 4
	Viscosity of air in Chapter 6
θ	The average roughness angle of the abrasive particle
ρ_a	Density of air
ρ_l	Density of liquid
ρ_{stg}	Stagnation air density
ν	Kinematic viscosity of the lubricant
σ_0	Normal tool tip stress
σ_w	Normal flank stress
τ_0	Shear tool tip stress
τ_{int}	Resolved shear stress at the tool-chip interface
τ_w	Shear flank stress
ΔT_{ch-s}	Temperature rise in the chip due to the primary heat source
ΔT_{ch-f}	Temperature rise in the chip due to the secondary heat source
ΔT_{t-f}	Temperature rise in the tool due to the secondary heat source
ΔT_{t-hl}	Temperature change in the tool due to the heat loss

ΔT_{t-r}	Temperature rise in the tool due to the rubbing heat source
ΔT_{wk-hl}	Temperature change in the workpiece due to the heat loss
ΔT_{wk-r}	Temperature rise in the workpiece due to the rubbing heat source
ΔT_{wk-s}	Temperature rise in the workpiece due to the primary heat source
Δt	Time interval

SUMMARY

The objective of this study is to develop a methodology to analyze the air quality and tool performance in turning process under near-dry condition. Near dry machining refers to the use of a very small amount of cutting fluid in the machining process. It was addressed in mid-1990's in order to reduce the machining cost, to alleviate the environment impact, and to improve the product surface quality. Although previous research showed near dry machining could be an alternative technology to dry and flood-cooled machining, those studies were restricted to qualitative experimental results.

In order to implement the near dry machining technology, this dissertation develops the analytical models for both tool life and aerosol generation prediction. This research includes predictive models of cutting temperatures, cutting forces, tool wear progressions, and aerosol generation. The comparison of air quality and tool performance among dry machining process, near dry machining process, and flood cooling machining process is also presented. It is found that according to the selected cutting conditions in the model-based comparisons, the predicted cutting forces, cutting temperature and power consumption under near dry lubrication are reduced as high as about 30% compared with those in dry cutting but these predicted values are higher than those in wet

cutting by about 10% under the same cutting conditions while the predicted tool wear land lengths are reduced by 60% compared with those in dry cutting but these values are higher than those in wet cutting about 1% under the same cutting conditions. However, the air quality for near dry machining with 12.5 ml/hr oil flow rate is worse than that for wet cutting due to different aerosol generation mechanisms.

After the physical behaviors in near dry turning are understood, it is possible to calculate the tool life and aerosol generation with given material properties and cutting conditions. The results of this research can support the future exploration of dimensional accuracy and cutting condition optimization.

CHAPTER 1

INTRODUCTION

In metal cutting processes, the use of cutting fluids is the most common strategy to improve the tool life, the product surface finish and the size accuracy. Cutting fluids also make chip-breaking and chip-transport easier. However, the introduction of cutting fluids often produces airborne mist, smoke and other particulates in the shop floor air quality. These products bring the environmental, health and safety concerns. In addition, the cost of using cutting fluids is several times higher than tool costs [1]. The economical and environmental concerns on the use of cutting fluids lead to the research of near dry machining (NDM) several years ago [1, 2].

In order to alleviate the economical and environmental impacts, near dry machining was addressed as an alternative to the traditional flood cooling application a decade ago [1, 2]. Near dry machining refers to the use of a small amount of cutting fluid, typically in the order of 100 ml/hr or less, which is about ten-thousandth of the amount of cutting fluid used in flood–cooled machining [3, 4]. The concept of near dry machining is

based on the principle of loss lubrication with dry surface after the machining process. This is the minimum quantity lubrication required in the machining process. Therefore, near dry machining is also recognized as minimum quantity lubrication (MQL) machining.

While showing possible benefits for both air quality control and tool performance improvement [1-8], near dry machining has only limited applications so far. This is because of the lack of scientific and quantitative studies on the appropriate near dry lubrication parameters, such as oil properties, oil flow rate and air pressure for different machining processes. The objective of this research is to develop a systematic and scientific methodology to analyze the air quality and tool wear in the cylindrical turning process.

In this research, the through-the-tool method will be utilized as the cutting fluid supply method. The lubricant is supplied from a pressurized reservoir and transmitted to the cutting zone as a mixture of fluid and air. This research includes: (1) development of temperature models for near dry machining process; (2) development of force models for near dry machining process; (3) development of tool wear models for near dry machining; (4) development of aerosol generation models for near dry machining; and (5) comparison of air quality and tool performance among dry, near dry, and flood cooling

machining process.

After the physical behaviors in near dry turning are understood, it is possible to predict the tool life and aerosol generation with given material properties and cutting conditions. With the study on tool wear rate and air quality as a beginning, the results from this research can support the future exploration of dimensional accuracy and cutting condition optimization as well as research on other machining processes, including milling, grinding, drilling and broaching.

This dissertation begins by providing background information and reviewing relevant research in the area of near dry machining in Chapters 1 and 2. Then, following a discussion of temperature modeling and force modeling in Chapters 3 and 4, the development of the tool wear modeling for near dry turning is presented in Chapter 5. In Chapter 6, the establishment of an analytical method to predict the aerosol generation in near dry turning is presented. Chapter 7 provides comparisons of tool performance and air quality under different cutting conditions among dry machining process, near dry machining process, and flood cooling machining process. This chapter evaluates the effect of near dry lubrication and cutting conditions on the performance of cutting tools. Studies on cutting temperature, cutting force, tool life, and air quality are discussed. The other application of the proposed model in this study is to apply the cooling and

lubricating affected tool wear model to estimate the tool life under conventional flood cooling. Although the approach is similar to the methods described in Chapters 2 ~ 5, it is worthwhile to present the tool wear model for flood cooling cutting in an independent chapter due to different material properties and heat transfer behavior. The results are presented in Chapter 8. Finally, a summary of major contributions and future work is given in Chapter 9.

CHAPTER 2

LITERATURE REVIEW

The literature review on near dry machining is categorized into three parts: (1) research on tool performance, (2) environmental, health impact from the use of cutting fluids and (3) research on air quality modeling. The research on tool performance will include discussions on the experimental observations on cutting forces, cutting temperatures, surface roughness and tool wear behavior with the implementation of near dry lubrication in different machining processes, such as drilling, turning, milling and grinding. The environmental and health impact from the use of cutting fluids will include the information about cutting fluids causing diseases and regulations from government organizations. The research on air quality modeling will discuss the analytical models developed in the past. These models were established based on aerosol concentration on the shop floor for flood cooling situations.

2.1 Researches on Tool Performance

2.1.1 Turning

Machado and Wallbank [3] applied 200-300 ml/hr of lubricant when turning steel bars. The lubricant was delivered in a flowing air stream at a pressure of 29-34 psi. The experimental results showed that surface roughness, chip thickness and cutting forces variations were improved compared to the conventional flood cooling situation. The authors found the following phenomena. (1) Cutting and feed forces were reduced with the use of cutting fluids when turning medium carbon steel bars under low cutting speeds and high feed rates. In some cases, cutting with near dry lubrication had better results than conventional flood cooling. (2) Near dry machining reduced variation in cutting forces and extended the tool life. (3) The effect of near dry lubrication on surface finish and chip thickness was only noticeable at low cutting speeds and high feed rates. (4) Application of near dry lubrication reduced the cost of cutting fluids and related equipments. However, the aerosol concentration increased compared with traditional flood cooling case.

Varadarajan *et. al.* [7] performed experiments in the area of hard turning AISI 4340 with 2 ml/hr oil in a flow of high pressure air at 20 MPa. It was found that cutting

under near dry lubrication had better performance than that in dry or wet cutting in terms of cutting forces, cutting temperatures, surface roughness, tool life, cutting ratio and tool-chip contact length. Lower cutting forces, lower cutting temperatures, better surface finish, shorter tool-chip contact length, larger cutting ratio and longer tool life were observed in near dry turning compared with those in dry or wet cutting. The method to estimate the cutting temperature was also provided but there was not any comparison between predicted cutting temperatures and measurements.

Chen *et. al.* [9] investigated the effects of oil-water combined mist on turning stainless steel with the use of 17 ml/hr oil and 150 ml/hr water mixture. The use of oil-water combined mist could prevent the production of built-up edge (BUE) while BUE was observed when cutting dry or with oil mist. BUE is an important factor of workpiece surface roughness. Therefore the workpiece surface finish under oil-water combined mist was better than that under dry, oil mist or water soluble oil applications. Lower cutting temperatures were also observed with the use of oil-water combined mist compared to cutting dry or with oil mist.

Diniz *et. al*. [10] applied 10 ml/hr oil in turning AISI 52100 steel with CBN tools. The supplied air pressure was 4.5 bar. According to the experimental data, the following conclusions were drawn. (1) Dry and near dry machining had similar performance in

terms of CBN tool flank wear, always better than the tool life under flood cooling. (2) The workpiece surface roughness measured in near dry cutting was close to that obtained from dry cutting.

Dhar *et. al.* [11] investigated the influence of near dry lubrication on cutting temperature, chip formation and dimensional accuracy when turning AISI 1040 steel. The lubricant was supplied at 60 ml/hr through an external nozzle in a flow of compressed air (7 bar). Based on the machining tests, the authors made the following conclusions. (1) Near dry lubrication resulted in lower cutting temperatures compared with dry and flood cooling. (2) The dimensional accuracy under near dry lubrication presented a notable benefit of controlling the increase of the workpiece diameter when the machining time elapsed where tool wear was observed. (3) Dimensional accuracy was improved with the use of near dry lubrication due to the diminution of tool wear and damage.

2.1.2 Milling

Rahman *et. al.* [4, 12] performed experiments in end milling with the use of lubricant at 8.5 ml/hr oil flow rate. The oil was supplied by the compressed air at 0.52 MPa. The workpiece material was ASSAB 718HH steel. The experimental results showed that: (1) tool wear under near dry lubrication was comparable to that under flood

cooling when cutting at low feed rates, low speeds and low depth of cuts; (2) the surface finish generated by near dry machining was comparable to that under flood cooling; (3) cutting forces were close in both near dry machining and flood cooling; (4) fewer burrs formed during near dry machining compared to dry cutting and flood cooling application; (5) the tool-chip interface temperature under near dry lubrication was lower than in dry cutting but higher than that in flood cooling.

Lopez *et. al.* [13] studied the effects of cutting fluid on tool wear in high speed milling. Both near dry lubrication and flood cooling were applied when cutting aluminum alloys. In addition to experiments, they also performed computational fluid dynamics (CFD) simulations for estimating the penetration of the cutting fluid to the cutting zone. The oil flow rates of 0.04 and 0.06 ml/min were studied. The pressurized air was applied at 10 bar. The results showed that (1) with the help of compressed air, the oil mist could penetrated the cutting zone and provide cooling and lubricating while the CFD simulation showed that the flood coolant was not able to reach the tool teeth; (2) the nozzle position relative to feed direction was very important for oil flow penetration optimization.

Sasahara *et al.* [8] reported that in the case of helical feed milling for boring aluminum alloy, cutting forces, cutting temperature and dimension accuracy under near dry lubrication were close to those under flood cooling condition.

2.1.3 Drilling

Braga et. al. [6] investigated the cutting forces, tool wear and hole quality when drilling aluminum-silicon alloys with a small amount of cutting fluid. The near dry lubrication was 10 ml/hr oil in a flow of 4.5 bar compressed air. The experiments showed the following trends when comparing the cutting performance between near dry lubrication and flood cooling. (1) The power consumed under near dry lubrication was lower than the power required in flood cooling, regardless of the tool material. It was inferred that with flood cooling, the workpiece did not heat as much and it required more power to cut the aluminum-silicon alloys. (2) The holes obtained with near dry lubrication offered either similar or better quality than those obtained with flood cooling. (3) The flank wear behavior was similar for these two lubrication conditions. (4) The hole roundness improvement was significant by introducing the near dry lubrication for the diamond coated drill and negligible for the uncoated drill.

Kelly and Cotterell [14] employed near dry lubrication to optimum drilling cast aluminum alloys. A flow of 20 ml/hr oil was delivered with the compressed air at the gauge pressure of 6 bar. The authors observed that the feed force, drill torque and surface roughness under near dry lubrication were the lowest compared with those in flood cooling, compressed air or dry cutting. However, the experimental results also showed

that the hole accuracy for near dry drilling was worse than that for flood cooling situation.

Heinemann *et. al.* [15] investigated the effect of minimum quantity lubricant on tool life when drilling carbon steels with high speed steel twist drills. The cutting fluid flow rate was 18 ml/hr. It was found that a continuous supply of minimum quantity lubricant conveyed a longer tool life while a discontinuous supply of lubricant resulted in a reduction of tool life. A low-viscous and high cooling-capable lubricant provided a longer tool life when different lubricants were used for an external MQL-supply in the tests.

2.1.4 Grinding

Hafenbraedl and Malkin [16] evaluated the near dry lubrication with ester oil based on internal cylindrical grinding tests. These tests were performed when cutting AISI 52100 hardened steel with the oil flow rate of 12 ml/hr mixing with 69 kPa compressed air. The experimental results showed that with the application of near dry lubrication, lower specific cutting energy, better surface finish and higher G-ratio were observed when comparing with cutting completely dry or under flood cooling. However, the elevated bulk temperature was observed as well as thermal distortion of the

workpiece for near dry grinding. This indicated that the cooling from the mixture of ester oil and cold air was not sufficient. The size accuracy would be a problem due to the thermal distortion.

Brinksmeier *et. al.* [17] applied minimum quantity lubrication in grinding. Two different work materials were used: hardened steel (16MnCr5) and tempered steel (42CrMo4V). The minimum quantity lubrication was implemented under 0.5 ml/min oil flow rate and 6 bar pressurized air. With reference to the grinding tests, the following results were observed: (1) both dry and near dry grinding would cause thermal damage on the hardened material with the creep feed grinding operation; (2) acceptable surface finish was obtained under minimum quantity lubrication if the material removal rate was low; (3) the type of lubricant used in minimum lubrication had a significant influence on the surface finish. The analysis of the cooling effect of cutting fluid for both minimum quantity lubrication and flood cooling was also presented. However, there was not a comparison between predicted and measured cutting temperatures.

2.2 Environmental and Health Impact of Using Cutting Fluids

Cutting fluids offer several important mechanical benefits in machining processes such as cooling, lubricating and chip flushing. A recent survey indicated that the cost of

cutting fluids and the auxiliary equipments compromise nearly 7-17% of the total machining costs [1]. Compared with the cost of the cutting tools (2-4%), the cutting fluid cost is significantly high. As a result, there is a need to reduce the use of the cutting fluids. Furthermore, machining processes often produce small lubricant droplets in the form of mist, smoke and gases that are harmful to the environment and human health. In this section, the effects of the cutting fluids on human health will be discussed.

During machining operations, workers could be exposed to cutting fluids by skin contact and inhalation [18]. Skin contact usually occurs in the following situations: (1) the worker directly touches cutting fluid without any protective equipment; (2) the worker handles work, machine, and equipment that are covered with cutting fluid; (3) the worker is exposed to cutting fluid splashes from the machine tool or workpiece. Skin exposure to cutting fluid can cause various skin diseases [19]. In general, skin contact with straight cutting oils cause folliculitis, oil acne, and keratoses while skin exposure to soluble, semi-synthetic and synthetic cutting fluid would result in irritant contact dermatitis and allergic contact dermatitis.

Another source of exposure to cutting fluids is by inhalation of mists or aerosols. The inhalation exposure will be higher if the worker is close to the machine that is not enclosed, if the metal cutting is operated with high cutting speeds and deep cuts, or if

ventilation equipment was not properly selected or maintained. Airborne inhalation diseases have been occurring with cutting fluid aerosols exposed workers for many years. These diseases include lipid pneumonia, hypersensitivity pneumonitis, asthma, acute airways irritation, chronic bronchitis, and impaired lung function [19].

In response to these health effects through skin contact or inhalation, the National Institute for Occupational Safety and Health (NIOSH) has recommended that the permissible exposure level (PEL) is 0.5 mg/m^3 as the metalworking fluid concentration on the shop floor [19, 20].

2.3 Research on Air Quality Modeling

The aerosol concentration is an index for the air quality on the shop floors. The mechanisms of cutting fluid aerosol generation have been studied for years. Yue *et al*. [21] initiated the use of an atomization theory to analyze the aerosol generation under flood cooling conditions. The theory covered diameters of cutting fluid drops in mist formation which were evaluated as a result of transformation between kinetic energy and surface energy. Bell *et al*. [22] observed three mechanisms of cutting fluid aerosol generation in machining processes. They were spin-off, splash and evaporation. The aerosol generation in machining process may come from either one or a combination of these mechanisms.

In addition to lubricant properties, the temperature in the cutting zone was also an important parameter in the aerosol concentration calculation. The cutting temperatures greatly affected the evaporation rate. In previous analyses [21-24], the spin-off mechanism was found to be dominant in flood machining. This may not be true in near dry machining. Because the amount of cutting fluid used in near dry machining is small, it is not easy for the fluid film develop on the workpiece. Thus the spin-off mechanism may be not significant and even not observed. Moreover, the compressed air will increase the kinetic energy of the applied cutting fluid and provide the cooling effect at the cutting zone. These mechanisms were not addressed in previous research. They will be discussed in Chapter 6.

2.4 Organization of this Dissertation

Near dry machining is of great interest in both air quality control and tool life extension as discussed in the literature review. Although previous researches showed this technology could be an alternative machining process other than dry machining or flood cooling machining, those studies are restricted to qualitative experimental results. It is necessary to develop a systematic methodology for near dry machining analysis on both aerosol generation and tool life prediction. The aerosol generation mechanisms should be

re-examined according to the features of near dry turning, i.e. mixture of lubricant and compressed air. The cutting forces, the cutting temperatures and the tool wear mechanisms need to reflect the existence of cutting fluid which may provide the action of lubricating and cooling.

To address the tool performance and environmental impact of near dry turning as a result of cooling and lubricating effects, this dissertation consists of the following tasks:

(1) Temperature modeling in near dry machining process and validation

(2) Force modeling in near dry machining process and validation

(3) Tool wear modeling in near dry machining and validation

(4) Aerosol generation modeling in near dry machining and validation

(5) Comparison of tool performance and air quality among dry machining process, near dry machining process, and flood-cooled machining process

The relationship between the above tasks is shown in Figure 2-1. The predictive values, including cutting forces, cutting temperatures, tool wear rate, and aerosol generation rate, are obtained with material properties and cutting conditions as inputs

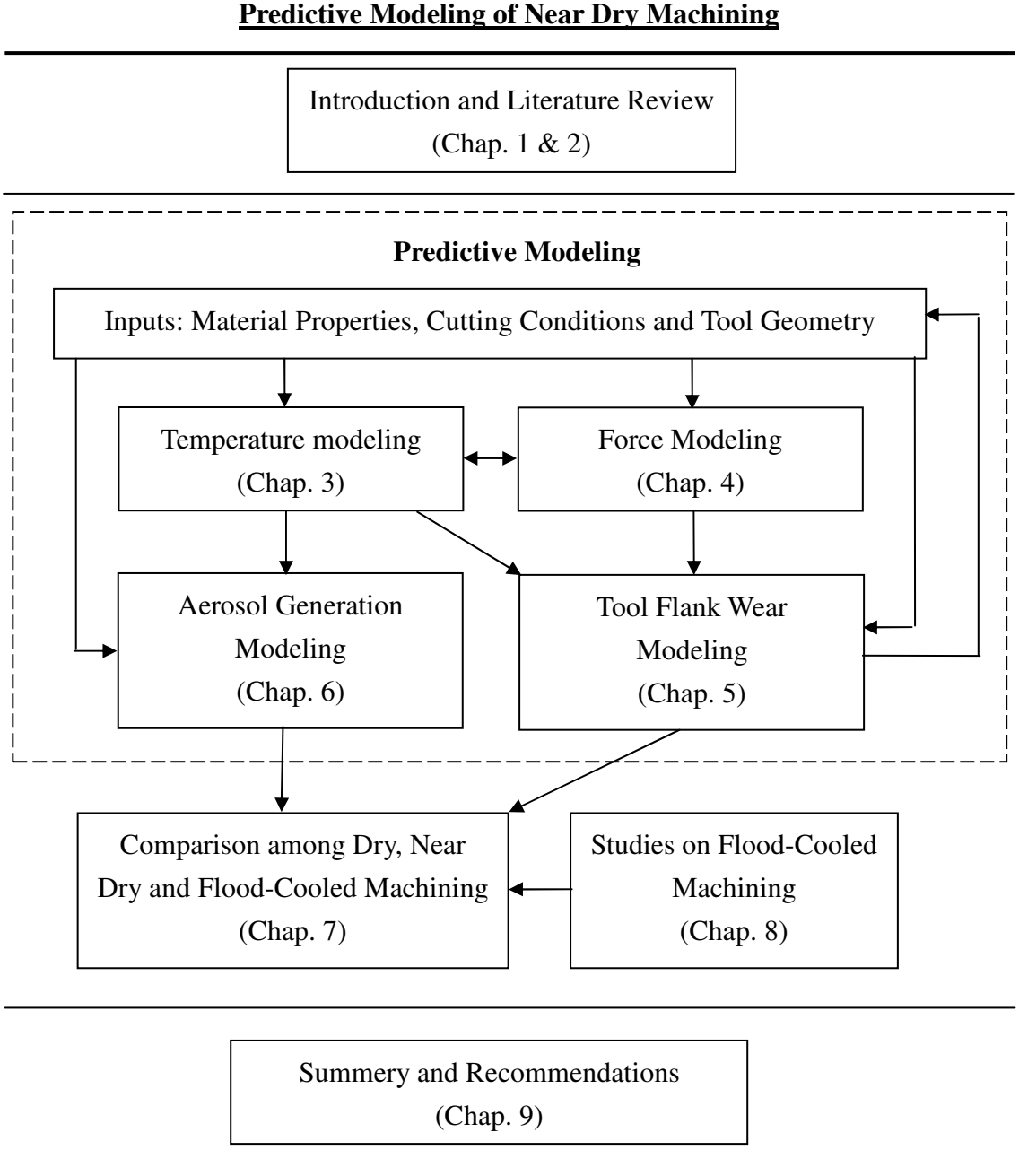

Figure 2-1: Organization of this dissertation.

CHAPTER 3

MODELING OF CUTTING TEMPERATURE IN NEAR DRY MACHINING

3.1 Introduction

The research on cutting temperature in metal cutting began as early as 1906 [25]. It was found that the cutting temperature was important to tool life. An empirical equation to estimate the tool life in terms of the cutting speed (consequently the tool temperature) was developed and subsequently widely used. Since that time, the steady state cutting temperature for dry machining has been studied by many researchers [26-35]. Among them, Komanduri *et. al.* [29] summarized and modified the work of Jaeger [26] and Hahn [31] to estimate the temperature distribution for a sharp tool in metal cutting. Temperature distribution on the tool-chip interface was attributed to the primary heat source (due to shear deformation in the shear zone) and secondary heat source (due to friction on the tool-chip interface) as specified in a moving oblique heat source model or

a stationary square heat source model. For example, the heat generated by the friction on the tool-chip interface was considered as a moving heat source for any fixed point on the chip, while it was considered as a stationary heat source for any fixed point on the tool. Huang and Liang [30] extended the heat source method to the application of worn tools. Unfortunately, those studies focused primarily on dry cutting conditions only. For machining under wet cutting conditions, the research pursued either experimental observations or finite element method simulations [36-38]. It was generally found that a small reduction of the cutting temperature required a large increase of the coolant flow rate [36].

The objective of this chapter is to model the cutting temperature for near dry machining. The understanding of temperature distributions in the near dry cutting zone is a prerequisite to the analysis of cutting tool wear behavior and shop floor air quality. The analysis of cutting temperatures in dry turning has been well documented in the literature. However, the effect of the oil mist under near dry lubrication has not yet been fully understood. In this study, the air-oil mixture is applied to the clearance between tool flank and machined surface with an in-tool nozzle. The heat source method is utilized to model the contributions of different heat sources and heat losses. The heat losses are considered in a two dimensional cutting model in which the cooling effect occurs on the tool flank

face and on an equivalent area on the workpiece just below the tool flank face. The cooling-effected area can then be specified by the tool insert thickness in length and the width of cut in width. The temperature in the chip is attributed to the primary heat source due to plastic shearing and the secondary heat source due to friction. The temperature in the tool is attributed to the secondary heat source, and the heat loss due to cooling on the tool flank face due to the air-oil mixture, while the rubbing heat source is also considered when the tool is worn. For a worn tool, the temperature on the interface between the tool flank face and the workpiece has to be estimated to calculate the heat partition factors on the tool-workpiece interface [30]. On the other hand, for a new tool, its flank face and the workpiece have a point contact. Therefore, the cutting temperature at the tool tip can be calculated according to the heat distribution on the tool-chip interface. The temperature change in the workpiece is caused by the primary heat source, the rubbing heat source, and heat the loss due to cooling. The proposed model is verified by experimental data of turning medium carbon steel AISI 1045 under near dry condition. The measured cutting forces are transferred to the equivalent cutting forces and thrust forces in orthogonal cutting according to the tool insert geometry [39]. The obtained forces are the inputs to estimate the heat source intensities. The temperatures are measured by an embedded thermocouple underneath the tool insert for comparison with model predictions.

3.2 Temperature on Sharp Tools under Near Dry Condition

In this study, fluid is applied through a small opening of 0.762-mm (0.03-inch) diameter in the tool holder just below the tool insert, as shown in Figure 3-1. The opening aims at the tool flank, thus the cooling effect is modeled as a heat loss at the gap between the tool flank and the workpiece surface below it.

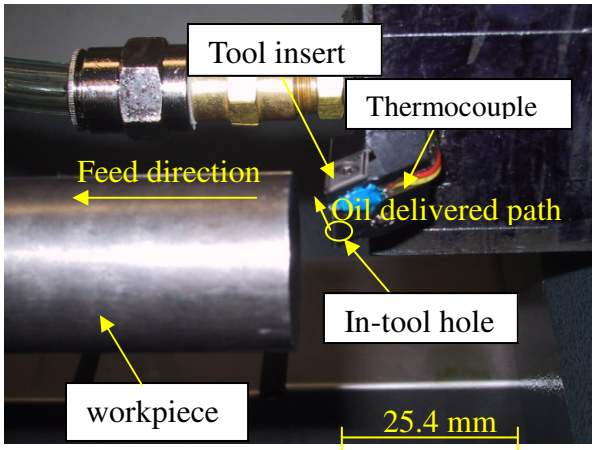

Figure 3-1: The in-tool hole and the thermocouple location

The temperature distribution on the tool-chip interface for sharp tool edges in dry machining can be calculated with an analytical model, as proposed by Komanduri *et. al.* [29]. It is believed that the temperature rise in dry machining is caused by the primary heat source at the shear plane and the secondary heat source at the tool-chip interface. In

near dry machining, three heat sources/losses are considered: the primary heat source due to shear deformation, the secondary heat source due to friction, and the heat loss due to air-oil mixture cooling, as shown in Figure 3-2. The following sections describe how the heat loss due to convection on the tool flank face and workpiece is calculated based on a stationary heat source model (for the tool) and a moving-band heat source model (for the workpiece). The temperature distribution on the tool-chip interface is then estimated by the superposition of temperature changes due to different heat sources and heat losses.

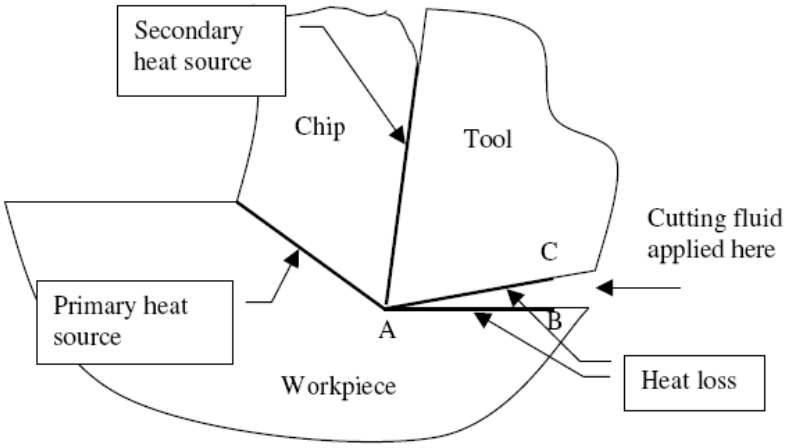

Figure 3-2: Heat sources and heat losses for the 2D model in near dry turning

3.2.1 Temperature rise on the tool-chip interface in chip

Temperature rise in the chip is attributed to both the primary heat source and the

secondary heat source. The effect of the primary heat source is considered as this heat source moving in a continuous chip flow. The back side of the chip is assumed to be adiabatic. Then, the primary heat source and the imaginary heat source are symmetric with respect to the back side of the chip. The schematic of the imaginary chip and the heat sources is shown in Figure 3-3. The temperature rise due to the primary heat source is expressed as [27]:

$$\Delta T_{ch-s} = \frac{q_s}{2\pi k_{ch}} \int_{l_i=0}^{L} e^{\frac{-(X-x_i)V_{ch}}{2a_{ch}}} \left\{ K_0\left(\frac{V_{ch}}{2a_{ch}} \sqrt{(X-x_i)^2 + (Z-z_i)^2} \right) + K_0\left(\frac{V_{ch}}{2a_{ch}} \sqrt{(X-x_i)^2 + (Z-(-2t_{ch}-z_i))^2} \right) \right\} dl_i \tag{3-1}$$

where $x_i = L - l_i \sin(\phi - \alpha)$, $z_i = l_i \cos(\phi - \alpha)$, $L = \frac{t_0}{\sin\phi}$

The above equation is valid only in the region of the chip physically removed, not the imaginary chip as depicted by the dash lines since there is not any material in the imaginary region.

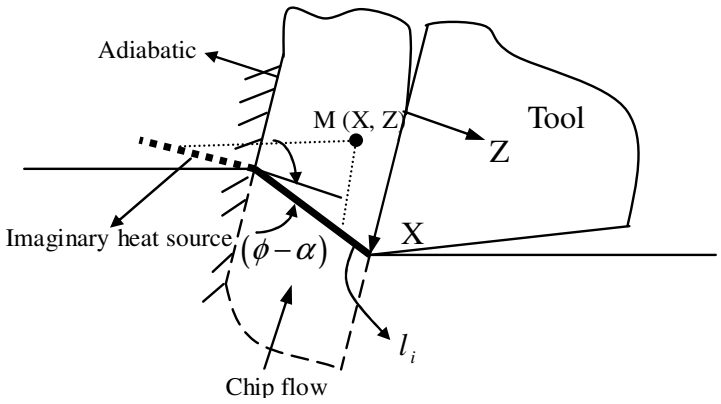

Figure 3-3: Schematics of the moving heat source model of the primary heat source for the chip

The effect of the secondary heat source is also considered as a continuous chip flow with an imaginary heat source [28], as shown in Figure 3-4. The direction of the moving heat source is opposite to the direction of the chip flow since the heat source is moving down with respect to the point M in the chip. The temperature rise due to secondary heat source is expressed as:

$$\Delta T_{ch-f} = \frac{q_f}{\pi k_{ch}} \int_{l_i=0}^{L} B_1(x) e^{-\frac{(X-l_i)V_{ch}}{2a_{ch}}} \left\{ 2K_0\left(\frac{R_i V_{ch}}{2a_{ch}}\right) + 2K_0\left(\frac{R_i' V_{ch}}{2a_{ch}}\right) \right\} dl_i \qquad (3\text{-}2)$$

where $R_i = \sqrt{(X-l_i)^2 + Z^2}$, $R_i' = \sqrt{(X-l_i)^2 + (Z+2t_{ch})^2}$

Again, the above equation is valid only in the region of the chip removed. Considering both the primary heat source and the secondary heat source, the temperature rise in the chip is $\Delta T_{ch-s} + \Delta T_{ch-f}$.

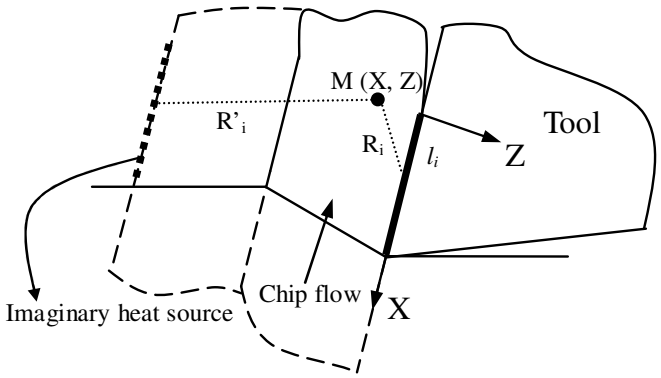

Figure 3-4: Schematic of the moving heat source model of the secondary heat source for the chip

3.2.2Temperature rise on the tool-chip interface in tool

The temperature rise in the tool comes from the friction heat source on the tool-chip interface and the heat loss on the tool flank face. The heat source is stationary with respect to any point in the tool. The imaginary heat source is shown as the dash line in Figure 3-5. The temperature rise due to the friction can be expressed as [28]:

$$\Delta T_{t-f} = \frac{q_f}{2\pi k_t} \int_0^{L_c} \left(1 - B_1(x_i)\right) \int_{-w/2}^{w/2} \left(\frac{1}{R_i} + \frac{1}{R_i'} \right) dy_i dx_i \qquad (3\text{-}3)$$

where $R_i = \sqrt{\left(X - x_i\right)^2 + \left(Y - y_i\right)^2 + Z^2}$ and $R_i' = \sqrt{\left(X - (2L_c - x_i)\right)^2 + \left(Y - y_i\right)^2 + Z^2}$

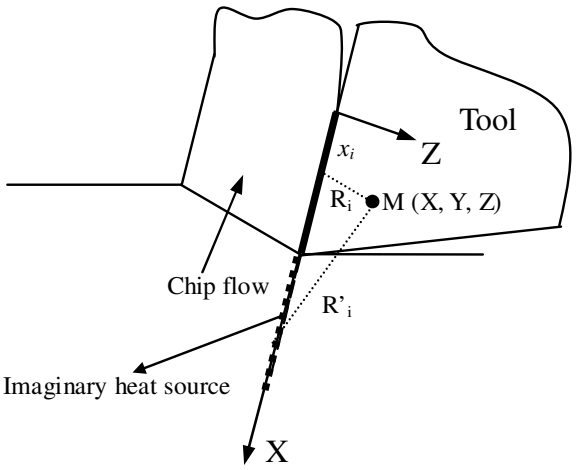

Figure 3-5: Schematic of the stationary heat source model of the secondary heat source for the tool

As near dry cooling is applied with an air-oil mixture on the tool-flank face, the affected region on the tool flank face acts as a heat sink. It is assumed that the affected region has an area of the tool insert thickness, L_t, by the width of cut, w (in the direction perpendicular to Figure 3-6). The heat loss is stationary with respect to the tool. The relative location of the imaginary heat loss is similar to that of the imaginary heat source in Figure 3-5. The heat loss and the imaginary heat loss due to air-oil mixture are plotted in Figure 3-6 in which the temperature change in the $X_1Y_1Z_1$ coordinate system follows Equation (3-3) as:

$$\Delta T_{t-hl} = \frac{q_{hl}}{2\pi k_t} \int_0^{L_c} \int_{-w/2}^{w/2} \left(\frac{1}{R_i} + \frac{1}{R_i'} \right) dy dx \qquad (3\text{-}4)$$

where $R_i = \sqrt{(X_1 - x_i)^2 + (Y_1 - y_i)^2 + Z_1^2}$ and $R_i' = \sqrt{(X_1 - (2L_t - x_i))^2 + (Y_1 - y_i)^2 + Z_1^2}$

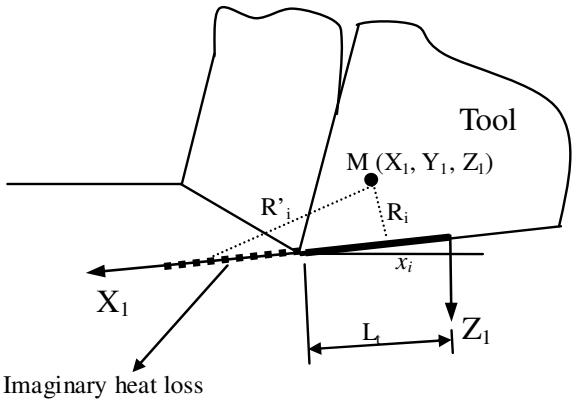

Figure 3-6: Schematic of the stationary heat source model of the heat loss for the tool

The heat loss intensity is calculated according to forced convection model as:

$$q_{hl} = \bar{h}(T_{flank} - T_0) \tag{3-5}$$

Since the flow of the applied air-oil mixture is parallel to the tool flank face and the machined workpiece, the forced convection effect can be considered as a fluid flow passing through parallel flat surfaces. The average heat transfer coefficient in the above equation can be estimated by the Nusselt number as following [40]:

$$\bar{N}_u = \frac{\bar{h}L_{eff}}{k_{air}} = 0.664\,\mathrm{Pr}^{1/3}\,\mathrm{Re}^{1/2} \tag{3-6}$$

In near dry machining, the air-oil mixture as a cutting fluid typically has relatively

low oil to air mass ratio. For example, in this study, the oil mass flow rate was about 2% of the air mass flow rate. Thus, it was assumed that the Prandtl number and Reynolds number can be estimated by the material properties of the compressed air. Moreover, it is necessary to check if the mixture flow is choked when passing through the small hole of 0.762-mm diameter. The condition of choked flow is given by [41]:

$$\frac{p^*}{p_{stg}} = \left(\frac{2}{1+\zeta}\right)^{\zeta/(\zeta-1)} \quad (\zeta = 1.4 \text{ for air}) \tag{3-7}$$

If the exit air pressure is larger than the critical air pressure, p^*, the flow is choked, and in which case the Mach number equals to 1. Regardless of the choking condition, the pressure, density, temperature, and velocity of the air flow at the exit of the hole can be calculated according to [41]:

$$\frac{p}{p_{stg}} = \left\{\frac{1}{1+\left[(\zeta-1)/2\right]Ma^2}\right\}^{\zeta/(\zeta-1)} \tag{3-8}$$

$$\frac{\rho}{\rho_{stg}} = \left\{\frac{1}{1+\left[(\zeta-1)/2\right]Ma^2}\right\}^{1/(\zeta-1)} \tag{3-9}$$

$$\frac{T}{T_{stg}} = \frac{1}{1+\left[(\zeta-1)/2\right]Ma^2} \tag{3-10}$$

$$V = Ma\sqrt{RT\zeta} \tag{3-11}$$

However, the heat transfer coefficient calculated in this way when only considering the cooling effect due to the air may be conservative for the cases where the

oil also contributes to the cooling effect in the machining process by convection or boiling. Considering that the cooling effect of the air-oil mixture flow is proportional to that of air flow, the effective heat transfer coefficient can be given as:

$$\bar{h}_{eff} = \lambda \bar{h} \tag{3-12}$$

The coefficient, λ, can be calibrated experimentally. With both the secondary heat source and the heat loss due to convection, the temperature rise in the chip is $\Delta T_{t-f} - \Delta T_{t-hl}$.

3.2.3 Temperature distribution on the tool-chip interface

The temperature rise on the tool-chip interface is considered the same as that in the chip and in the tool. The heat partition function $B_1(x_i)$ is solved by the following relationship.

$$\Delta T_{ch-s} + \Delta T_{ch-f} + T_0 = \Delta T_{t-f} - \Delta T_{t-hl} + T_0 \tag{3-13}$$

If a total of n points are of interest on the tool-chip interface, the same number of equations can be solved for the heat partition factors, $B_1^{(1)} \sim B_1^{(n)}$. Subsequently, the temperature distribution on the tool-chip interface can be obtained.

3.3 Temperature on Worn Tools under Near Dry Condition

In estimating the cutting temperature with tool flank wear in dry machining, Huang and Liang [30] developed a new model to predict the heat generation due to the

tool flank wear. A rubbing heat source, as a result of the presence of tool wearland, was added to the aforementioned heat sources methods under dry machining condition. The cutting temperature distribution was thus calculated with the tool flank wear effect. The schematic of the heat sources and heat losses in near dry machining with tool flank wear is shown in Figure 3-7. The effective area of the heat losses decreases with the increase of the wearland length L_t.

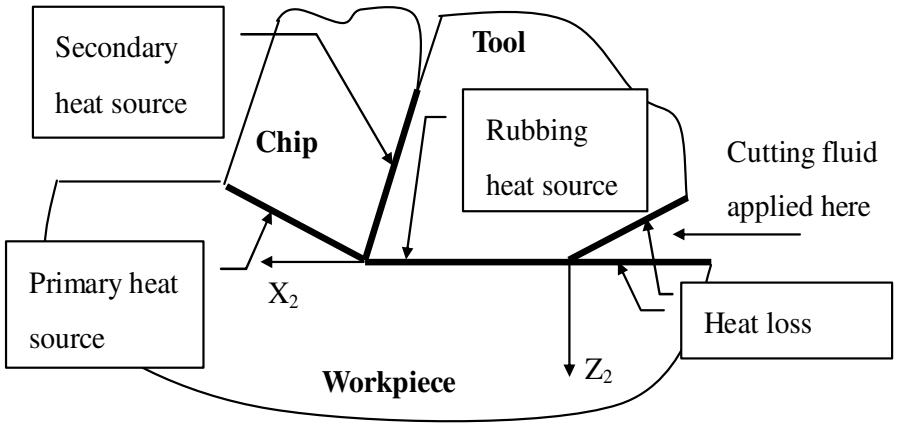

Figure 3-7: Heat sources and heat losses for the 2D model in near dry turning with the tool wear effect

3.3.1 Temperature rise in chip

With the tool flank wear, the temperature rise in the chip is caused by the primary

heat source and the secondary heat source. The temperature rise in the chip is calculated by equations (3-1) and (3-2).

3.3.2 Temperature rise in the tool

The temperature rise in the tool with the tool flank wear is attributed to the secondary heat source, the heat loss, and the rubbing heat source. The effects of the secondary heat source and the heat loss on the cutting temperature are calculated by equations (3-3) and (3-4). There is a part, $B_2(x_i)$, of the rubbing heat transferred into the workpiece, while the other part, $1-B_2(x_i)$, transferred into the tool. The effect of the rubbing heat source on the tool is calculated in the $X_2Y_2Z_2$ coordinate system as shown in Figure 3-7 by the following equation [30]:

$$\Delta T_{t-r} = \frac{q_r}{2\pi k_t} \int_0^{L_{VB}} \int_{-w/2}^{w/2} \left(1-B_2(x_i)\right)\left(\frac{1}{R_i}+\frac{1}{R_i'}\right) dy_i dx_i \qquad (3\text{-}14)$$

where $R_i = \sqrt{\left(X_2 - x_i\right)^2 + \left(Y_2 - y_i\right)^2 + Z_2^{\,2}}$ and $R_i' = \sqrt{\left(X_2 - (2L_{VB} - x_i)\right)^2 + \left(Y_2 - y_i\right)^2 + Z_2^{\,2}}$

The temperature rise in the tool under the tool flank wear effect is $\Delta T_{t-f} - \Delta T_{t-hl} + \Delta T_{t-r}$.

3.3.3 Temperature rise in the workpiece

The temperature rise in the workpiece is caused by the primary heat source, the rubbing heat source, and the heat loss. The heat sources and the heat loss are considered

as moving heat bands with respect to any fixed point in the workpiece. The temperature rise in workpiece was estimated by the moving heat bands models [27, 30] with proper coordinate systems. The imaginary part of the primary heat source is plotted in Figure 3-8. The heat source is assumed to move in a semi-infinite material with imaginary material. The effect of the primary heat source is expressed as:

$$\Delta T_{wk-s} = \frac{q_s}{2\pi k_{wk}} \int_{l_i=0}^{L} e^{\frac{-(X_2-x_i)V_c}{2a_{wk}}} \left\{ K_0\left(\frac{V_c}{2a_{wk}} \sqrt{(X_2 - x_i)^2 + (Z_2 - z_i)^2} \right) + K_0\left(\frac{V_c}{2a_{wk}} \sqrt{(X_2 - x_i)^2 + (Z_2 - (-2t_0 - z_i))^2} \right) \right\} dl_i \tag{3-15}$$

where $x_i = L_{VB} + l_i \cos\phi$, $z_i = l_i \sin\phi$.

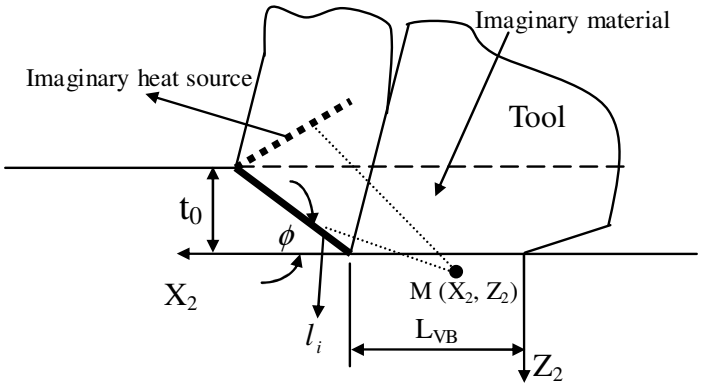

Figure 3-8: Schematic of the moving heat source model of the primary heat source for the workpiece

Similarly, the effect of rubbing heat source is considered as a heat source moving along the X_2 axis in a semi-infinite material as shown in Figure 3-9. The effect of the rubbing heat source is expressed as [28, 30]:

$$\Delta T_{wk-r} = \frac{q_r}{\pi k_{wk}} \int_0^{L_{VB}} B_2(x_i) e^{-\frac{(X_2 - x_i)V_c}{2a_{wk}}} \left\{ K_0 \left(\frac{V_c}{2a_{wk}} \sqrt{(X_2 - x_i)^2 + Z_2^2} \right) \right\} dx_i \qquad (3\text{-}16)$$

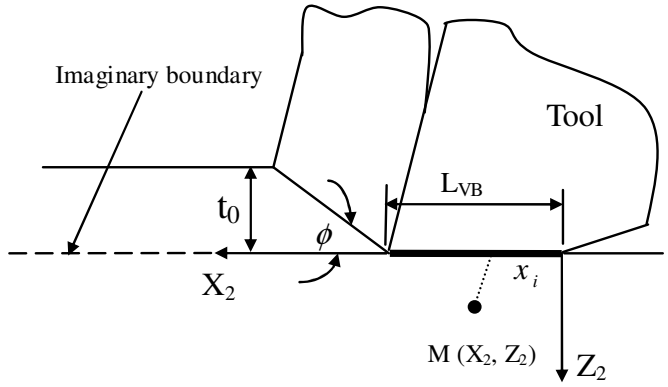

Figure 3-9: Schematic of the moving heat source model of the rubbing heat source for the workpiece

The temperature decrease due to heat loss is also calculated in the $X_2Y_2Z_2$ coordinate systems, as depicted in Figure 3-10 according to:

$$\Delta T_{wk-hl} = \frac{q_{hl}}{\pi k_{wk}} \int_0^{L_t} e^{-\frac{(X_2 - x_i)V_c}{2a_{wk}}} \left\{ K_0 \left(\frac{V_c}{2a_{wk}} \sqrt{(X_2 - x_i)^2 + Z_2^2} \right) \right\} dx_i \qquad (3\text{-}17)$$

where $q_{hl} = \bar{h}(T_{flank} - T_0)$ and the effective length L_t is the partial tool insert thickness

outside of the wearland.

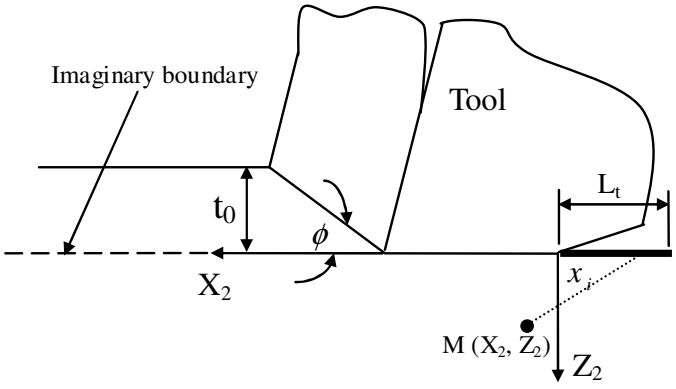

Figure 3-10: Schematic of the moving heat source model of the heat loss for the workpiece

The temperature rise in workpiece then equals to $\Delta T_{wk-s} + \Delta T_{wk-r} - \Delta T_{wk-hl}$.

3.3.4 Temperature distribution on the tool-chip interface and tool-workpiece interface

It is assumed that the temperature rise on the tool-chip interface in the chip and in the tool is the same. Under the effect of tool flank wear, the relationship is:

$$\Delta T_{ch-s} + \Delta T_{ch-f} + T_0 \;=\; \Delta T_{t-f} - \Delta T_{t-hl} + \Delta T_{t-r} + T_0 \quad \text{(on tool rake face)} \qquad (3\text{-}18)$$

Similarly, the temperature distribution on the tool-workpiece interface should be the same in the tool and in the workpiece, thus:

$$\Delta T_{wk-s} + \Delta T_{wk-r} + \Delta T_{wk-hl} + T_0 \;=\; \Delta T_{t-f} - \Delta T_{t-hl} + \Delta T_{t-r} + T_0 \quad \text{(on tool flank face)} \qquad (3\text{-}19)$$

Both the equations (3-18) and (3-19) contain the heat partition factors $B_1(x_i)$ and $B_2(x_i)$. If the contact length on the tool-chip interface is divided into *n* points, $B_1^{(1)} \sim B_1^{(n)}$, and the contact length on the tool-workpiece is divided into *m* points, $B_2^{(1)} \sim B_2^{(m)}$. The heat-partition factors can be obtained by solving the (*n*+*m*) equations according to (3-18) and (3-19).

3.4 Experimental Model Validation

3.4.1 Cutting conditions and estimated parameters

The validation of cutting temperatures in near dry turning is verified by measuring the temperatures with an embedded thermocouple (Omega K-type) located under the tool insert when cutting AISI 1045 with uncoated carbide tool inserts (Valenite DPMT-2A) on a lathe (CMS GT-27) under various cutting conditions, as shown in Table 3-1. The cutting conditions are selected in the ranges of cutting speed = 45.75-137.25 m/min, feed = 0.0508-0.1016 mm/rev and depth of cut = 0.508-1.016 mm according to the design of experiment [42]. The workpiece is 31.75 mm in diameter and 76.2 mm long. Each cut takes away 50.8 mm long material. The shortest cutting time in the tests is about 20 seconds (the 9th test) which is long enough to reach the steady state of the cutting temperature measurement. The cutting fluid is delivered to the tool flank face through a

0.762-mm in-tool hole by a cutting fluid applicator (UNIST uni-MAX Coolubricator). The UNIST system is used to supply the air-fluid mixture of 12.5 ml/hr at a pressure of 275.8 kPa (40 psi). Coolube 2210, a vegetable oil, is chosen as the cutting fluid. The cutting forces are recorded by a tool-post dynamometer (Kistler model 9257B). The arrangement of the in-tool hole and the thermocouple is shown in Figure 3-1. In the figure, it is shown that the in-tool hole was located underneath the tool insert. The thermocouple is covered by the thermal conductive composite as indicated in the figure.

Table 3-1: Test cutting conditions for both sharp tools and worn tools

Test No.	Speed (m/min)	Feed (mm/rev)	Depth of cut (mm)
1	45.75	0.0508	0.508
2	45.75	0.0762	1.016
3	45.75	0.1016	0.762
4	91.5	0.0508	1.016
5	91.5	0.0762	0.762
6	91.5	0.1016	0.508
7	137.25	0.0508	0.762
8	137.25	0.0762	0.508
9	137.25	0.1016	1.016

The equivalent 2D cutting forces and thrust forces can be calculated from the measured 3D force data according to the tool insert geometry [39]. Assuming that the

heat intensities are uniform on the shear plane, on the tool-chip interface, and on the tool-workpiece interface, they can be calculated as:

$$q_s = \frac{F_s V_s}{w(t_0 / \sin\phi)} \tag{3-20}$$

$$q_f = \frac{F V_{ch}}{w L_c} \tag{3-21}$$

$$q_r = \frac{F_{cw} V_c}{w L_{VB}} \tag{3-22}$$

where forces and velocities, F_s, F, V_s, V_{ch} can be calculated with the cutting force, the thrust force, cutting velocity and the shear angle [43]. The different heat generations in the cutting zones for dry and near dry cutting conditions are conveyed by the measured cutting forces which represent the lubricating effect in different circumstances. With the oil lubrication, the measured cutting forces in near dry machining are expected smaller than those in dry cutting and so are the heat generations. The shear angle, ϕ, and the contact length, L_c, were obtained by [43, 44]:

$$\frac{F_t}{F_c} = \tan(\beta - \alpha) \tag{3-23}$$

$$\phi = \frac{\pi}{4} - \frac{1}{2}(\beta - \alpha) \tag{3-24}$$

$$L_c = \frac{t_0 \sin\beta}{\sin\phi \cos(\phi + \beta - \alpha)} \tag{3-25}$$

The shear angle and the chip thickness are almost constant as the tool wears [30]. Thus, the rubbing force F_{cw} can be obtained from the experimental data by subtracting the sharp tool cutting force from the worn tool cutting force.

A carbide tool insert (Valenite DPMT-2A) with 0^0 rake angle and 11^0 clearance angle was used in this study. The material properties of the tool insert, the workpiece (AISI 1045) and the air are listed in Table 3-2.

Table 3-2: Material properties for the tool insert, the workpiece and the air

Tool insert	AISI 1045		Air (at atmosphere pressure, $20\,^oC$)			
Thermal conductivity (k_t)	Thermal conductivity (k_{ch})	Thermal diffusivity (a_{ch})	Density (ρ)	Prandtl Number (Pr)	Absolute viscosity (μ)	Thermal conductivity (k_{air})
84.02 W/mK	50.8 W/mK	0.134×10^{-4} m^2/s	1.164 kg/m^3	0.71	1.824×10^{-5} Ns/m^2	0.0251 W/mK

Source: Shackelford *et. al.*[45], ASM handbook [46], and Munson [41]

The estimated parameters according to the measured cutting forces for sharp tool are listed in Table 3-3 and the estimated parameters according to the measured cutting forces for worn tools are listed in Table 3-4. When investigating the near dry lubrication effect on the cutting temperatures, the values of rubbing force on the tool-workpiece interface F_{cw} and wearland length L_{VB} in Table 3-4 are used in order to compare the cutting temperatures in dry and near dry situations under the same tool wear conditions.

Table 3-3: The estimated parameters for sharp tools

(a) Near dry machining				
Test No.	F_c (N)	F_t (N)	ϕ (degrees)	L_c (mm)
1	67.15	35.52	31.61	0.0813
2	212.98	133.56	29.48	0.1608
3	194.79	115.20	30.61	0.1857
4	189.81	170.56	24.42	0.1940
5	197.25	150.50	26.90	0.2166
6	159.47	109.50	28.72	0.2298
7	125.19	97.57	26.61	0.1495
8	117.4	76.57	29.36	0.1602
9	283.17	177.45	29.30	0.2188

(b) Dry machining				
Test No.	F_c (N)	F_t (N)	ϕ (degrees)	L_c (mm)
1	165.07	99.91	29.41	0.0981
2	219.47	141.71	28.58	0.1807
3	211.43	134.37	28.78	0.2351
4	222.84	219.83	22.69	0.2397
5	209.79	185.79	24.24	0.2998
6	170.33	134.12	25.89	0.3296
7	132.08	100.69	26.34	0.1564
8	135.97	103.83	26.32	0.2353
9	287.01	168.72	29.78	0.2088

In this study, the air flow is choked according to the choked flow analysis from equations (3-7) ~ (3-11). Thus, the air flow velocity equals to the sound speed at $20^0 C$ as $313\, m/s$. The coefficient, λ, in Equation (3-12) is determined to be 64.02 by

comparing the predicted temperature and the measured temperature with the embedded thermocouple for the 5th test for sharp tool. The measured temperature for calibration is the 5th set of experimental data in Figure 3-11.

Table 3-4: The estimated parameters for worn tools for near dry machining

Test No.	F_c (N)	F_t (N)	L_{VB} (μm)	F_{cw} (N)	ϕ (degrees)	L_c (mm)
1	67.15	33.89	28.5	4.77	31.61	0.0813
2	212.98	128.16	55.6	3.61	29.48	0.1608
3	194.79	107.03	89.9	4.54	30.61	0.1857
4	189.81	165.95	119.8	41.13	24.42	0.1940
5	197.25	144.37	110.4	27.87	26.90	0.2166
6	159.47	101.80	129.5	36.03	28.72	0.2298
7	125.19	93.59	153.0	61.25	26.61	0.1495
8	117.4	71.34	110.6	38.69	29.36	0.1602
9	283.17	172.85	155.1	83.56	29.30	0.2188

3.5 Results and Discussion

The model-predicted temperatures and the measured temperatures under the tool insert for different cutting conditions are shown in Figures 3-11 and 3-12. The deviations are within 12 % of error except for case 7 for sharp tool and case 4 for worn tool. Most of the predicted temperatures for worn tool (except case 4) are a little bit higher than the recorded temperature.

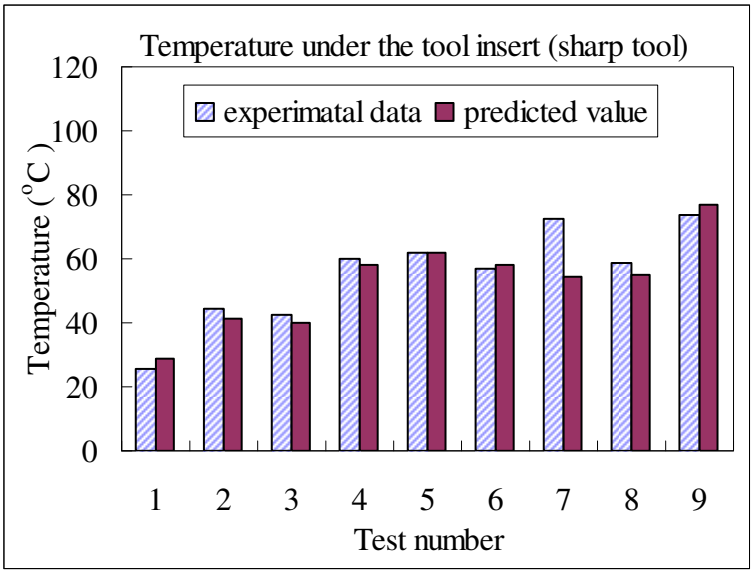

Figure 3-11: Temperature comparison between predicted values and measured values at thermocouple location for sharp tool

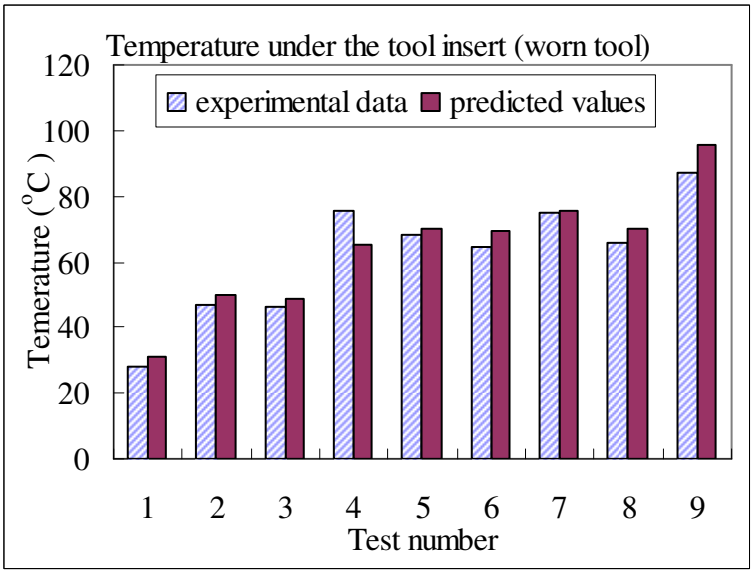

Figure 3-12: Temperature comparison between predicted values and measured values at thermocouple location for worn tool

Figure 3-13 shows the effect of the tool flank wear on the cutting temperature. It is observed that at higher cutting speeds the effect of the tool flank wear is more significant. For example, the cutting temperature increases 26% for case 8 (cutting speed was 137.25 m/min), while the temperature only increases 10% for case 5 (cutting speed was 91.5 m/min) when the tool flank wear length is about 110 μm.

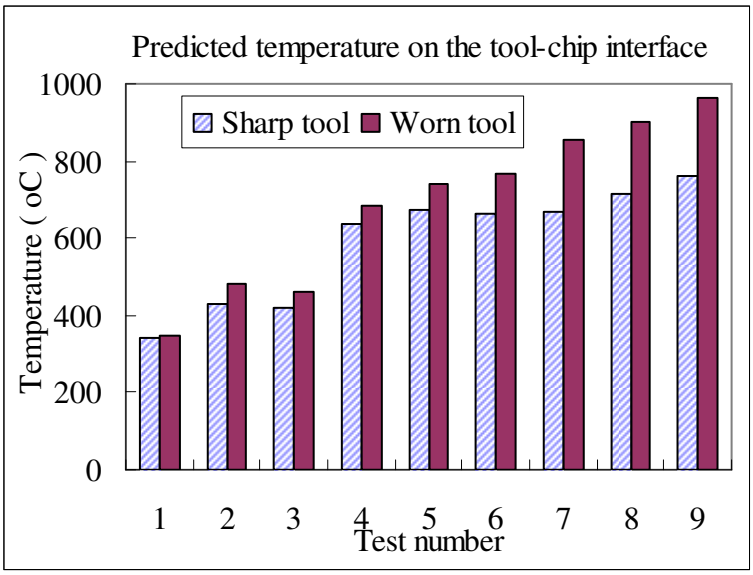

Figure 3-13: Temperature comparison of predicted values at thermocouple location between sharp tool and for worn tool

The effect of near dry cooling can be established by comparing cutting temperatures between dry and near dry machining as shown in Figures 3-14 and 3-15, in

which the cutting forces are based on Tables 3-3 and 3-4. Figure 3-16 presents the tool-workpiece temperature for worn tool. It can be seen that the average reduction in cutting temperature (excluding case 1 due to a significant distinction in measured cutting forces) is about 8.1% for the tool-chip interface temperatures for sharp tools, 9.0% for the tool-chip interface temperatures for worn tools, and 4.6% for the tool-workpiece interface temperatures for worn tools. The difference in cutting temperatures for dry and near dry conditions is closely related to the difference in cutting forces. The greater the cutting forces the more heat is generated and consequently the higher cutting temperatures. Moreover, the average cutting temperature reduction, relative to dry machining, on the tool-chip interface in near dry machining is below 10%. This insignificant effect can be understood based on the mechanics of the cooling process. First, the tool flank face, where heat is removed, is far away from the cutting zone as compared to the dimensions of the heat sources. The temperatures difference between the tool flank and the mixture are not as much as that between the air-oil flow temperature and the maximum temperature at the tool-chip interface. Thus, the heat taken away from the tool flank face is relatively insignificant. Even if more cutting fluid is applied, the temperature reduction on the tool-chip interface is still limited by a low heat transfer coefficient. A similar relationship between temperature reduction and fluid flow rate was observed in wet

cutting situations in a previous research [36]. Secondly, the heat transfer rate is proportional to the heat coefficient of the medium. In this study, it was found that the heat intensity for the cooling process is almost two orders of magnitude less than the heat intensity generated in the primary shear zone or the tool-chip interface. Therefore, only a small portion of the heat can be removed from the cutting zone.

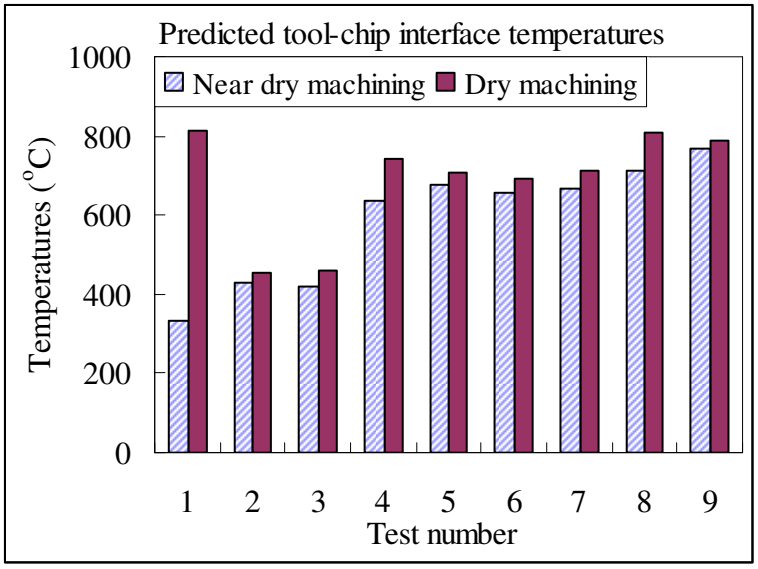

Figure 3-14 : Temperature comparison of predicted values between near dry machining and dry machining on the tool-chip interface for sharp tool

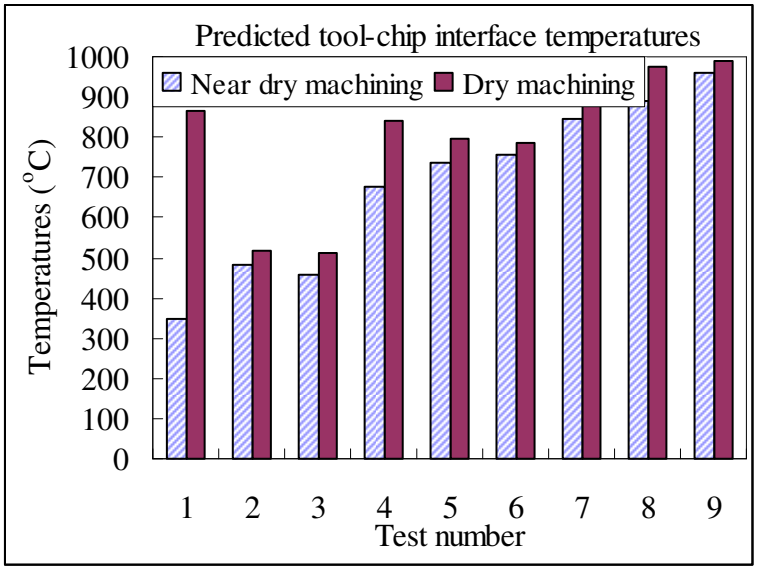

Figure 3-15: Temperature comparison of predicted values between near dry machining and dry machining on the tool-chip interface for worn tool

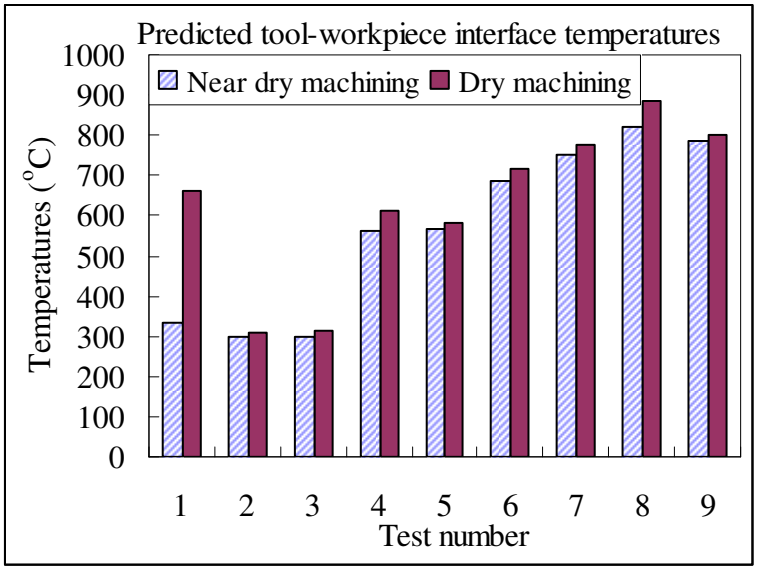

Figure 3-16: Temperature comparison of predicted values between near dry machining and dry machining on the tool-workpiece interface for worn tool

The cooling effect of the oil-air mixture is also observed by the heat partition coefficients. Figure 3-17 shows the average heat partition coefficients (B1) for sharp tools under both near dry and dry situations. The trends of heat partition coefficients for worn tools are similar. As shown in Figure 3-17, the heat partition coefficients in near dry machining are smaller than those in dry machining. This indicates that the heat is taken away by the near dry cooling. Less heat remains in the chip. Nevertheless, the heat partition coefficients only change a little which implies that the near dry cooling for the selected cutting conditions is limited. To sufficiently reduce the cutting temperatures, it is suggested to apply the cutting fluid as close as possible to the heat generation area, such as the shear zone, the tool-chip interface, and the tool-workpiece interface, or to use a cutting fluid with a high heat coefficient.

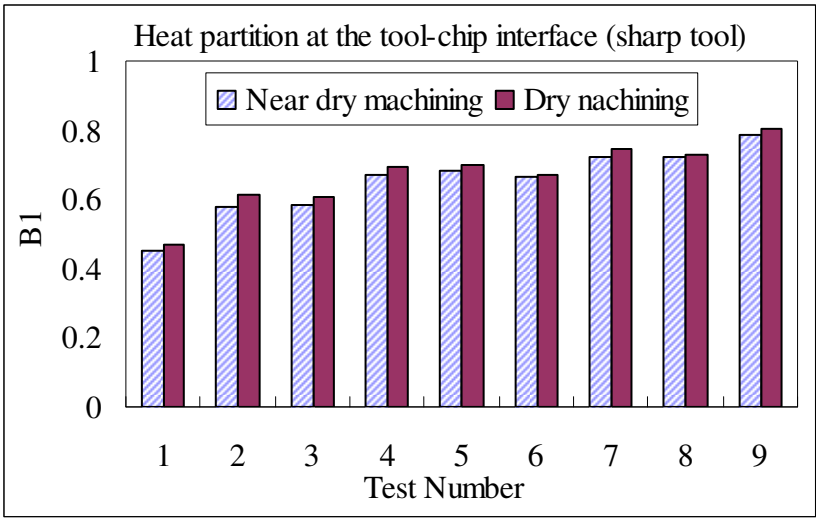

Figure 3-17: The average heat partition coefficients (B1) comparison between near dry machining and dry machining on the tool-chip interface for sharp tool

The effects of cutting parameters on the cutting temperature in near dry turning process are shown in Figures 3-18, 3-19, and 3-20 according to the design of experiments [42]. It is shown that the cutting speed is the dominant factor among the cutting conditions, followed by the feed, and then the depth. It is interesting that the effect of the depth of cut on tool-workpiece temperature for worn tool has no obvious trend.

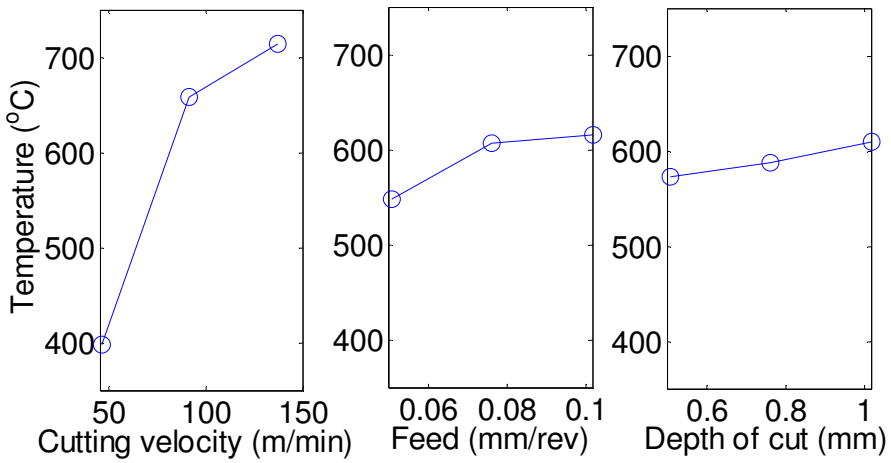

Figure 3-18: Tool-chip interface temperature trend for sharp tool with respect to cutting conditions

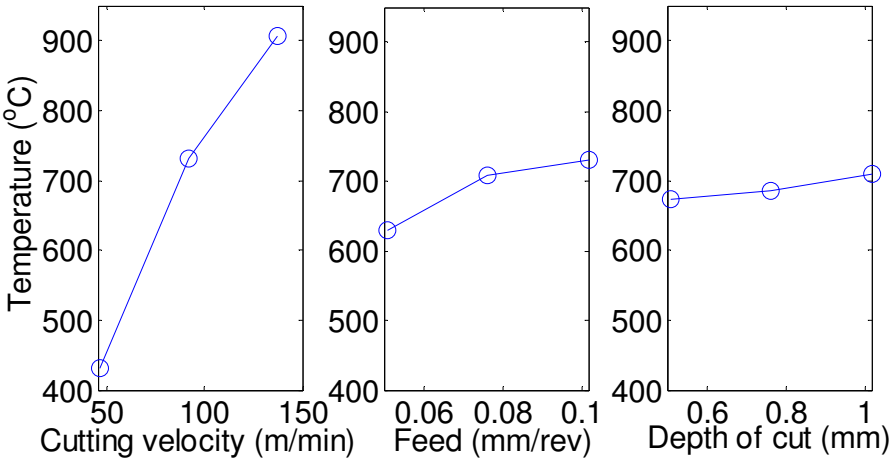

Figure 3-19: Tool-chip interface temperature trend for worn tool with respect to cutting conditions

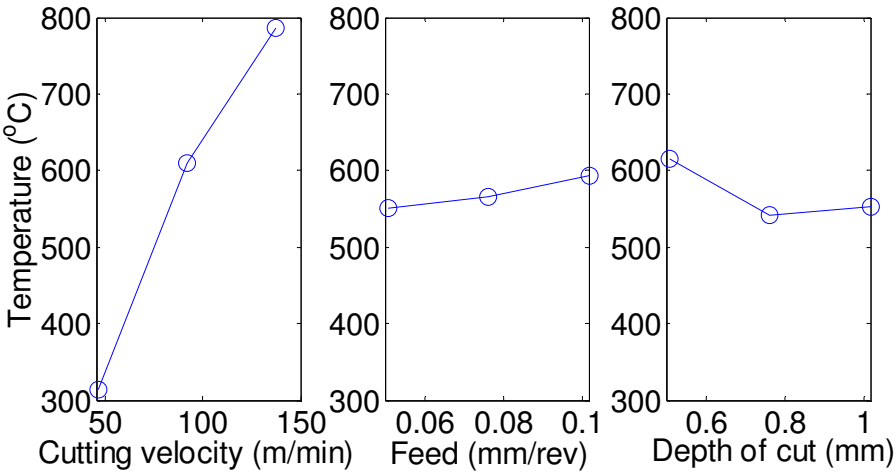

Figure 3-20: Tool-workpiece interface temperature trend for worn tool with respect to cutting conditions

3.6 Conclusion

This study addresses the effect of the oil mist on the cutting temperature in near dry turning with a different approach, analytical models, from other researches. The understanding of temperature distributions in machining under near dry situations is extremely important to the analysis of tool wear progressions and shop floor air quality. A temperature model based on heat source and heat sink mechanisms for near dry machining is presented. With cutting forces and the material properties as inputs, the average tool-chip interface temperature and the average tool-workpiece temperature are obtained. In this chapter, the cooling effect in near dry situations is modeled as heat losses on the tool flank face and the workpiece surface below the tool. In addition, the

lubricating effect on cutting temperatures in near dry machining is considered by the change of cutting forces which lead to different heat intensities in the cutting zone. For the temperature rise in the chip on the tool-chip interface, the effects of the shearing heat source on the shear plane and the frictional heat source on the tool-chip interface are modeled as moving heat sources. For the temperature rise in the tool on the tool-chip interface or on the tool-workpiece interface, the effects of the secondary heat source due to friction and the heat loss due to cooling on the tool flank face are modeled as stationary heat sources, while the rubbing heat source is also considered as another stationary heat sources when the tool was worn. For the temperature rise in the workpiece on the interface between the tool flank face and the workpiece, the shearing heat source on the shear plane and the heat loss due to cooling on the machined surface are modeled as moving heat sources, while the rubbing heat source is also considered as another moving heat sources when the tool is worn. It is found that the tool flank wear has a larger effect on cutting temperature for high cutting speed. The results also show that the cutting velocity plays an important role for the temperature rise in turning processes. Moreover, the reduction in the cutting temperatures is small by considering the lubricating effect as the reduction in cutting forces, and consequently the cooling effect on the tool flank wear face is insignificant when the differences in cutting forces between

dry and near dry turning are small.

CHAPTER 4

MODELING OF CUTTING FORCE IN NEAR DRY MACHINING

4.1 Introduction

The knowledge of cutting forces is a prerequisite to cutting temperature estimation, tool life prediction, cutting process planning, and chatter analysis, etc. The mechanics of machining processes and the prediction of cutting forces have been extensively analyzed and modeled for decades by many researchers. Although a number of studies have been documented in the field, these models are not suited for near dry lubrication condition without considering the effects of lubricating and cooling resulting from the small amount of cutting fluid transmitted to the cutting zone as an air-oil mixture. In order to support the planning, optimization, and control of near dry machining process, it is necessary to establish a set of predictive thermo-mechanical models for estimating the cutting forces as functions of near dry lubrication parameters and cutting conditions.

In a recent study, it was shown that most documented studies on near dry machining were empirical and qualitative [47]. Although an evaporative heat transfer model was proposed for near dry machining by Varadarajan *et. al.* [7], no experimental evidence was presented. In this chapter, an analytical approach is taken to quantitatively model the cutting forces in near dry machining by including the cooling and lubricating effects in the Oxley's force model. The analysis is further expanded to use the obtained flow stress, contact length, and shear angle to predict the cutting forces due to tool flank wear based on Waldorf's model, considering that shear angle and chip thickness do not vary significantly with tool wear [48]. The cutting forces can be calculated as the summation of the forces attributed to the sharp tool and the forces attributed to the tool flank wear [49, 50].

The objective of this chapter is to estimate the cutting forces for near dry machining under either sharp or worn tool conditions. In this study, the in-tool configuration of near dry lubrication is used as shown in Figure 3-1 in Chapter 3. The lubricant is applied to the tool flank face with compressed air through an opening below the tool insert. Based on the physics of the near dry machining, modifications are made for Oxley's model [39] for sharp tools and for Waldorf's model [49] for worn tools. First, the friction angle describing the ratio of tangential to normal forces at the tool-chip

interface is calculated based on the boundary lubrication model presented by Kato *et. al.* [51]. The resulting friction angle is then used in Oxley's model for considering the lubricating effect in near dry machining. Subsequently, the cooling effect of the air-oil mixture in near dry machining is calculated by the moving heat source method as discussed in Chapter 3. The predicted shear angle and flow stresses are then used in Waldorf's model for force prediction under the effect of tool flank wear. For validation, the predicted cutting forces are compared with experimental data in the cutting of AISI 1045 with uncoated carbide inserts.

4.2 Proposed Force Modeling for Sharp Tools

4.2.1 Friction coefficient in near dry machining based on the boundary lubrication theory

A prominent effect of the applied air-oil mixture in near dry machining is lubrication, which changes the friction coefficient at the tool-chip interface. In near dry machining, hydrodynamic lubrication model cannot be used to accurately predict cutting forces in view of the limited amount of lubricant. A cutting fluid film cannot be fully established under this condition. Instead, the boundary lubrication theory is a more proper description of the near dry machining condition. In boundary lubrication, part of the load is carried by the asperity contacts and the other part is carried by the cutting fluid. The

friction force and the normal load in boundary lubrication can be expressed following as [52]:

$$F = s_m A_m + s_b A_b \tag{4-1}$$

$$N = p_m A_m + p_b A_b \tag{4-2}$$

Then the friction coefficient is calculated from equations (4-1) and (4-2) as

$$\mu = \frac{s_m A_m + s_b A_b}{p_m A_m + p_b A_b} = \frac{C_1 A_m + C_2 C_3 A_b}{A_m + C_2 A_b} \tag{4-3}$$

where

$$C_1 = \frac{s_m}{p_m}, C_2 = \frac{p_b}{p_m}, C_3 = \frac{s_b}{p_b} \tag{4-4}$$

The metallic contact area A_m and the adsorbed lubricant film contact area A_b are calculated as follows according to the model presented by Kato *et. al.* [51]:

$$A_m = \frac{\pi R n_0 D^2 a_s^3}{6H_{\max}^2} \tag{4-5}$$

$$A_b = \frac{\pi R n_0 D^2 \left\{ \left(a_s + t_b \right)^3 - a_s^3 \right\}}{6H_{\max}^2} \tag{4-6}$$

Substituting equations (4-5) and (4-6) in to Equation (4-1), a cubic equation to estimate the approach of two surfaces a_s is obtained.

$$a_s^3 + 3C_2 t_b a_s^2 + 3C_2 t_b^2 a_s + \left(C_2 t_b^3 - \frac{N}{p_m Q} \right) = 0 \tag{4-7}$$

where

$$Q = \frac{\pi R n_0 D^2}{6H_{\max}^2} \tag{4-8}$$

From equations (4-3), (4-5), and (4-6), the friction coefficient can be calculated as:

$$\mu = \frac{C_1 a_s^3 + C_2 C_3 \left\{ \left(a_s + t_b \right)^3 - a_s^3 \right\}}{a_s^3 + C_2 \left\{ \left(a_s + t_b \right)^3 - a_s^3 \right\}} \tag{4-9}$$

4.2.2 Modification of Oxley's machining theory to near dry machining

In order to extend the cutting force model to the condition of near dry machining, modifications are attempted by considering both the lubricating effect and the cooling effect.

A modification of Oxley's machining theory in the following discussion is used to account for the lubricating effect on the friction angle. The initial guess of the normal load N in Equation (4-7) is obtained by Oxley's model for completely dry condition. It is also noticed that when the adsorbed lubricant film thickness t_b equals to zero, there is an absence of lubrication in the machining process, i.e., the completely dry condition. In addition, when t_b equals zero, Equation (4-9) becomes

$$\mu = C_1 \tag{4-10}$$

Therefore, the coefficient C_1 in Equation (4-9) can be estimated by the friction angle from Oxley's model for completely dry machining condition. The coefficients C_2 and C_3 are determined from experimental data and material properties. They will be discussed later in the chapter.

The second modification is to model the cutting temperature with a moving heat source method, instead of using the empirical equations in Oxley's work [39]. The method to estimate the cutting temperature under near dry lubrication was discussed in Chapter 3.

4.2.3 Equivalent cutting edge model for oblique cutting conditions

In order to take advantage of the predictive orthogonal cutting model, the concept of the equivalent cutting edge is adopted [53] when considering the oblique cutting cases. This three dimensional oblique cutting force modeling was established by several researchers, including Oxley [39] and Arsecularatne *et. al.* [53, 54]. The method to determine the cutting forces in the oblique cutting with the proposed equivalent cutting edge is briefly described as follows. The equivalent cutting edge is determined by the chip flow direction. The development of the predicted chip flow direction on a tool with a nose radius, an end cutting edge, and an inclination angle is based on the experimental observations [39]. The chip flow direction due to the effect of the nose radius is determined on an imaginary tool with zero rake angle and zero inclination angle. The equivalent cutting edge is taken as the line perpendicular to the chip flow direction. The imaginary line is then projected to the tool rake face. The projected line is defined as the

equivalent cutting edge, as shown in Figure 4-1.

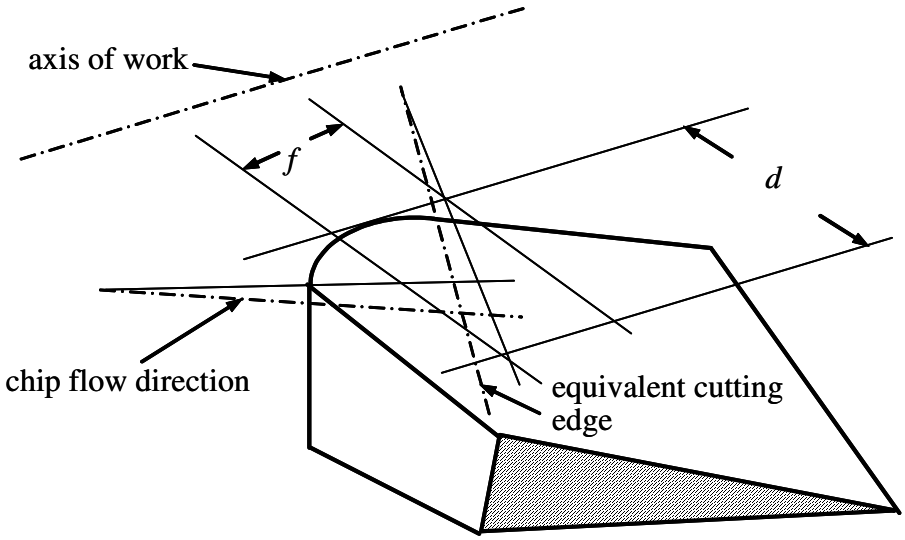

Figure 4-1: Equivalent cutting edge and tool angles [53]

With the equivalent cutting edge and the equivalent side cutting angle C_c^*, the equivalent undeformed chip thickness t^* and the equivalent width of cut w^* are given by the following equations.

$$t^* = f \cos C_s^* \tag{4-11}$$

$$w^* = \frac{d}{\cos C_s^*} \tag{4-12}$$

Once the chip flow direction is defined, the chip flow angle η_c^* which is the angle between the normal to the equivalent cutting edge and the chip flow direction on

the tool rake face is determined based on Stabler's flow rule [55] as:

$$\eta_c^* = i^* \tag{4-13}$$

Then the cutting force and the thrust force, F_c and F_t, in the equivalent orthogonal machining can be calculated with the equivalent undeformed chip thickness, width of cut, and corresponding tool angles. The cutting forces are transformed from the orthogonal cutting to 3D oblique cutting by the following equations [53]:

$$P_1 = F_c \tag{4-14}$$

$$P_2 = F_t \cos C_s^* + F_r \sin C_s^* \tag{4-15}$$

$$P_3 = F_t \sin C_s^* - F_r \cos C_s^* \tag{4-16}$$

where P_1, P_2 and P_3 are the forces acting in the cutting velocity, the axial and the radial directions and

$$F_r = \frac{F_c\left(\sin i^* - \cos i^* \sin \alpha_n^* \tan \eta_c^*\right) - F_t \cos \alpha_n^* \tan \eta_c^*}{\sin i^* \sin \alpha_n^* \tan \eta_c^* + \cos i^*} \tag{4-17}$$

The detailed equations relating to the cutting forces in oblique case are discussed in the work of Arsecularatne *et. al.* [53].

4.3 Proposed Force Modeling for Worn Tool Effect

The cutting forces with the use of worn tools can be calculated by summing up the cutting forces attributed to the effect of the sharp tool and those attributed to the effect

of the tool flank wear land [49]. This section will discuss the methodology for finding the forces due to tool flank wear. The forces in the thrust force direction F_{tw} and in the cutting force direction F_{cw} can be calculated by integrating the normal flank stress and the shear flank stress respectively [49, 50]. The forces due to tool flank wear are depicted in Figure 4-2. Therefore, the cutting forces due to tool flank wear are given by

$$F_{tw} = w\int_0^{L_{VB}} \sigma_w(x)dx \tag{4-18}$$

$$F_{cw} = w\int_0^{L_{VB}} \tau_w(x)dx \tag{4-19}$$

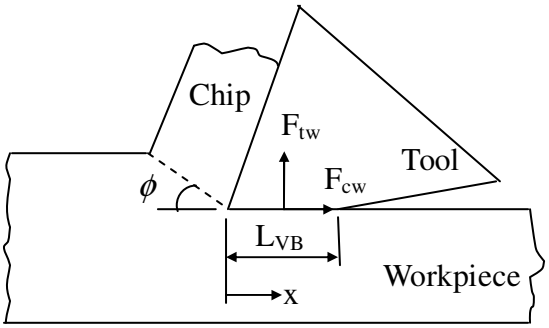

Figure 4-2: Cutting forces due to tool flank wear in orthogonal cutting model [50]

In order to estimate the cutting forces due to tool flank wear, the normal stress and the shear stress have to be found first. Waldorf [49] proposed polynomial-shaped distributions for both the normal and shear stresses. Those stress distributions are also

affected by a critical flank wear land length L_{VB}^{*}, at which plastic flow is initiated at the front of the wear land. If the tool flank wear land length is less than the critical value ($L_{VB} \le L_{VB}^{*}$), purely elastic contact between tool wear land and the workpiece is presented. If $L_{VB} > L_{VB}^{*}$, both elastic contact and plastic contact exist. Based on the experimental observations, the critical wear land length L_{VB}^{*} for steel workpieces is $0.38\,mm$, as suggested by Smithey *et. al.* [50]. Due to different wear land lengths, the expressions for the normal and shear stresses can be calculated with appropriate equations as listed below:

$$\text{If} \quad L_{VB} \le L_{VB}^{*}$$

$$\begin{aligned} \sigma_w(x) &= \sigma_0 \left(\frac{L_{VB} - x}{L_{VB}} \right)^2 \quad \text{for} \quad 0 < x < L_{VB} \\ \tau_w(x) &= \tau_0 \quad \text{for} \quad 0 < x < L_{VB}\left(1 - \sqrt{\frac{\tau_0}{\sigma_0}}\right) \\ \tau_w(x) &= \mu \sigma_w(x) \quad \text{for} \quad L_{VB}\left(1 - \sqrt{\frac{\tau_0}{\sigma_0}}\right) < x < L_{VB} \end{aligned} \tag{4-20}$$

$$\text{If} \quad L_{VB} > L_{VB}^{*}$$

$$\begin{aligned} \sigma_w(x) &= \sigma_0 \quad \text{for} \quad 0 < x < L_{VB} - L_{VB}^{*} \\ \sigma_w(x) &= \sigma_0 \left(\frac{L_{VB} - x}{L_{VB}} \right)^2 \quad \text{for} \quad L_{VB} - L_{VB}^{*} < x < L_{VB} \end{aligned} \tag{4-21}$$

$$\tau_w(x) = \tau_0 \quad \text{for} \quad 0 < x < L_{VB} - L_{VB}^{*}\sqrt{\frac{\tau_0}{\sigma_0}}$$

$$\tau_w(x) = \mu\sigma_w(x) \quad \text{for} \quad L_{VB} - L_{VB}^{*}\sqrt{\frac{\tau_0}{\sigma_0}} < x < L_{VB}$$

where the flow stresses σ_0 and τ_0 are obtained from the modified Oxley's force modeling for sharp tools. The required information, such as shear angle, for the Wardolf's model [49] can be also obtained from the modified Oxley's machining theory [39].

The total cutting force and the total thrust force for a worn tool in the orthogonal case are the summation of the sharp tool cutting forces and the worn tool cutting forces. With the equivalent cutting edge model for oblique cutting [Arsecularatne *et. al.*, 2000], the total cutting forces in the tangential, axial, and radial directions can be estimated by equations (4-14), (4-15), and (4-16).

4.4 Model Validation

4.4.1 Cutting conditions and estimated parameters

The validation of cutting forces in near dry turning is measured by a tool-post dynamometer (Kistler model 9257B) when cutting AISI 1045 with uncoated carbide tool inserts (Valenite DPMT-2A) on a horizontal lathe (CMS-GT27). The cutting tests are performed under different cutting conditions, as shown in Table 3-1 in Chapter 3. The

carbide tool insert had 0^0 rake angle, 11^0 clearance angle, 6^0 inclination angle, and thermal conductivity of $84.02\,W/mK$ [45]. The workpiece (AISI 1045) has thermal conductivity of 50.8 W/mK and thermal diffusivity of $0.134\times10^{-4}\ m^2/s$ [46]. The flank wear land length is recorded with a Nikon microscope MICROPHOT-FXL before the cutting forces are measured. The cutting fluid is delivered to the tool flank face through a 0.762-mm in-tool hole by a cutting fluid applicator (UNIST uni-MAX Coolubricator). The UNIST system is used to supply the air-fluid mixture of 12.5 ml/hr at a pressure of 275.8 kPa. Coolube 2210, a vegetable oil, is chosen as the cutting fluid. The arrangement of the in-tool hole and the thermocouple is shown in Figure 3-1 in Chapter 3.

Before the friction coefficients in near dry machining processes are obtained according to Equation (4-9), several parameters have to be determined. First, the shear strength at the adsorbed lubricant film contact area was estimated by the kinematic viscosity, density, and shear strain rate [56].

$$\nu = \frac{s_b}{\rho\dot{\gamma}} \tag{4-22}$$

Assuming that the lubricant shear strain rate is close to the chip shear strain rate which is calculated by Oxley's model, the shear strength at the adsorbed lubricant film contact area can be determined according to Equation (4-22). The representative value of the coefficient C_2 is determined by Kato *et. al.* [51] as 0.5 in the boundary lubrication.

The coefficient C_2 was used to estimate the mean contact pressure p_b as well as the coefficient C_3.

The total asperity number n_0 on the tool-chip contact area is estimated by the assumed linear distribution density of asperities per unit length [51]:

$$n_0 = A_0 z^2 \tag{4-23}$$

The linear distribution density z was estimated by measuring a new tool insert with the white light interferometer (Zygo NewView 200). It was found to be 100 ($1/mm$). The distribution height of asperities $H_{\max}$ was also measured to be 5 μm. The estimated parameters for predicting the friction coefficient in near dry turning are summarized in Table 4-1.

Table 4-1: Parameters in boundary lubrication calculation

Parameter	t_b (μm)	C_2	$H_{\max}$ (μm)	R (μm)	D	z ($1/mm$)	ν (mm^2/s)	ρ (g/cm^3)
Representative value	0.15	0.5	5	20	1.5	100	10	0.89

4.5 Results and Discussion

The force comparisons for sharp tools for the axial forces, radial forces, and

tangential cutting forces are shown in Figures 4-3, 4-4, and 4-5 respectively. Each figure shows the predicted cutting forces in near dry machining and the measured cutting forces for near dry machining, as well as the predicted and measured cutting forces for dry machining. It is observed that the forces in dry cases are larger than the forces in near dry cases for both predicted values comparison and experimental data comparison except for the experimental data in the 9^{th} case. However, in case 9, the maximum deviation between the measured forces for the dry and near dry condition is less than 5%. It is found that if the predicted cutting forces for dry machining are close to the experimental data, the estimated forces for near dry machining have better agreement with the measured data, such as the 2^{nd}, 7^{th} and 9^{th} cases for the axial direction forces, the 5^{th} and 8^{th} cases for the radial direction forces, and the 2^{nd}, 5^{th}, 6^{th}, 7^{th}, 8^{th} and 9^{th} cases for the cutting velocity direction forces. Generally, the model provides an average prediction error of 14% in the tangential cutting force direction, 21% in the axial directions and 30% in the radial directions within the experimental test condition range.

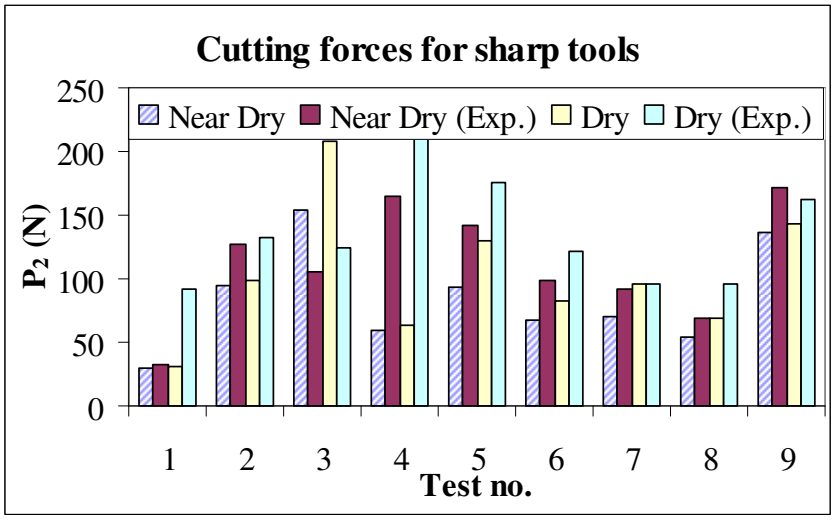

Figure 4-3: Force comparisons for the axial direction for sharp tools

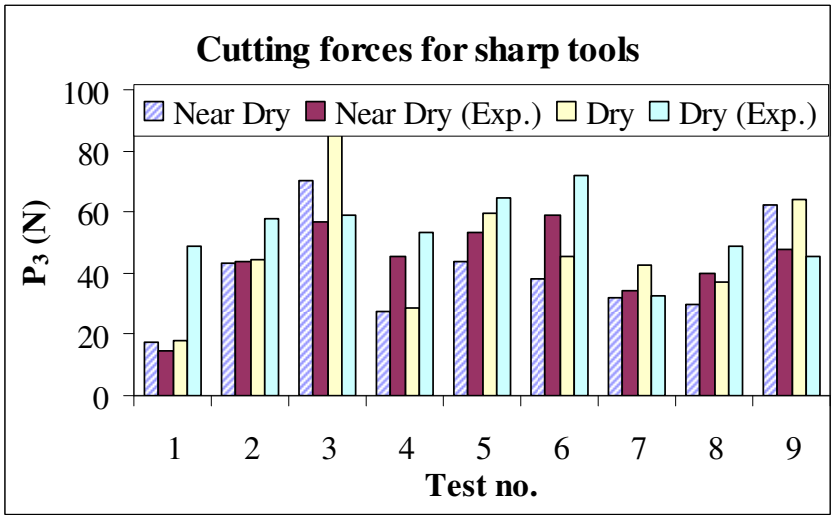

Figure 4-4: Force comparisons for the radial direction for sharp tools

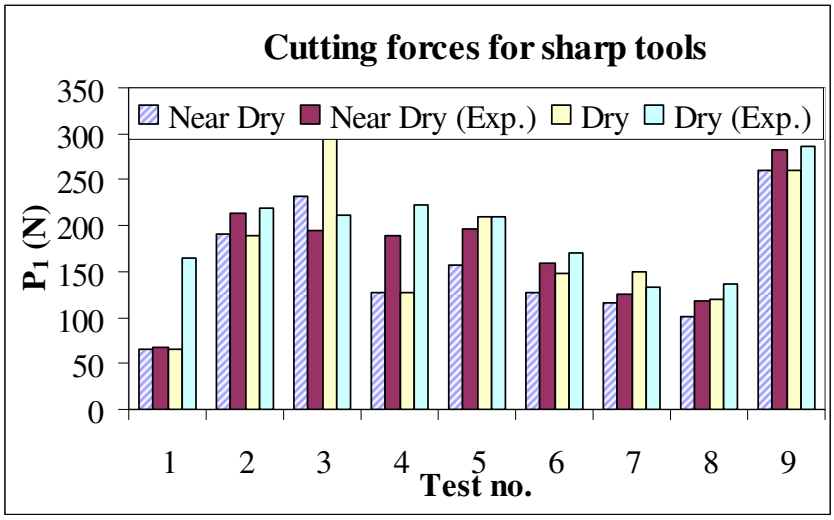

Figure 4-5: Force comparisons for the cutting velocity direction for sharp tools

The built-up edge (BUE) is observed when cutting AISI 1045 at low cutting speed; i.e., case 1, case 2 and case 3. One example of the BUE is shown in Figure 4-6. The existence of BUE is a deviation from the assumptions of Oxley's machining theory [39] due to the difference in the equivalent cutting edge. Therefore, a significant difference between the predicted forces and the measured forces is found, as depicted in Figures 4-3, 4-4 and 4-5. For the forces measured at the cutting speed of 91.5 m/min and 137.25 m/min, the predicted force reductions for near dry machining from dry machining are 5% - 39% for axial cutting forces, 3% - 36% for radial cutting forces, and 1% - 32% for tangential cutting forces while the measured force reductions are 4% - 37% for axial cutting forces, 5% - 22% for radial cutting forces, and 1% - 17% for tangential cutting

forces. The differences between the predicted forces for near dry machining and dry machining seem to be overestimated when compared to the experimental data.

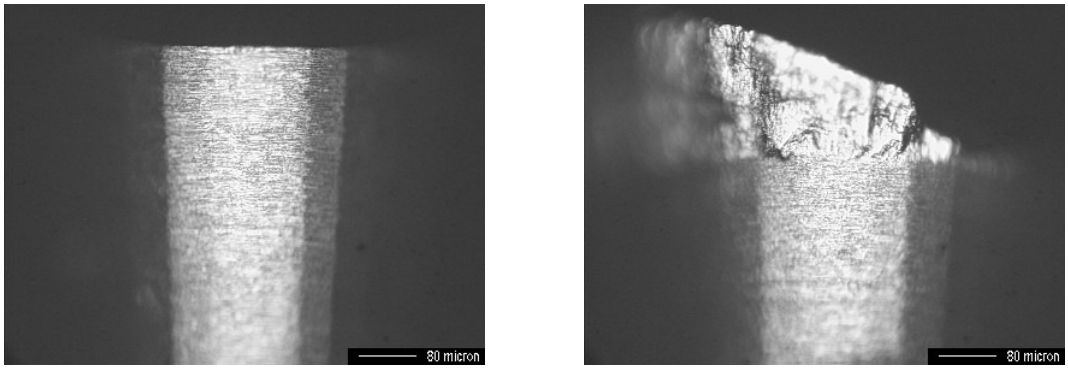

(a) (b)

Figure 4-6: Tool profile comparison: (a) new tool (b) BUE observed at the beginning of test (Cutting velocity = 45.75 m/min, feed = 0.0762 mm/rev, depth of cut = 1.016 mm)

For near dry machining, the combination of the lubricating and cooling effects on machining AISI 1045 with uncoated carbide results in lower cutting forces in all directions. Since the cutting temperatures are higher in dry machining than those in near dry machining, the cutting forces should be less under dry machining due to the material softening effect when only the cooling effect is considered. Thus, it is inferred that the lubricating mechanism has a stronger effect on cutting forces than the cooling mechanism when cutting AISI 1045 with uncoated carbide tools.

In addition to the lubricating and cooling effects, the temperature dependent material properties may play an important part in the cutting forces. The high cutting temperatures are usually observed in the cutting zone. As shown in the Figure 3-13, the predicted tool-chip interface temperatures can be as high as about 700 ºC for sharp tools and 950 ºC for worn tools. The high temperature would affect the material properties such as yield stress, conductivity, elastic modulus and so on. The thermal softening of the material causes lower cutting forces in dry cutting than those in near dry cutting. This explains the overestimation of cutting forces in some cases in force predictions. Another temperature dependent property of materials is phase transformation. The high cutting temperature as predicted in the study may cause phase transformation of carbon steels. When the material phase transformation happens, these material properties should be reconsidered. They should be treated as different materials than the bulk materials. The change of the cutting forces due to the material phase transformation can be calculated according to the developed force model with the suitable material properties of the phase transformed materials.

The force comparisons for worn tools between analytical values and experimental data are similar in the selected cutting condition in Table 3-1 in Chapter 3. Thus, case 5 and case 8 are selected as the representative data for force comparison because the

deviations of the cutting forces in dry machining between analytical values and experimental data are close for the cutting speed of 91.5 m/min and 137.25 m/min, respectively. The predicted forces and experimental data for near dry machining are depicted as solid lines and circles in Figures 4-7 and 4-8 for case 5 and case 8 respectively. The data for dry machining are also presented in the same figures for comparing the differences between the cutting forces for dry and near dry conditions.

It is observed that slopes of circles and solid lines are close in Figures 4-7 and 4-8. Therefore, it is deduced that if the predicted cutting forces for sharp tools match well with the experimental data, the predicted cutting forces with the progress of the tool flank wear have good agreements with the measured cutting forces, such as radial forces in case 5 and axial forces and tangential cutting forces in case 8. There are discrepancies for forces in axial and tangential cutting directions between the predicted forces and the measured values at the beginning (small tool wear land length) or the end (large tool wear land length) of the test. The discrepancies may come from two sources. First, at the beginning or the end of the test, the tool wear is unstable and not uniform as assumed for worn tool force calculation. Chipping or obvious non-uniform tool wear are usually observed at the end of each test. Figure 4-9 shows one example of non-uniform tool flank wear when the tool wear length is large. Secondly, the measurement error for the tool

flank wear length is approximately $\pm 5\mu m$, which is comparable to small tool flank wear and consequently results in a considerable error in predicted cutting forces. In addition, the discrepancies for radial forces in case 8 were observed, not limited to either the beginning or the end of the test. The possible error source for the radial forces is that the effective inclination angle may change during the progress of the tool flank wear since the inclination angle is the important parameter for the cutting forces in the radial direction.

In general, the proposed model shows the best estimation for the forces for worn tools in the tangential cutting direction followed by the estimation for the axial forces and for the radial forces. In this study, although the predicted cutting forces have comparable errors with respect to the experimental data, the differences between the forces for dry and near dry cases are similar for both the predicted cutting forces and measured data. The similar dissemblance of about 10% - 20% between cutting forces for dry and near dry machining was also observed by Rahman *et. al.* [12] when cutting ASSAB 718H steel with a Sumitomo Electric Carbide 20 mm diameter single-tooth end mill.

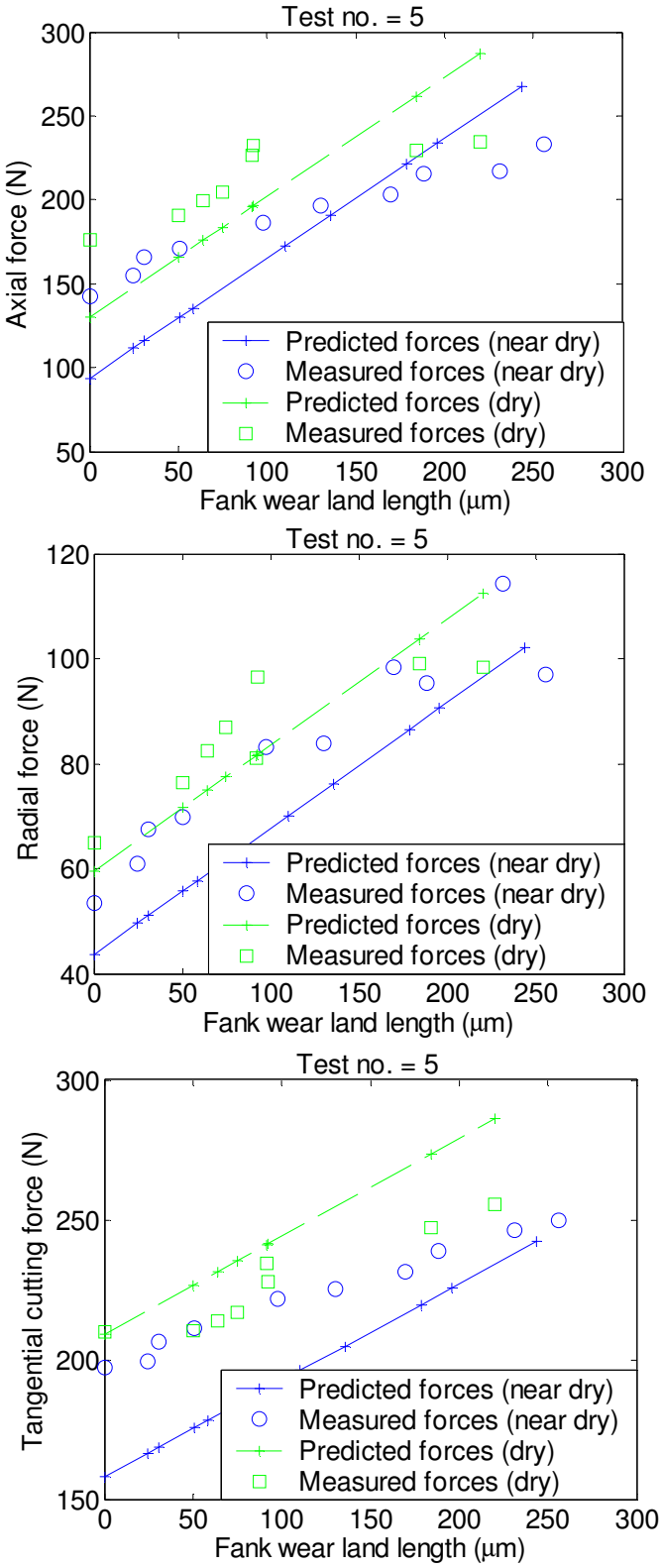

Figure 4-7: Cutting force comparisons for case 5

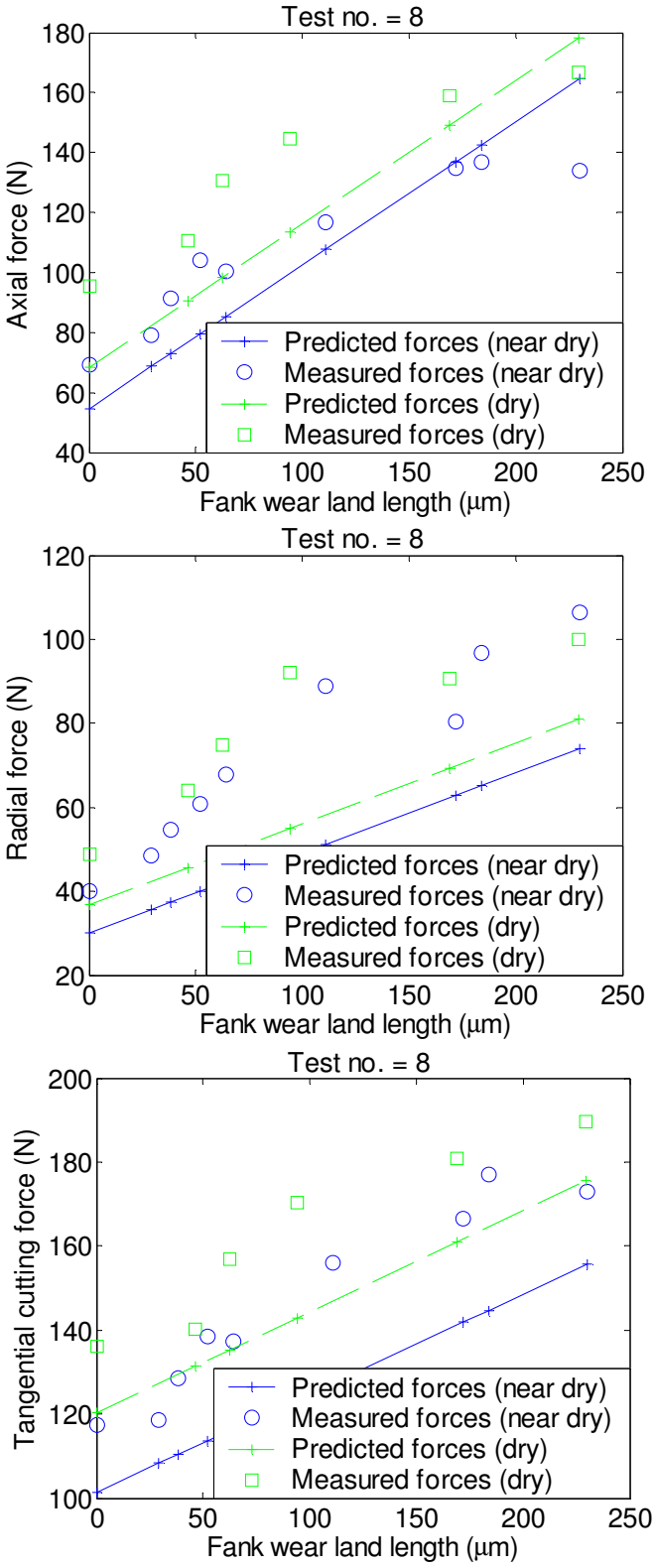

Figure 4-8: Cutting force comparisons for case 8

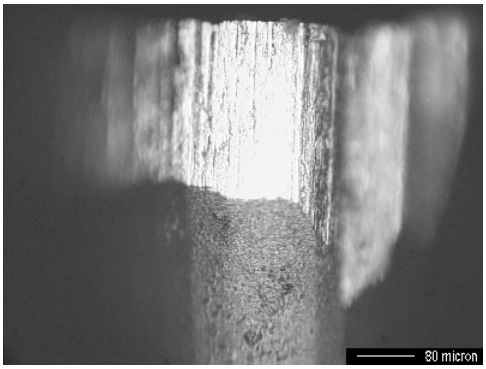

Figure 4-9: Non-uniform tool flank wear when the average tool flank wear length is about $250\,\mu m$ (Cutting velocity = 137.25 m/min, feed = 0.0762 mm/rev, depth of cut = 0.508 mm)

4.6 Conclusions

In this chapter, a force modeling is presented for estimating the cutting forces in near dry machining based on the Oxley's machining theory and the Waldorf's worn tool model. Lubricating effect and cooling effect for near dry machining are considered in the proposed model. The predicted cutting forces are compared to the experimental data in cutting medium carbon steels with uncoated carbide tools. For sharp tool cutting force predictions, it is found that the proposed model had a better prediction on cutting forces when the predicted forces for dry machining were close to the experimental data. The predicted cutting forces in completely dry machining are the initial guesses of the normal loads for calculation in the proposed lubrication model for near dry machining. Moreover, the predicted forces in the tangential cutting direction have better agreement than the

forces in the other two directions. The predicted parameters of modified Oxley's model can be used in worn tool cutting forces estimation or tool life prediction in the future.

For worn tool cutting force predictions, the total cutting forces are obtained by summing up the predicted forces without any tool wear and the forces due to the flank wear. It is observed that the predicted forces match better in the tangential cutting direction and the axial direction than in the radial direction with the progress of tool flank wear. It is also found that the cutting forces under near dry machining can reduce 10% - 20% cutting forces compared with the forces under dry machining conditions when cutting the AISI 1045 with uncoated carbides, suggesting that lubricating has a stronger effect on cutting forces than cooling under these conditions.

CHAPTER 5

MODELING OF TOOL FLANK WEAR IN NEAR DRY MACHINING

5.1 Introduction

Near dry machining refers to the use of cutting fluids of only a small amount, typically three to four orders of magnitude lower than the amount of cutting fluids commonly used in flood cooling condition. Many studies confirmed a lower cutting temperature and a longer tool life by near dry machining over dry machining [1-7]. However, the research only focused on qualitative observations. Predictive capability of tool life in near dry machining offers possible benefits for choosing proper cutting conditions without excessive experimental studies. The main focus of this chapter is to establish the near-dry tool life prediction capability based on analytical modeling and experimental validation.

Many models have been proposed to estimate the volumetric loss and/or wear rate in machining processes, such as abrasive wear [57, 58], adhesive wear [59], and diffusive

wear [59, 60]. Generally, the tool wear is modeled as one of the above wear mechanisms or any combination of them depending on the tool-workpiece combination [58, 59, 61, 62]. Unfortunately, the research only focused on the completely dry condition.

This chapter first discusses the volumetric loss wear models based on the primary wear mechanisms of abrasion, adhesion, and diffusion. Second, the flank face wear rate model is developed by relating the volumetric loss due to different wear mechanisms to the tool insert geometry. At the same time, the force models and temperature models for near dry turning are also introduced based on the in-tool hole configuration of near dry lubrication as shown in Figure 3-1. The lubricant is applied to the tool flank face with compressed air from the opening below the tool insert to achieve near-dry lubrication. Finally, the presented model is calibrated in turning AISI 1045 steel under dry machining and verified in turning the same material with the oil flow rate of 12.5 ml/hr at different cutting conditions under both dry and near dry conditions.

5.2 Modeling of Wear Mechanisms

5.2.1 Abrasive wear model

Abrasive wear exists when two surfaces slide against each other with hard particles. Most engineering metals contain impurities that are imparted to improve

material strength. If the hard particles are securely constrained in the metal matrix composite, these particles will cause two-body abrasive wear, representing hard particles in the metal sliding over a soft surface [61]. On the other hand, if the particles are released to the interface of the tool and the workpiece or the chip in cutting, the hard particles roll between the contacting surfaces, causing three-body abrasive wear [62].

Rabinowicz [63] developed empirical equations for calculating the volumetric loss of the three-body abrasive wear based on a lapping process. The equations for volumetric loss per particle are shown as below:

$$V_{ab-3b} = \frac{xN\tan\theta}{3H_t}, \quad \frac{H_t}{H_a} < 0.8;$$

$$V_{ab-3b} = \frac{xN\tan\theta}{5.3H_t}\left(\frac{H_t}{H_a}\right)^{-2.5}, \quad 0.8 < \frac{H_t}{H_a} < 1.25; \tag{5-1}$$

$$V_{ab-3b} = \frac{xN\tan\theta}{2.43H_t}\left(\frac{H_t}{H_a}\right)^{-6}, \quad 1.25 < \frac{H_t}{H_a}$$

The above equations were rearranged and used in turning process according to the work of Huang *et. al.* [62] with the assumption of uniform stress distribution between the tool flank face and the workpiece:

$$V_{abrasion} = K_{abrasion} K\left(\frac{H_a^{n-1}}{H_t^n}\right) V_c w L_{VB} \sigma \Delta t \tag{5-2}$$

where n = 1.0, K = 0.333, for $\frac{H_t}{H_a} < 0.8$;

n = 3.5, K = 0.189, for $0.8 < \frac{H_t}{H_a} < 1.25$;

n = 7.0, K = 0.416, for $1.25 < \frac{H_t}{H_a}$

The coefficient $K_{abrasion}$ is associated with the hard particle properties. It is taken as a constant for a given tool and workpiece combination [62]. The hardness data of the hard particles (Fe_3C for plain carbon steel) and the uncoated tungsten carbide are listed below [58]:

$$H_{Fe_3C} = 11760e^{-16.3\times10^{-4}T}$$
$$H_{WC} = 23054e^{-3.62\times10^{-4}T} \quad (5\text{-}3)$$

For two-body abrasive wear, the equation for volumetric loss per particle is [64]

$$V_{ab-2b} = \frac{xN\overline{\tan\theta}}{\pi H_t} \quad (5\text{-}4)$$

Similarly, the volumetric loss of the tool flank face for two-body abrasion can be calculated as:

$$V_{abration} = K_{abrasion}\frac{1}{H_t}V_c w L_{VB}\sigma\Delta t \quad (5\text{-}5)$$

General forms of the abrasive wear can be written as:

$$V_{abration} = K_{abrasion}K\left(\frac{H_a^{n-1}}{H_t^n}\right)V_c w L_{VB}\sigma\Delta t \quad \text{for three-body abrasion;} \quad (5\text{-}6)$$

$$V_{abration} = K_{abrasion} \frac{1}{H_t} V_c w L_{VB} \sigma \Delta t \quad \text{for two-body abrasion}$$

5.2.2 Adhesive wear model

The contact area between the tool flank and the workpiece is only a small portion of the apparent area. The contact is among the asperities of the tool flank and the workpiece surfaces. The asperities weld together due to the high temperature and high stress on the tool-workpiece interface during machining. As the tool and the workpiece slide against each other, the asperity junctions are torn off. This results in the removal of the tool material. The volumetric loss of the tool flank face due to the adhesive wear is calculated as [62]:

$$V_{adhesion} = K_{adhesion} e^{aT} V_c w \sigma \Delta t \tag{5-7}$$

The coefficient $K_{adhesion}$ is associated with the probability of the formation of a sizable wear particle of the tool material, the hardness of the tool, the hardness of the workpiece, and the asperity characteristic height. It is a constant for a given tool and workpiece combination.

5.2.3 Diffusive wear model

The tool material diffusion across the tool-workpiece interface is dominant at high

temperature [61, 62]. The diffusive wear accelerates the tool flank wear when the temperature is higher than a critical temperature. In machining processes, the temperature along the tool-workpiece interface is considered uniform and the concentration of the diffusing species is assumed to be constant. Based on the Fick's laws of diffusive wear, the volumetric loss of the tool flank face due to the diffusive wear is calculated as [59]:

$$V_{diffusion} = K_{diffusion} \sqrt{V_c L_{VB}} e^{-(\frac{K_Q}{T+273})} \tag{5-8}$$

The coefficient $K_{diffusion}$ is associated with the diffusion species, the concentration of diffusion, the atomic weight of the diffusion species, and the density of the tool material. It is taken as a constant for the same tool and workpiece combination. The coefficient K_Q is associated with the activation energy in diffusion [59].

5.3 Composite Wear Rate

The volumetric loss of the tool flank is the summation of the abrasive wear, the adhesive wear, and the diffusive wear. The tool flank wear rate model is presented by relating the aforementioned wear mechanisms and the tool geometry. The geometric volumetric loss of the tool flank face for orthogonal cutting is shown in Figure 5-1 Suppose that after a period of time Δt, for a worn tool with the width of cut w, the reduction in the depth of cut is Δh. The tool flank face volume removed is:

$$\begin{aligned}\Delta V_{wear} &= \frac{1}{2} w\Delta L_1 \Delta h + w(L_{VB} - \Delta L_1)\Delta h + \frac{1}{2} w\Delta L_2 \Delta h \\ &= \frac{1}{2} w\Delta h^2 \tan\alpha + w(L_{VB} - \Delta h \tan\alpha)\Delta h + \frac{1}{2} w\Delta h^2 \cot\gamma\end{aligned} \tag{5-9}$$

By eliminating the high order term Δh^2, the above equation becomes:

$$\Delta V_{wear} = wL_{VB}\Delta h = \frac{wL_{VB}}{\cot\gamma - \tan\alpha}\Delta L_{VB} \tag{5-10}$$

where $\Delta L_{VB} = \Delta L_2 - \Delta L_1$

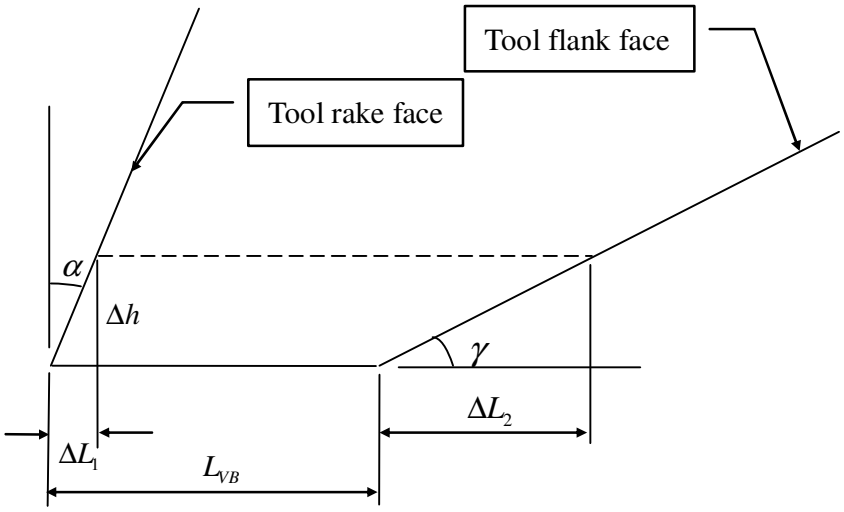

Figure 5-1: Geometric schematic of the tool flank face volumetric loss in orthogonal cutting

At the same time, the total volumetric loss of the tool flank face is assumed to be attributed to abrasion, adhesion, and diffusion. The relationship between the geometric model and the tool wear mechanisms is:

$$\Delta V_{wear} = V_{abrasion} + V_{adhesion} + V_{diffusion} \tag{5-11}$$

Substituting appropriate terms in Equation (5-11), results in the following:

$$\begin{aligned}\frac{wL_{VB}}{\cot\gamma - \tan\alpha}\Delta L_{VB} &= K_{abrasion}K\left(\frac{H_a^{n-1}}{H_t^n}\right)V_c w L_{VB}\sigma\Delta t + K_{adhesion}e^{aT}V_c w\sigma\Delta t \\ &\quad + K_{diffusion}\sqrt{V_c L_{VB}}\,e^{\frac{-K_Q}{T+273}}w\Delta t \quad \text{for three-body abrasive wear;} \\ \frac{wL_{VB}}{\cot\gamma - \tan\alpha}\Delta L_{VB} &= K_{abrasion}\left(\frac{1}{H_t}\right)V_c w L_{VB}\sigma\Delta t + K_{adhesion}e^{aT}V_c w\sigma\Delta t \\ &\quad + K_{diffusion}\sqrt{V_c L_{VB}}\,e^{\frac{-K_Q}{T+273}}w\Delta t \quad \text{for two-body abrasive wear}\end{aligned} \tag{5-12}$$

When the time interval approaches to zero, the flank wear rate is given as:

$$\begin{aligned}\frac{dL_{VB}}{dt} &= \frac{\cot\gamma - \tan\alpha}{L_{VB}}\left\{K_{abrasion}K\left(\frac{H_a^{n-1}}{H_t^n}\right)V_c L_{VB}\sigma + K_{adhesion}e^{aT}V_c\sigma\right. \\ &\quad \left. + K_{diffusion}\sqrt{V_c L_{VB}}\,e^{\frac{-K_Q}{T+273}}\right\} \quad \text{for three-body abrasive wear;} \\ \frac{dL_{VB}}{dt} &= \frac{\cot\gamma - \tan\alpha}{L_{VB}}\left\{K_{abrasion}K\left(\frac{1}{H_t}\right)V_c L_{VB}\sigma + K_{adhesion}e^{aT}V_c\sigma\right. \\ &\quad \left. + K_{diffusion}\sqrt{V_c L_{VB}}\,e^{\frac{-K_Q}{T+273}}\right\} \quad \text{for two-body abrasive wear;}\end{aligned} \tag{5-13}$$

The constants, $K_{abrasion}$, $K_{adhesion}$, a, $K_{diffusion}$ and K_Q, in the above equations can be obtained from the experimental calibration under completely dry conditions. These coefficients are then used to predict the tool wear rate under near dry lubrication by assuming that the cutting fluids do not significantly affect the tool wear coefficients. In

this study, plain carbon steel, AISI 1045, is used. The hard particles (Fe_3C) are securely constrained within pearlites, which causes two-body abrasive wear [61]. Therefore, the tool wear rate model considering the two-body abrasive wear is adopted in this research. Although the conventional turning process is chosen as the machining process for model validation, the tool flank face wear model for orthogonal cutting still works as long as the parameters such as the width of cut and the undeformed chip thickness are substituted by the equivalent width of cut and the equivalent undeformed chip thickness according to the model of an equivalent cutting edge [65].

5.4 Considering the Built-Up Edge Effect on Tool Flank Wear

For cutting steels of carbon content within the range from 0.2 % to 0.38 %, it has been shown that the built-up edge (BUE) formation is closely related to the dynamic strain aging [66]. By observing the BUE formation in the machining tests, it was proposed that:

1. if $T_{\text{mod}} > 700K$, there would be no BUE but for lower T_{mod} , there will be;

2. even if $T_{\text{mod}} < 700K$ there will be no BUE if $T_{\text{int}} > 1000K$

where T_{int} is the average tool-chip interface temperature and T_{mod} is the modified temperature in Oxley's machining theory [39].

The above criteria also show good predictions under oblique cutting conditions using cutting tools with nose radius [67]. However, in this study when cutting steels of 0.45 % carbon content, the experimental results obtained from machining tests are inconsistent with the above criteria, especially for cutting under flood cooling conditions (which will be discussed in Chapter 8). Accordingly the above criteria are modified in the context of critical T_{mod} as:

1. if $T_{\text{mod}} > 550K$, there would be no BUE but for lower T_{mod}, there will be;

2. even if $T_{\text{mod}} < 550K$ there will be no BUE if $T_{\text{int}} > 1000K$.

The BUE deposits on the tool surface and it tends to protect the tool from direct rubbing and abrasive wear with the workpiece, thereby extending the tool life. Therefore, if the cutting process parameters meet the above criteria and BUE is anticipated, the model assumes that the abrasive wear does not participate in the tool wear mechanisms.

5.5 Estimated Cutting Forces and Cutting Temperatures

It is found that in Equation (5-13), in addition to the tool geometry, the material properties, and the cutting conditions, the normal stress σ and the temperature T at the tool-workpiece interface are required for the flank face wear rate model. The normal

stress can be estimated by the method described in Chapter 4. Moreover, the tool flank-workpiece interface temperature can be estimated from the moving heat source method. The details for calculating the average temperature on the tool-workpiece interface is presented in Chapter 3.

As shown in Equation (5-13), with known wear coefficients and required parameters such as material properties, tool geometry, and cutting conditions, the tool flank wear rate can be calculated with respect to a specific tool flank wear length. According to the predicted wear rate, the new flank wear length can be calculated after a short time interval. The new flank wear length is used to update the tool geometry for calculating the stress and the temperature on the tool-workpiece interface for the next step. Figure 5-2 shows the steps for calculating the flank tool wear.

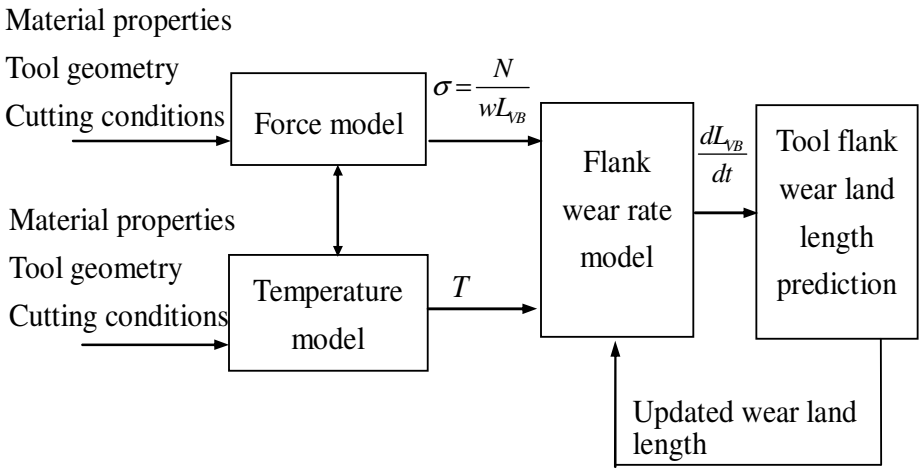

Figure 5-2: Flow chart for calculating the flank wear progression

5.6 Model Calibration

5.6.1 Turning experiments

The flank wear land length is recorded with an optical microscope when cutting AISI 1045 with uncoated carbide tool inserts (Valenite DPMT-2A) on a lathe. The machining tests are performed under different cutting conditions, as shown in Table 3-1 in Chapter 3. For model calibration (calibrating the coefficients: $K_{abrasion}$, $K_{adhesion}$, a, $K_{diffusion}$ and K_Q), the cutting forces and the cutting temperatures are also recorded. Cutting forces are measured by a tool-post dynamometer (Kistler model 9257B) while cutting temperatures are measured with an embedded thermocouple (Omega K-type) located under the tool insert. The carbide tool insert had 0^0 rake angle, 11^0 clearance

angle, 6^0 inclination angle, and the thermal conductivity of $84.02\,W/mK$ [45]. The workpiece (AISI 1045) has the thermal conductivity of 50.8 W/mK and the thermal diffusivity of $0.134\times10^{-4}\ m^2/s$ [46]. The cutting fluid is delivered to the tool flank face through a 0.762-mm in-tool hole by a cutting fluid applicator (UNIST uni-MAX Coolubricator). The UNIST system is used to supply the air-fluid mixture of 12.5 ml/hr at a pressure of 275.8 kPa. Coolube 2210, a vegetable oil, is chosen as the cutting fluid. The arrangement of the in-tool hole and the thermal couple is shown in Figure 3-1 in Chapter 3.

5.6.2 Model calibration

The coefficients in Equation (5-13) are determined based on experimental data. The experimental data of tool flank wear in the dry turning process are recorded with a microscope. The predicted tool wear rates are calculated according to the cutting forces and the cutting temperatures measured in machining processes. Then, the coefficients in tool wear rate model are determined by minimizing the least square errors between experimental tool wear rates and predicted tool wear rates according to Equation (5-13) at different times as tool wear progressed. The measured wear rates of the 6^{th} cutting condition are used in calibrating these coefficients. As indicated by Kwon [61], in

machining plain carbon steel (hot rolled AISI 1045 in this study), the complex lamella cementite is securely constrained with ferrite matrix phase in the pearlite structure, causing two-body abrasive wear. Therefore, the tool wear rate model associated with the two-body abrasive wear is used in this study. With the calibrated coefficients, Equation (5-13) becomes:

$$\frac{dL_{VB}}{dt} = \frac{\cot\gamma - \tan\alpha}{L_{VB}} \left\{ 7.394\times10^{-7} K \left(\frac{1}{H_t} \right) V_c L_{VB} \sigma + 5.147\times10^{-16} e^{7.456\times10^{-4} T} V_c \sigma + 1.29\times10^{5} \sqrt{V_c L_{VB}}\, e^{\frac{-20570}{T+273}} \right\} \tag{5-14}$$

5.7 Results and Discussion

The proposed model is used to predict the tool flank wear rates and wear progressions for near dry turning according to the cutting conditions listed in Table 3-1 with known tool geometry and material properties. The comparisons of predicted and measured tool wear progression are shown in Figure 5-3. The solid lines represent the predicted tool wear progressions while the circles represent the measured tool wear progressions. The predicted values show good agreement with the experimental data for conditions 5 thru 9. The conditions represented the medium cutting speed (91.5 m/min) and high cutting speed (137.25 m/min) in this study. The causes of modeling errors under

low cutting speed conditions (condition 1 - 3) may come from the following sources. (1) The tool wears very fast at the beginning of cutting tests. The initial wear is not correctly captured by the proposed model. Nevertheless, when the tool wear went to steady state tool wear, the predicted tool wear behaviors are close to those of measurements. (2) The inexact wear coefficients are calibrated by using only the data under condition 6. In this study, the model calibration tries to include the data of condition 5. However, the obtained tool wear coefficient results in extremely large errors under conditions 7, 8, and 9. Therefore, when the tool wear coefficients are calibrated, the data of condition 5 are dropped. The calibration of tool wear coefficients is based on cutting condition 6 which had a higher cutting speed than conditions 1 - 3. Therefore, the possible tool wear coefficient deviations could cause errors in predicted tool lives. (3) The errors of predicted tool flank wear land lengths could accumulate due to the use of the estimated process information instead of directly measured values. In this study, the cutting temperatures have to be estimated from other process information, such as material properties and cutting forces. Although the cutting temperatures are verified by comparing with the cutting temperatures measured by the thermocouple located under the tool insert, the real tool-workpiece temperatures may be different from the predicted values. The BUE are expected for cases 1 - 4 in the model. However, the BUE actually

appears for cases 1 - 3 and only at the beginning of cases 4 - 8. This discrepancy of the BUE formation prediction in case 4 leads to a large inconsistency of the tool progressions between calculation and measurements.

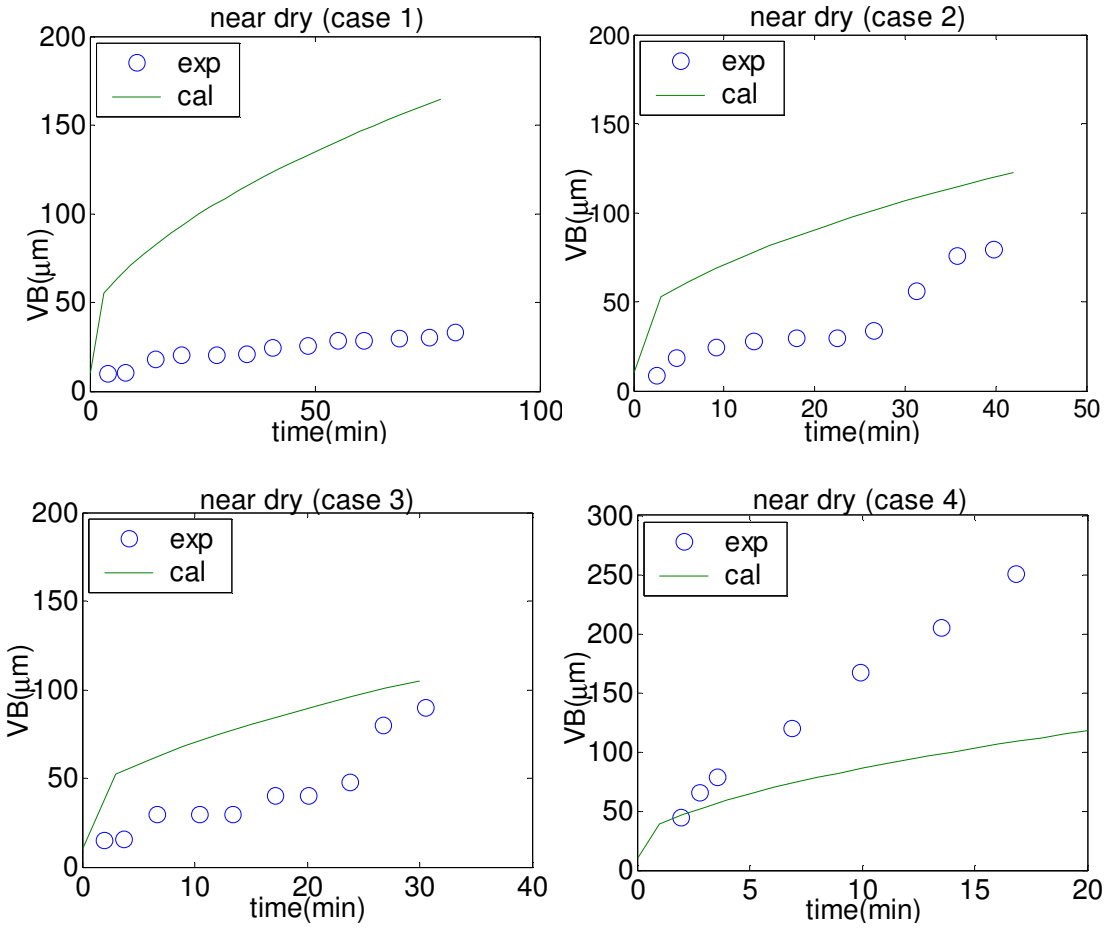

Figure 5-3: The comparisons of tool flank wear progressions for near dry machining

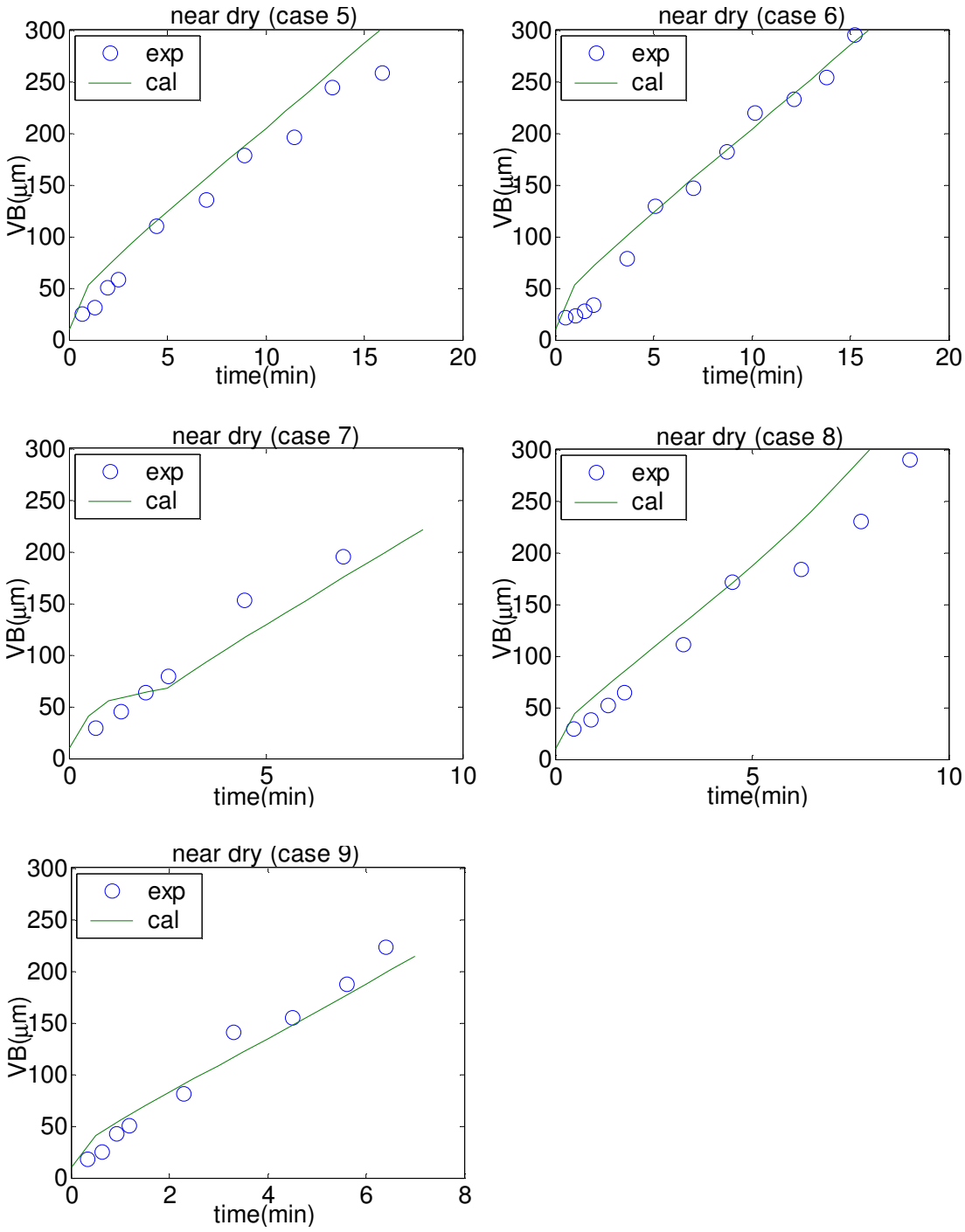

Figure 5-3 continued: The comparisons of tool flank wear progressions for near dry machining

The comparisons of predicted and measured tool wear progression under dry conditions are shown in Figure 5-4. It is seen that the predicted tool wear progressions are under-estimated for conditions 2, 4, 5, 7, 8 and 9. Similar to the predictions for near- dry cutting, the BUE are expected for cases 1 - 4 in the model. However, the BUE physically appears for cases 1 and 2 and only at the beginning of cases 3 and 4. This discrepancy of the BUE formation prediction in case 4 leads to a large inconsistency of the tool progressions between calculation and measurements. The under-estimation may also come from the non-uniform tool flank wear as shown in Figure 5-5. The equivalent tool flank wear for non-uniform tool wear is the average of five randomly picked flank wear lengths. It is possible to under-estimate the effective wear land lengths when the model only considers the uniform tool flank wear. Moreover, the predicted wear land length is used to predict cutting forces and cutting temperatures in the next step. The predicted error of tool life would accumulate and propagate. For near dry machining, the tool flank wear is more uniform than the tool wear under completely dry condition. The predicted tool wear progressions for near dry turning show a better agreement with the measured data compared with the data for dry turning.

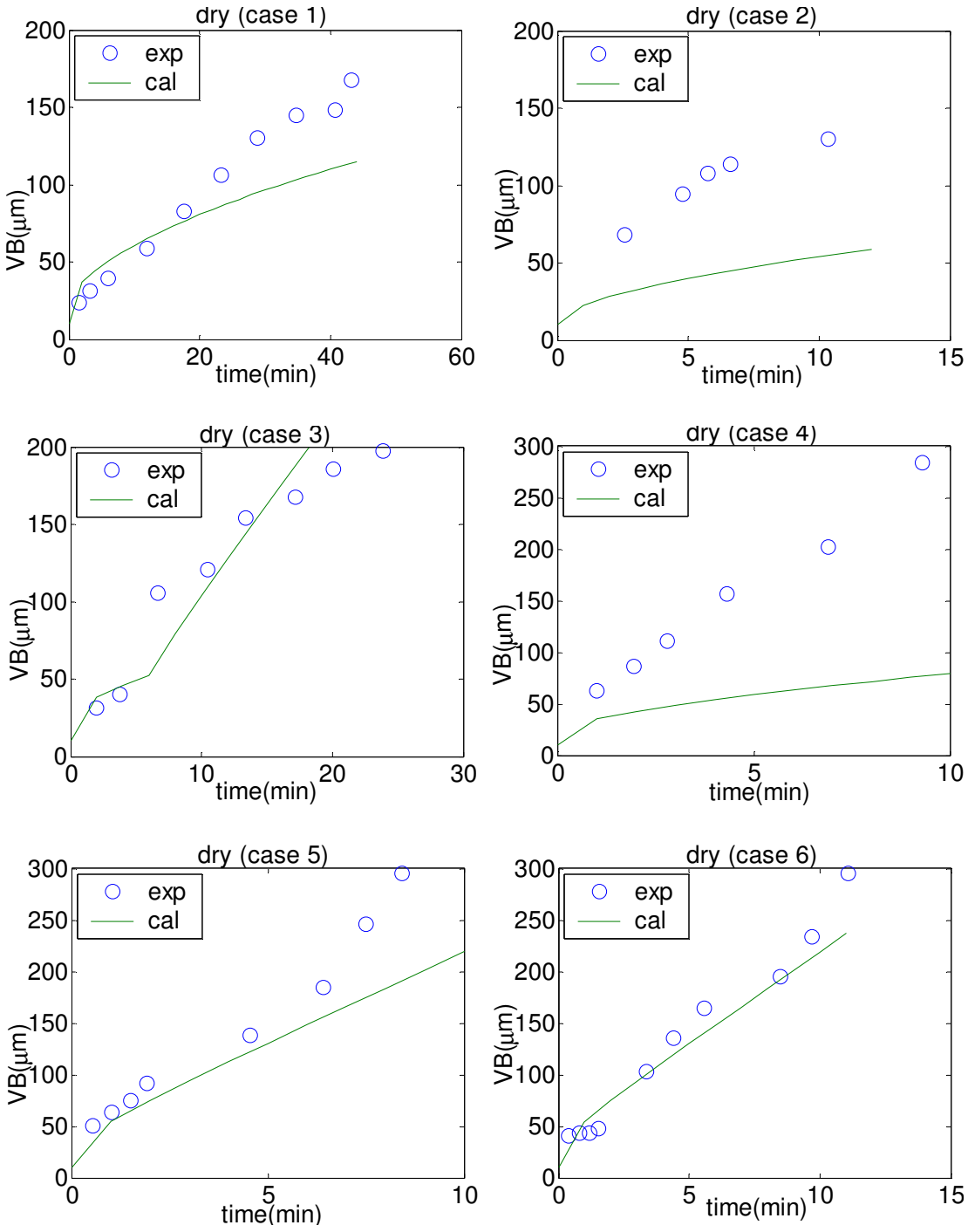

Figure 5-4: The comparisons of tool flank wear progression for dry machining

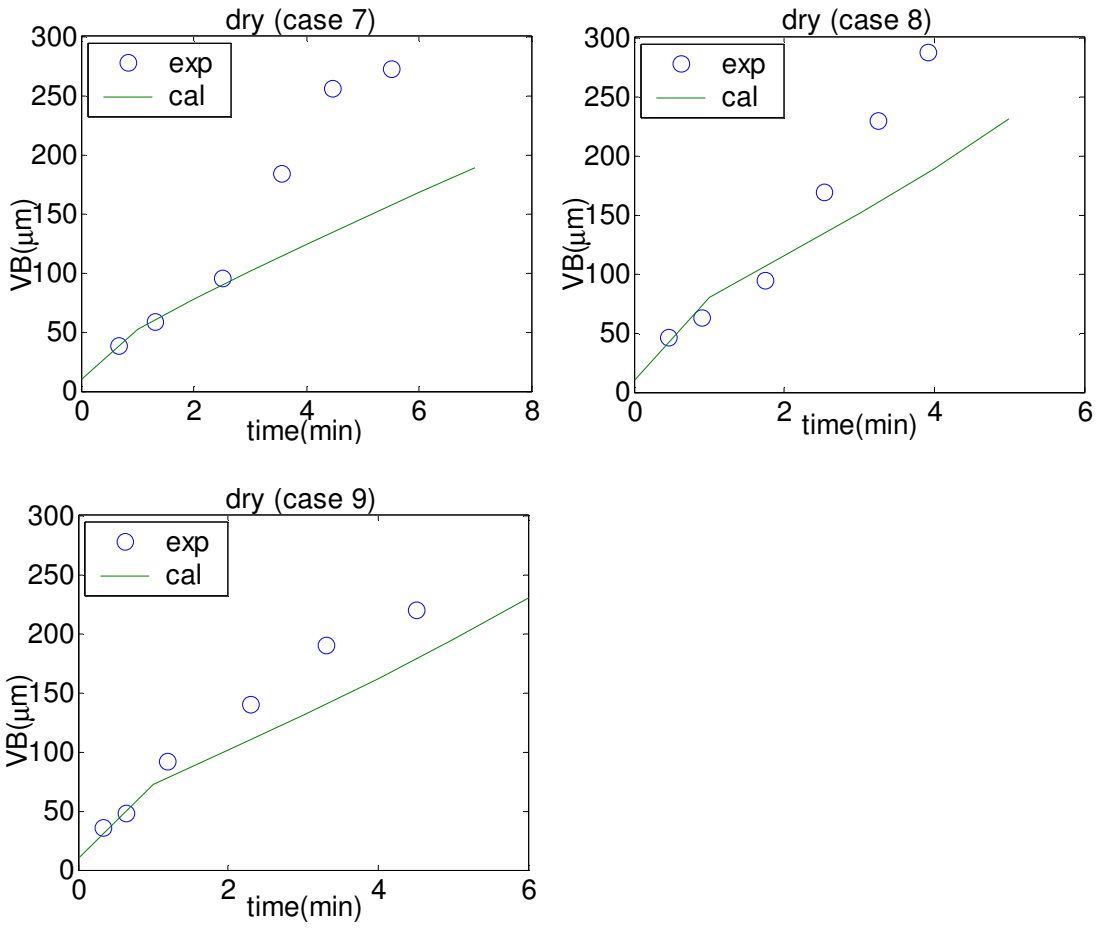

Figure 5-4 continued: The comparisons of tool flank wear progression for dry machining

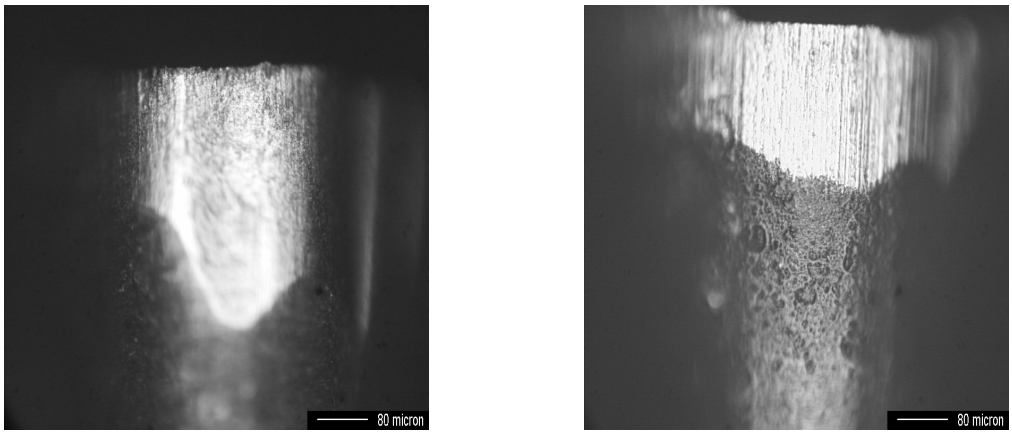

(a) (b)

Figure 5-5: Tool flank wear conditions under dry and near dry conditions after the same time interval for condition 5. (a) Dry machining. (b) Near dry machining.

The effects of cutting parameters on the tool wear rates in near dry turning process are shown in Figure 5-6 according to the principle of design of experiments [42]. It is shown that the cutting speed is the dominant factor among the cutting conditions. The effect of the depth of cut on the wear rate shows a decreasing trend. There is not any trend of the effect of the feed on the tool flank wear rate.

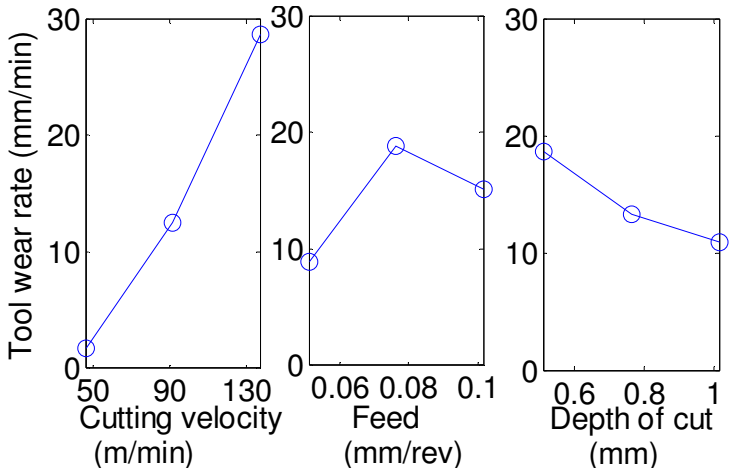

Figure 5-6: Tool flank wear rate trend for near dry machining with respect to cutting condition

The trends shown in Figure 5-6 do not exactly match the observations for dry cutting in the literatures [43, 48]. The effects of cutting parameters on the tool wear rates for dry cutting are essentially due to the cutting velocity, followed by feed and then depth of cut. The effects caused by feed and then depth of cut could be either minor or

insignificant, depending on the tool geometry. The inconsistency of the prediction in Figure 5-6 and the previous observations could attribute to the BUE formation model in this study. If the BUE formation is not considered in the tool wear predictions, the effects of cutting parameters on the tool wear rates in near dry turning process are close to the prior reports, as shown in Figure 5-7.

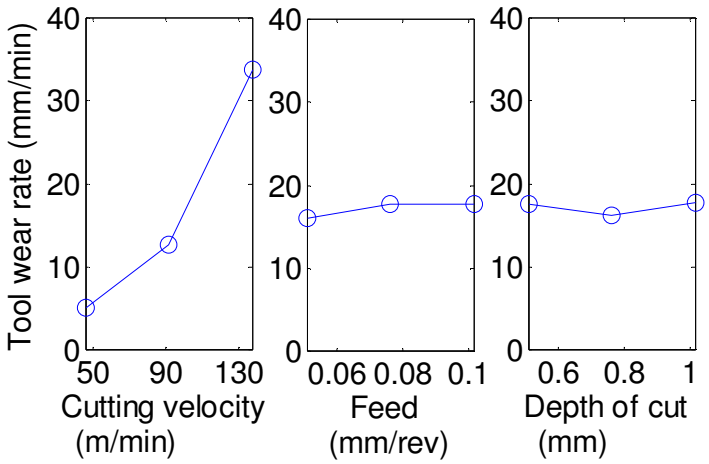

Figure 5-7: Tool flank wear rate trend for near dry machining with respect to cutting condition without considering BUE formation

5.8 Conclusion

The methodology for tool flank wear modeling in near dry turning is presented. This chapter integrated the cutting force model and the temperature model with the tool flank wear mechanisms. The cutting force model is developed based on Oxley's model

with modifications for lubricating and cooling effect for near dry lubrication. The cutting temperature is obtained by considering a moving or stationary heat source in the tool. Three wear mechanisms are considered: abrasion, adhesion, and diffusion. The BUE formation is also formulated in the tool flank wear model based on a dynamic strain aging relationship. The tool wear progressions as well as the cutting forces and the cutting temperatures are estimated based on material properties, tool geometry, and cutting conditions. The coefficients for wear rate model are calibrated by the measured tool wear lengths when turning AISI 1045 steel with uncoated tungsten carbide. The model is validated by comparing the predicted tool wear progressions with experimental data over different cutting conditions. The predicted tool wear progressions show good agreement with the measured data under near dry lubrication. It is observed that non-uniform tool flank wear or inexact prediction of BUE would lead to estimate less accurate cutting forces and cutting temperature and consequently less precise tool life. It is suggested that the geometry of non-uniform tool flank wear should also be considered when establishing tool wear models. It is also found that the cutting velocity is the dominant factor for tool wear progression prediction. This is the same phenomenon as observed in dry machining processes.

CHAPTER 6

MODELING OF CUTTING FLUID AEROSOL GENERATION IN NEAR DRY MACHINING

6.1 Introduction

Near dry machining was addressed several years ago [1, 2] as an alternative to the traditional flood cooling application. Although near dry machining has already attracted great notice since the mid-1900's, the previous research only focused on the tool performance and product dimension accuracy while very little study has been conducted on the issue of air quality. To achieve a better understanding of the machining process planning with environmental concerns as a factor of consideration, the cutting fluid generated from near dry machining has to be quantitatively understood. This chapter develops a predictive model on an analytical basis to provide a quantitative description of the cutting fluid atomization behavior in near dry turning process in order to estimate the resulting air quality.

The model of aerosol generation of cutting fluid for traditional flood cooling can be described as atomization and evaporation, as shown in Figure 6-1 [21]. The total quantity of applied cutting fluid in conventional flood cooling can be divided to three independent forms [21, 22, 68]: (1) mist due to atomization, including spin-off mechanism and splash mechanism; (2) steam due to evaporation; (3) liquid cutting fluid remaining on workpiece, machine tool and/or shop floor. By the basic definition of near dry turning, the workpiece is almost dry after the machining process is completed. Meanwhile, it is expected that there is no cutting fluid left on the machine tool, cutter, or on the shop floor. Thus the cutting fluid applied in near dry machining can be considered to contribute only to the mechanisms of mist and steam.

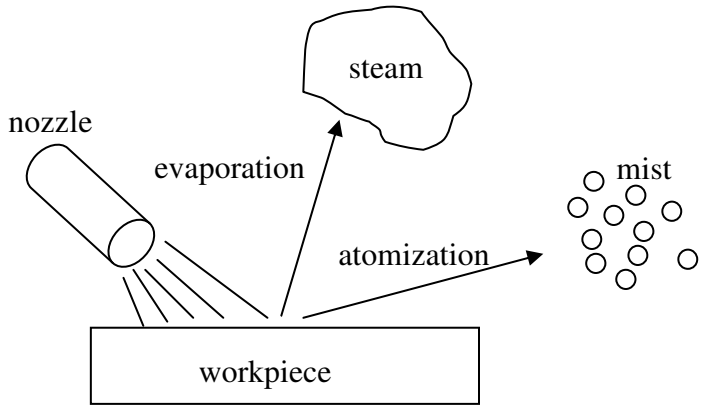

Figure 6-1: Various cutting fluid atomization mechanism [21]

At the same time, the aerosol concentration is different everywhere in the space. It is necessary to establish a diffusion model for aerosol dissipation. The aerosol is dissipated from the cutting zone in the radial direction due to the aerosol concentration gradient. Thus a diffusion model with a point source is suitable for the aerosol concentration [68].

In this chapter, analytical models for near dry turning are proposed to predict the aerosol generation and diffusion. The primary interests of this study focus on (1) the formation of the air-fluid mixed flow, (2) the aerosol generation mechanisms and (3) the aerosol diffusion model. Following the analytical modeling, experimental testing has been performed for calibration and validation.

6.2 Analytical Modeling

Generally speaking, the cutting fluid aerosol generated in the turning process is from either one of, or a combination of, spin-off, splash, and evaporation mechanisms [22]. Spin-off is the result of centrifugal force on the workpiece in rotational motion. Splash comes from the energy transformation from kinetic energy to surface energy. Evaporation is the result of the high temperature at the cutting zone. In near dry turning, the cutting fluid is applied to the cutting zone in the form of air-cutting-fluid mixture

(aerosol) instead of abundant cutting fluid. Therefore the cutting fluid aerosol generation mechanisms for traditional flood cooling may be not suitable for estimating the aerosol generation in near dry turning. It is necessary to modify the current models according to the characteristics of near dry lubrication. A suitable approach is to estimate the spray transfer efficiency (TE) first when the aerosol hits the workpiece surface. The transfer efficiency is defined as the mass fraction of applied air-cutting-fluid mixture which is deposited on the workpiece. The runaway aerosol corresponds to the aerosol generation due to splash mechanism in flood cooling situation. The deposited cutting fluid on the workpiece will generate the aerosol by either evaporation or spin-off mechanisms or both. At the same time, the contribution of spin-off mechanism is assumed to be insignificant because the lubricant quantity is small and is insufficient to form an oil film on the workpiece after the machining process. This assumption is also verified by non-machining tests which will be discussed later in the chapter.

6.2.1 Cutting fluid aerosol generated by the lubricant applicator

In this section, the cutting fluid aerosol supplied by the lubricant applicator is described. The droplet diameter distribution is assumed to be fit the Rosin and Rammler distribution [69]. The generated aerosol is delivered to the cutting zone as both the

lubricant and coolant for machining processes. The basic assumptions made in the following analysis are: (1) the cross area of the air-liquid mixture flow equals to the nozzle cross area of the applicator before the mixture reaches the cutting zone; (2) the presence of dust particles in the air is negligible.

The air-cutting-fluid aerosol is composed of droplets of different sizes. A widely used empirical expression is described by the Rosin and Rammler distribution function as [69]:

$$1 - Q(D) = \exp\left[-\left(\frac{D}{X} \right)^{q} \right] \tag{6-1}$$

where q and X are determined from experiments.

The momentum of liquid to the momentum of atomizing air ratio satisfies the relation [70]

$$\gamma = \frac{m_l v_l}{m_a v_a} \leq 1 \tag{6-2}$$

Since the liquid-air mass ratio is a known parameter of the cutting fluid applicator, the velocity of drops at the atomizer outlet satisfies the relation:

$$v_l \leq \frac{m_a}{m_l} v_a \tag{6-3}$$

The discharged air velocity from the cutting fluid applicator can be estimated by air flow rate. Assuming that the drops have attained their maximum velocities, the drop

velocities can be obtained.

6.2.2 Runaway aerosol generation

In this section, the runaway aerosol as well as the distribution parameter and mean drop diameter are to be determined. The runaway aerosol comes from the undesirable overspray in the cutting process. The mass fraction of the deposited cutting fluid on the workpiece is close related to the spray momentum rate (SMR) and droplet size based on experimental results [71]. The relationship among the mass fraction of the deposited cutting fluid (defined as transfer efficiency, TE), SMR and droplet size is expressed as [71]:

$$TE = a + b(SMR) + C(SMR)^2 + d \times D_{32} \tag{6-4}$$

$$SMR = \frac{(\dot{m}_l)^2}{\rho_l A_{nozzle}} \tag{6-5}$$

where a, b, c and d are coefficients dependent on the cutting fluid properties and to be determined by experiments.

It is assumed that the droplet distribution parameter and mean droplet diameter are similar to those in grinding [68] from the splash mechanism because the splash atomization in grinding is caused by the kinetic energy transformation as well as the disturbances due to the existence of the air. The drop diameter distribution in aerosol

runaway mechanism is still the Rosin and Rammler distribution function in Equation (6-1). The distribution parameter, q, and the mean diameter, X, are estimated by the following equations [68, 72]:

$$q = K\,\mathrm{Re}^{n} \tag{6-6}$$

$$X = \frac{C_a \mu^{0.5} m_l^{0.1} \left(1 + \frac{m_l}{m_a}\right)^{0.5} d_{avg}^{0.1} \sigma^{0.2}}{\rho_a^{0.3} v_l} \tag{6-7}$$

The amount of cutting fluid used in near dry turning is very small. In order to sufficiently deliver the cutting fluid to the cutting zone, a through-the-tool technique is used in this study. A 0.762-mm in-tool channel is made by electric discharge machining (EDM). Thus the d_{avg} equals 0.762 mm here. Moreover, the vegetable oil, Coolube 2210, is chosen as the lubricant in this study. Then Equation (6-7) can be simplified as:

$$X = \frac{C_a' \mu^{0.5} m_l^{0.1} \left(1 + \frac{m_l}{m_a}\right)^{0.5}}{\rho_a^{0.3} v_l} \tag{6-8}$$

where $C_a' = C_a d_{avg}^{0.1} \sigma^{0.2}$.

6.2.3 Evaporation atomization

In the evaporation atomization analysis, the evaporation rate and the temperature models are presented. The heat flux between the tool, the workpiece and cutting fluid

provides the energy to evaporate the cutting fluids. Then the condensation of vapor around spontaneously generated liquid nuclei or other foreign particles forms aerosol in the form of droplets. Considering a simplified model that the temperature distribution in the cutting zone is uniform, the net rate of evaporation is calculated by the Hertz-Knudsen equation as following [73]:

$$Q_{net} = \sqrt{\frac{M}{2\pi R}}\left(\frac{Ep_{tr}}{\sqrt{T_{tr}}} - \frac{Cp_{atm}}{\sqrt{T_v}}\right) \tag{6-9}$$

When a state of equilibrium is reached, the evaporation coefficient and the condensation coefficient are equal. Then the equation for evaporation of the cutting fluid can be rewritten as:

$$Q_{net} = \alpha\left(\frac{p_{tr}}{\sqrt{T_{tr}}} - \frac{p_{atm}}{\sqrt{T_v}}\right) \tag{6-10}$$

The knowledge of the cutting fluid surface temperature, as the segment AB and AC show in Figure 3-2 in Chapter 3, is a prerequisite to the evaporation rate. The temperature distributions along tool-chip interface, along tool clearance face and along the workpiece can be estimated by considering the oblique moving band heat source or stationary rectangular heat sources as presented in Chapter 3.

6.2.4 Diffusion model

The small fluid drops generated in the near dry turning process diffuse into the air due to the aerosol concentration gradient. The aerosol dissipates in the radial direction away from the cutting zone, as shown in Figure 6-2. The aerosol diffusion can be modeled as a point source with an origin located at the point of cutting action in a 3-D space [68], as following:

$$D_{AB}\frac{1}{r^2}\frac{\partial}{\partial r}\left(r^2\frac{\partial Q_a}{\partial r}\right)=\frac{\partial Q_a}{\partial t} \tag{6-11}$$

With the boundary condition and initial condition, the equation above is rewritten as [68]:

$$Q_a(r,t)=Q_{a,o}+\frac{Q_{flux}S^2}{D_{AB}r}\times \left[erfc\left(\frac{r-S}{\sqrt{4D_{AB}t}}\right)-\exp\left(\frac{r-S}{S}+\frac{D_{AB}t}{S^2}\right)erfc\left(\frac{r-S}{\sqrt{4D_{AB}t}}+\frac{\sqrt{D_{AB}t}}{S}\right)\right] \tag{6-12}$$

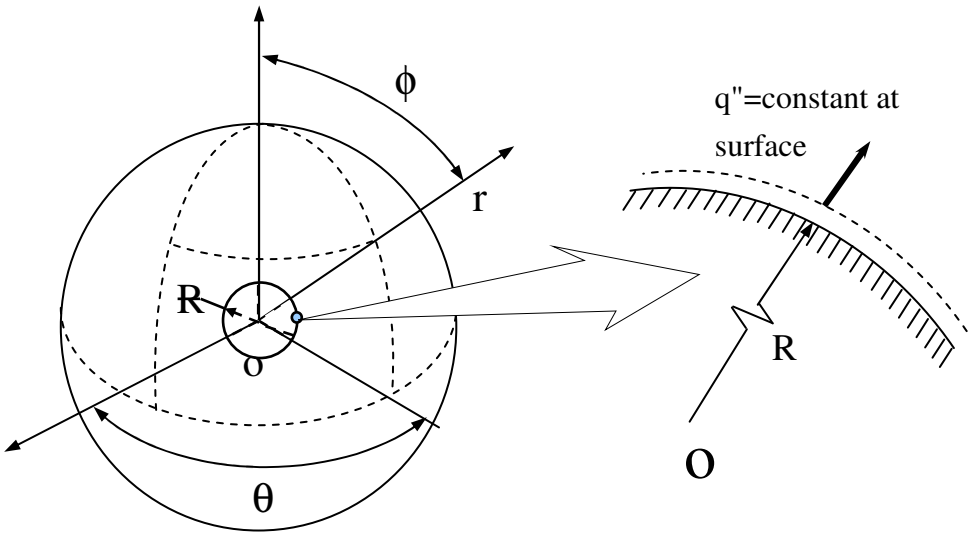

Figure 6-2: Schematic of diffusion model [68]

6.3 Experimental setup

Figure 6-3 shows the experimental setup consisting of a horizontal lathe (CMS GT29), an in-tool cutting fluid applicator (UNIST uni-MAX Coolubricator), a tool-post dynamometer (Kistler model 9257B), thermocouples, an aerosol spectrometer (PMS-CSASP-100 or MIE DataRam 2000 aerosol monitor) and a PC-based data acquisition system. The UNIST system is used to supply the air-fluid mixture of 12.5 ml/hr at a pressure of 275.8 kPa. Coolube 2210, a vegetable oil, is chosen as the cutting fluid. The air-fluid mixture is applied to the flank face of the insert through a 0.762-mm in-tool hole as shown in Figure 3-1 in Chapter 3. Medium carbon steel, AISI 1045, is machined with the uncoated carbide inserts (DCMT-2A).

In order to verify that the aerosol generation due to spin-off mechanism is assumed to be insignificant, non-machining tests are planned. When the workpiece is not rotated, the aerosol generation is attributed to the aerosol runaway mechanism with supplied oil and air mixture. When the workpiece is rotated without machining, the aerosol generation is attributed to the combination of the aerosol runaway and spin-off mechanism. Comparing the results from the above two non-machining tests, the fraction of generation due to the aerosol runaway and spin-off mechanisms can be determined.

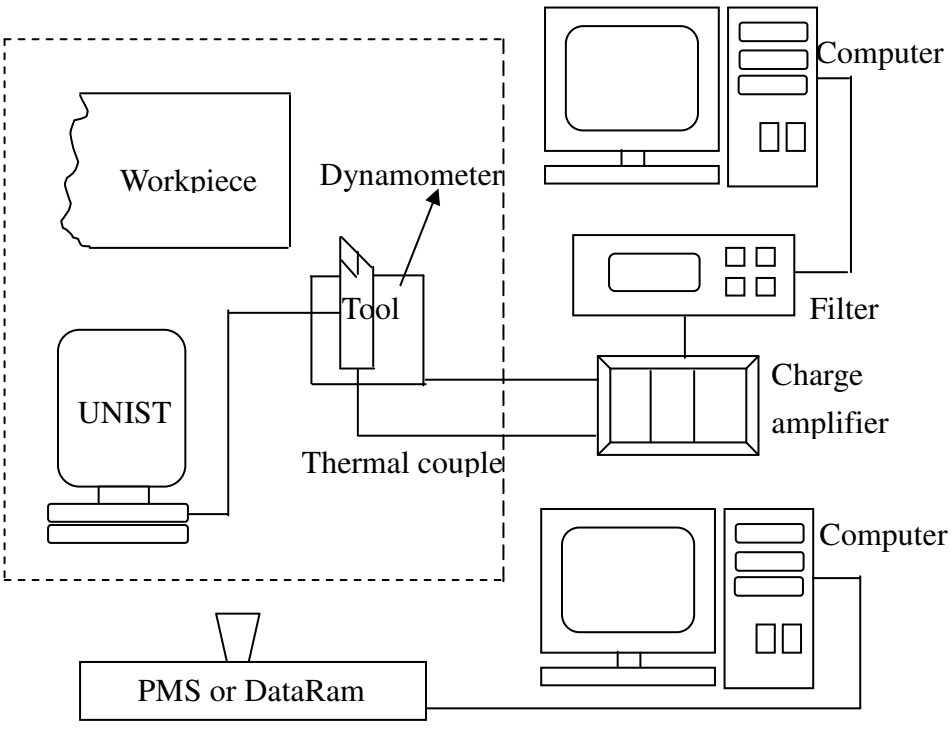

Figure 6-3: Schematic diagram of experiment set-up and some instruments

A non-machining test with different airflow rate is performed to calibrate the constants in Equations (6-6) and (6-8). The constant, α, in Hertz-Knudsen equation was calibrated by heating a certain amount of cutting fluid to 200°C The heat generation rate is calculated by the cutting model [39, 43] as described in Chapters 3 and 4. Then dry turning, near dry turning and flood cooling turning experiments are performed under the selected cutting conditions in order to validate the proposed model.

6.4 Results and Discussions

The comparison of aerosol generation due to aerosol runaway and spin-off mechanisms is shown in Figures 6-4, 6-5 and 6-6. In the figures, the aerosol generation rate due to the aerosol runaway and spin-off mechanism is only slightly higher than the aerosol generation due to the aerosol runaway mechanism. Therefore, it is reasonable to assume that aerosol generation due to the spin-off mechanism is insignificant.

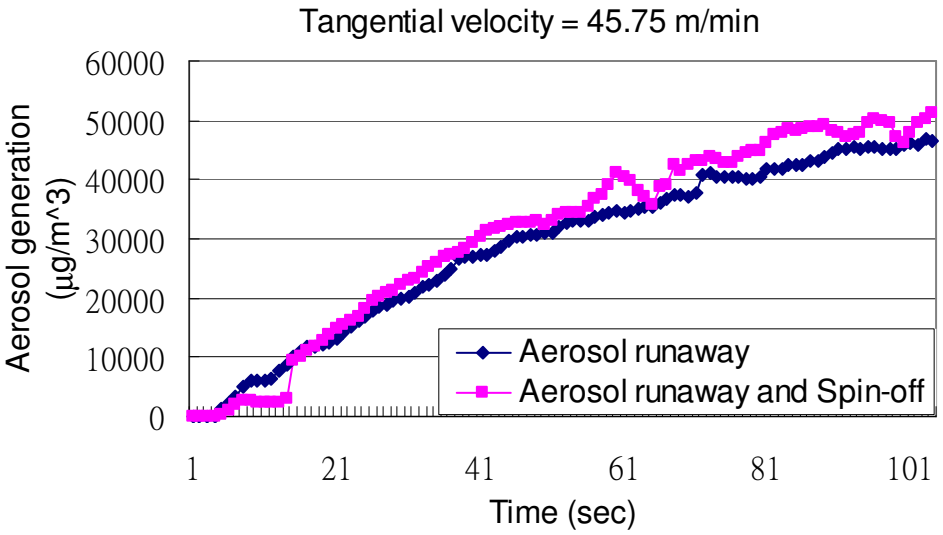

Figure 6-4: Comparison between aerosol runaway and spin-off mechanism at 45.75 m/min tangential speed for the oil flow rate of 12.5ml/hr

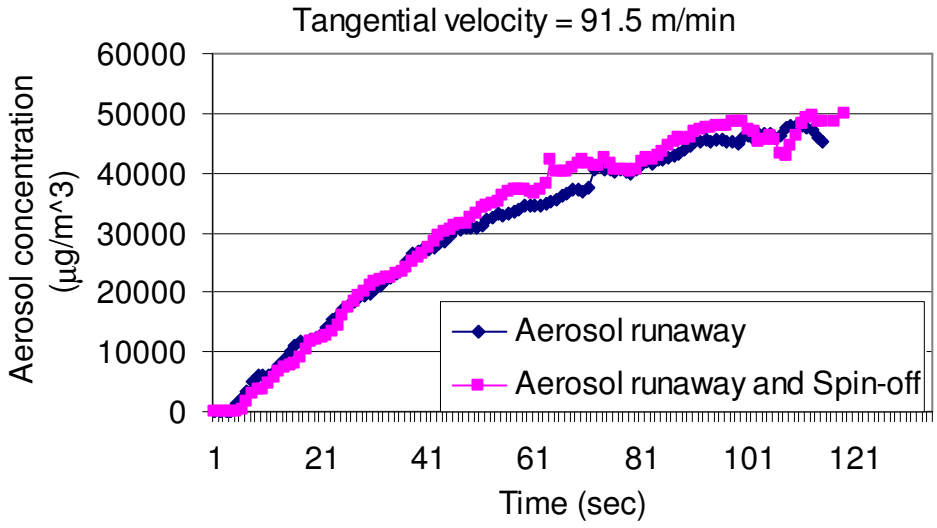

Figure 6-5: Comparison between aerosol runaway and spin-off mechanism at 91.5 m/min tangential speed for the oil flow rate of 12.5ml/hr

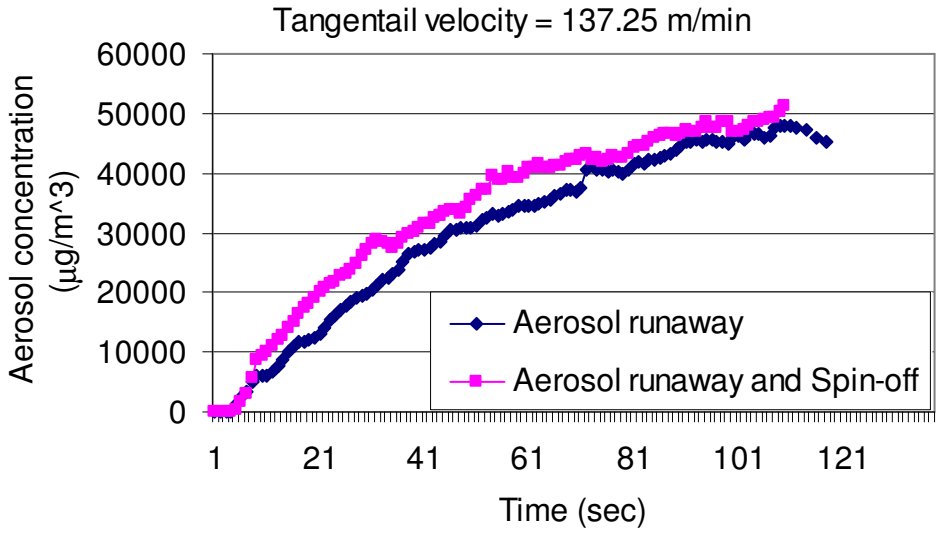

Figure 6-6: Comparison between aerosol runaway and spin-off mechanism at 137.25 m/min tangential speed for the oil flow rate of 12.5ml/hr

The coefficients for transfer efficiency in Equation (6-4) are determined with experimental data from non-machining test with oil flow rate of 9.38 18.75, 30.0, 46.88 and 56.25 ml/hr. With the calibrated coefficients, Equation (6-4) becomes

$$TE = 39.7 - 36.6SMR + SMR^2 + 54.3SMD \qquad (6\text{-}13)$$

The distribution function constants are calibrated with experiments of different air flow rate. These constants in Equation (6-6) are $K = 0.3954$ and $n = 0.137$ which were obtained when the air flow rates were 39.6, 70.8, 96.3 and 114.3 l/min and the oil flow rate was 12.5 ml/hr. Also, the constant, $C_a^{'}$, in Equation (6-8) is 0.307. These coefficients are valid for the 0.762-mm in-tool hole and Coolube 2210 as used in the

experiments in this study.

After the cutting temperatures are determined with the method presented in Chapter 3, the evaporation rate can be obtained by Equation (6-10). The coefficient, α, in Hertz-Knudsen equation is calibrated by heating 150 ml cutting fluid (Coolube 2210) with a hot plate from 160°C to 200°C. It is found that for Coolube 2210, α is sensitive to the temperature and can be expressed as following:

$$\alpha = 0.01921T^2 - 7.6669T + 774.9 \qquad (6\text{-}14)$$

With the Hertz-Knudsen equation, the evaporation rate in near dry turning is found to be small relative to the aerosol runaway. For example, if the average tool flank face temperature in steady state is 160°C in near dry turning, the evaporation rate is less than one millionth of aerosol generation rate due to the aerosol runaway mechanism.

In a prior study [68], it was shown that the aerosol generation rate achieves a constant level in a relatively short time with a constant cutting conditions. In order to minimize the influence of aerosol generated in the closed machining space, sampling time should be relatively short. A sampling time less than 100 seconds is recommended. In this research, the shortest machining time is around 30 seconds. Thus the aerosol generation rates of analysis results and experimental results are compared on the basis of 30 seconds sampling time, as shown in Figures 6-7 to 6-9. In near dry turning, the air

flow velocity, which is the main cause of the aerosol runaway mechanism, is much higher than the fluid flow velocity in flood cooling. As a result, it is found that the aerosol generation rate is not sensitive to the cutting parameters in the planned experiments. At the same time, the aerosol generation rate is primarily governed by the cutting fluid flow rate as shown in Figure 6-10. The errors of the predicted aerosol generation rates in Figure 6-10 are within 4%. It is found in Figures 6-7 to 6-10 that the aerosol generation rate for near dry turning under the cutting conditions in this study approximately ranged from 1000 to 8000 $\mu g / m^3 s$. Compared with the aerosol generation in flood cooling, the aerosol generation in near dry turning is mainly caused by the aerosol runaway, not spin-off. It is found that reducing the rotational speed in turning process does not effectively lower the aerosol generation rate because the rotational speed is the primary parameter for the spin-off mechanism, not for aerosol runaway.

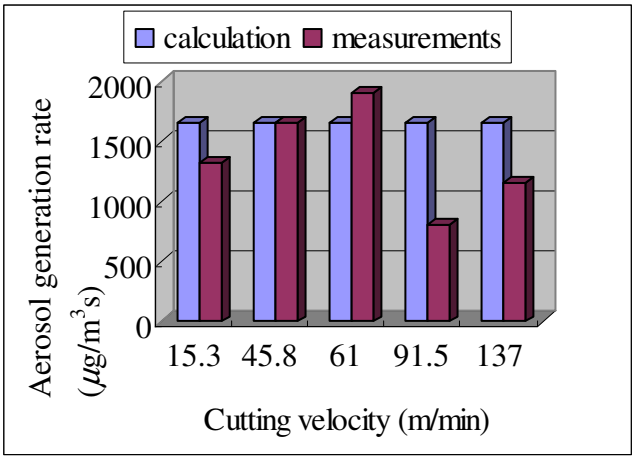

Figure 6-7: Aerosol generation rate comparison for different cutting velocity (feed rate = 0.0762 mm, depth of cut = 0.508mm, oil flow rate = 12.5 ml/hr)

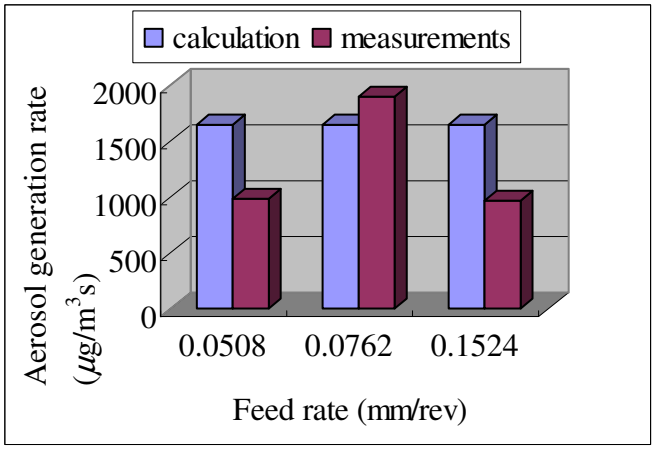

Figure 6-8: Aerosol generation rate comparison for different feed rate (cutting velocity = 61 m/min, depth of cut = 0.508mm, oil flow rate = 12.5 ml/hr)

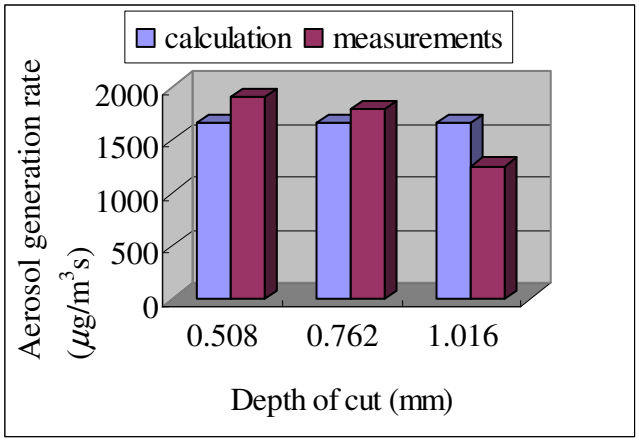

Figure 6-9: Aerosol generation rate comparison for different depth of cut (cutting velocity = 61 m/min, feed rate = 0.0762 mm, oil flow rate = 12.5 ml/hr)

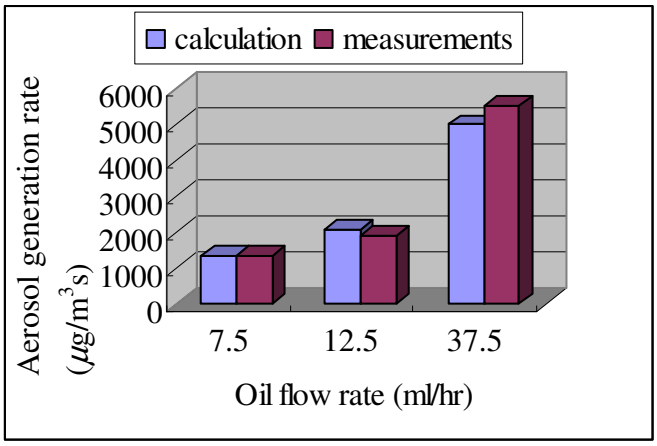

Figure 6-10: Aerosol generation rate comparison (cutting velocity = 61 m/min, feed rate = 0.0762 mm, depth of cut = 0.508mm)

The trend of transfer efficiency with respect to the cutting fluid flow rate is shown in Figure 6-11. There is a decreasing trend for the conditions of the cutting fluid flow rate higher than 40 ml/hr. Nevertheless, the decrease of the transfer efficiency is only within

3%. Combined with the effect of oil flow rate on the aerosol generation, it still leads to an increasing aerosol generation for higher oil flow rate. According to Figures 6-10 and 6-11, it is recommended that the most effective solution to reduce the aerosol concentration in near dry turning is to limit the use of cutting fluid.

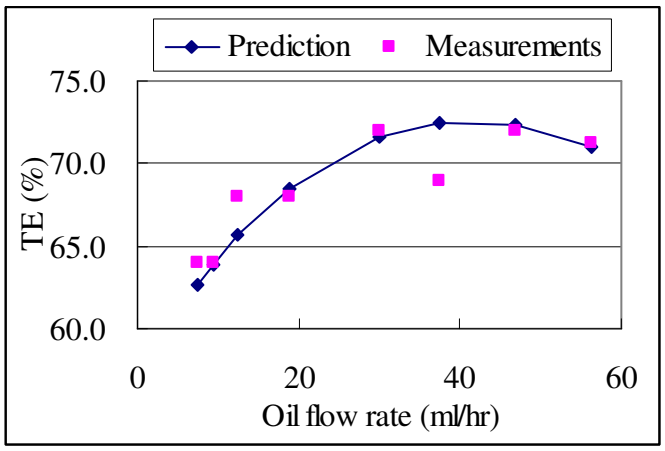

Figure 6-11: Predicted transfer efficiency for different oil flow rate

In addition, the characteristic diameter calculated from Equation (6-8) as well as the measured droplet diameter for near dry turning is about $1\mu m$. Compared with the characteristic diameter in turning under flood cooling condition, the droplet diameter is around $10\mu m$ [68]. The smaller droplet diameter indicates that the generated droplets under near dry condition will suspend in the air for a longer time and become harmful to

the human. The best way to minimize the aerosol generation in near dry machining is to minimize the use of oil or to find the "optimal quantity" of cutting fluid which is sufficient for lubricating or cooling in metal cutting.

6.5 Conclusion

To address the issue of the environmental concerns of cutting fluids in near dry machining, this chapter presents an analytical model to predict the cutting temperature, aerosol generation rate and mean aerosol size distribution. This study focuses on the turning process with air-fluid mixture applied to the insert flank face. Two primary aerosol formation mechanisms are considered: aerosol runaway and evaporation. Both the analysis and the experimental results show that the aerosol runaway has a significantly higher effect on aerosol generation in near dry turning.

It is found that the aerosol generation rate under normal cutting condition (for example with 61 m/min cutting speed, 0.0762 mm feed rate, and 0.508 mm depth of cut) is on the order of $1000 \mu g / m^3 s$. The model is verified by comparing the analytical results with the measured cutting temperature and aerosol generation. The analytical results show a good agreement with the experimental results.

This study provides a fundamental investigation of the aerosol generation

prediction in near dry turning. The analysis can be expanded to other machining processes, such as milling and drilling. The resulting model can also be incorporated with the tool performance evaluation to achieve the requirements of air quality on the machine shop floor and cost in machining processes.

CHAPTER 7

MODEL-BASED PERFORMANCE PROFILING OF NEAR DRY MACHINING

7.1 Introduction

Near dry lubrication in machining refers to the use of cutting fluids of only a small amount as an alternative to completely dry or flood cooling methods to address the environmental, economical, and mechanical process performance concerns [1, 3]. Much research has suggested that near dry lubrication shows its potential competitiveness in terms of tool life, surface finish and cutting forces in turning [3], milling [12], drilling [6, 74], reaming [74], and tapping [74]. Most documented studies concerning near dry lubrication thus far are built upon experimental observations with individual and separate treatment of machining performance measures such as cutting force, temperature, tool wear progress, chip formation, surface roughness, or air quality [74].

In profiling the performance capability of near dry lubrication to support its

broad-range process planning, this chapter presents the development of a realm of physics-based predictive models to quantitatively describe both the environmental and mechanical effects of near dry lubrication relative to completely dry and flood cooling conditions in turning. It involves the analysis of cutting forces, temperatures, tool wear modes of abrasion, adhesion, and diffusion, as well as aerosol generation mechanisms of evaporation, runaway aerosol, and dissipation. The sensitivity analysis of tool utilization, power consumption, and air quality with respect to near dry lubrication attributes is discussed to profile the performance capability of near dry lubrication for both mechanical and environmental considerations.

7.2 Parameters Used in Sensitivity Analysis

The capability profile of near dry lubrication is herein evaluated based on its sensitivity to machining and near dry lubrication application parameters. Predictive models in Chapters 3 - 6 are used for workpiece of AISI 1045, tool of carbide insert with 0^0 rake, 11^0 clearance, and 6^0 inclination, and near dry lubrication of vegetable oil Coolube 2210. Additonally, the boundary lubrication parameters are $t_b = 0.15\mu m$, $C_2 = 0.5$, $H_{max} = 5\ \mu m$, $\rho = 0.89\ g/cm^3$, $z = 100/mm$, $D_{inc} = 1.5$, $R = 20\mu m$, and $\nu = 10\ mm^2/s$. All these parameters can be found in Chapter 4. In flood cooling, 1:20

Valcool is the fluid in over-head delivery. The effective fluid film thickness, t_b, is found to be 0.4 μm from the measured forces in flood. The details of the predictive models for conventional flood cooling will be presented in Chapter 8.

7.3 Comparisons of Machining Performance for Dry, Near Dry, and Flood Cutting

7.3.1 Cutting forces

Figure 7-1 shows that the forces decrease with increasing speed for all lubrication cases. It is also shown that lubrication is more effective for lower cutting speeds, a characteristic that is well documented [43]. At high speeds, the lubrication effect is much less significant. It is observed that cutting fluid is most effective for the tangential cutting forces at low cutting speed (91.5 m/min) where the force reduces by 24.4% and 32.2% relative to dry cutting for near dry machining (NDM) and flood conditions respectively. This is consistent with the variation of fluid penetration into the cutting zone with cutting speeds [43].

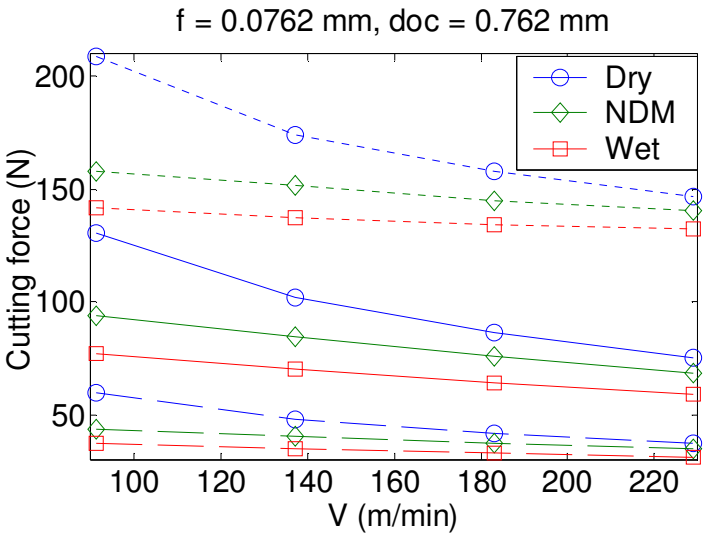

Figure 7-1: Effect of cutting speed on cutting forces (feed, radial, and tangential: solid, dash and dot lines).

Figure 7-2 shows that as the tool flank face wears, the contact between the tool and workpiece leads to an increase of total cutting forces. The increase is more pronounced when the wear is larger. For example, after cutting for 8 minutes, the tangential forces increase by 54.7%, 51.2%, and 45.5% for dry, NDM, and flood conditions. Also, the trends of cutting force components with respect to time are similar for machining under NDM and flood cooling as well as the magnitudes of the cutting force components.

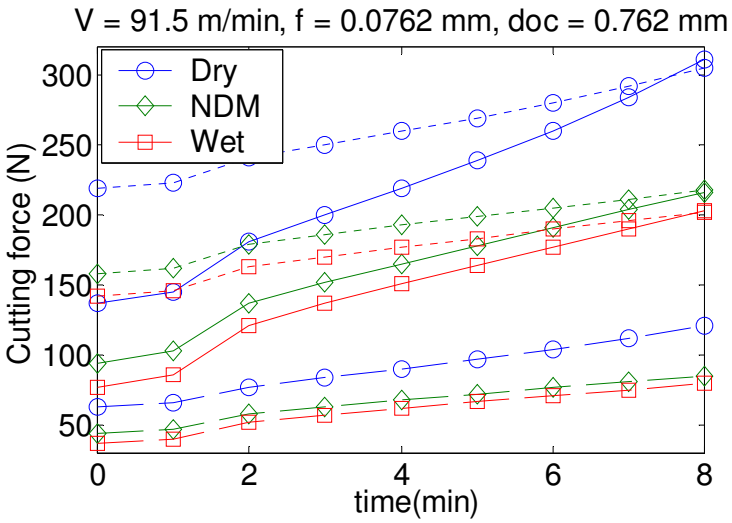

Figure 7-2: Time traces of cutting forces (feed, radial, and tangential directions: solid, dash and dot lines).

7.3.2 Temperatures

The tool flank temperature is important for tool life and aerosol generation. Figure 7-3 shows the flank temperatures with a $10\,\mu m$ initial wearland where the heat generated in the cutting zone is estimated from the predicted cutting forces. The highest temperatures are in dry cutting, followed by NDM and then the flood. It shows that the small amount of air-oil mixture of NDM presents a strong cooling effect. At 91.5 m/min, the temperature reduces by 22.1% from dry to NDM compared with the 31.4% reduction in flood. Also, the tool flank temperature increases with cutting speed due to a higher heat generation in the cutting zone.

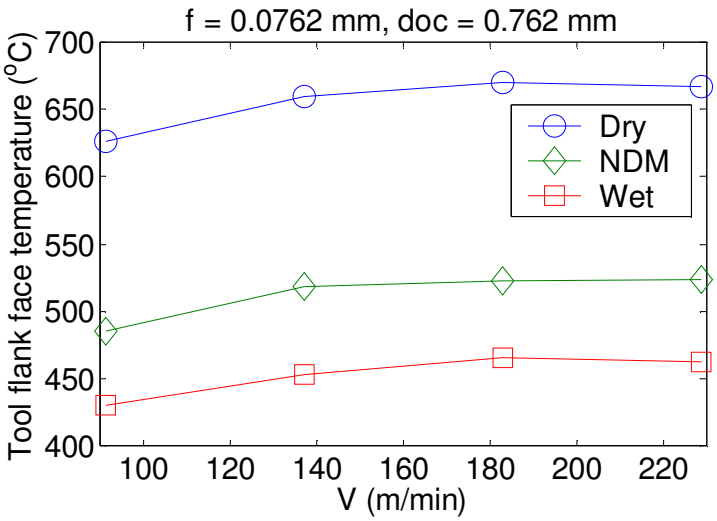

Figure 7-3: Effect of cutting speed on tool temperature.

Figure 7-4 shows that the tool flank temperature increases with time and thus the increase of wearland. The trends of tool flank face temperatures for all the situations are similar. Nevertheless, the temperatures for NDM and flood cooling conditions are comparable in the figure.

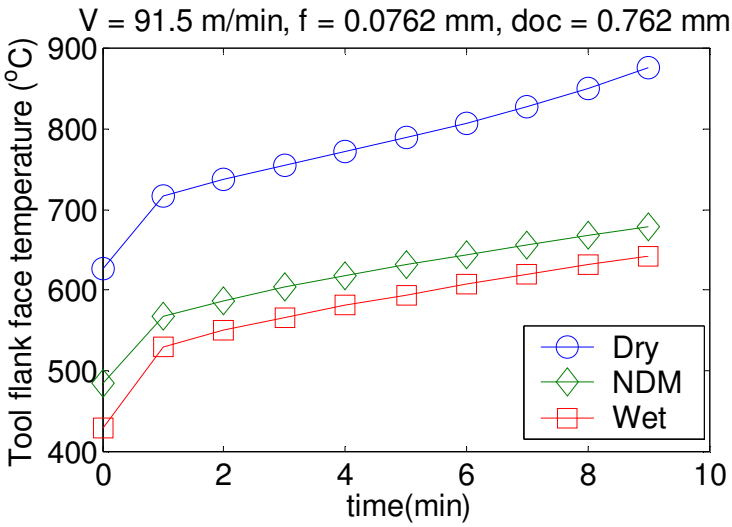

Figure 7-4: Effect of cutting time on tool flank temperature.

7.3.3 Tool flank wear

Figure 7-5 shows that tool wear progresses in NDM and in flood cooling in similar ways. Also seen is that in dry machining, the end of the tool wear shows a rapid increase. This phenomenon is attributed to the high flank face temperature where the diffusive mechanism is dominant.

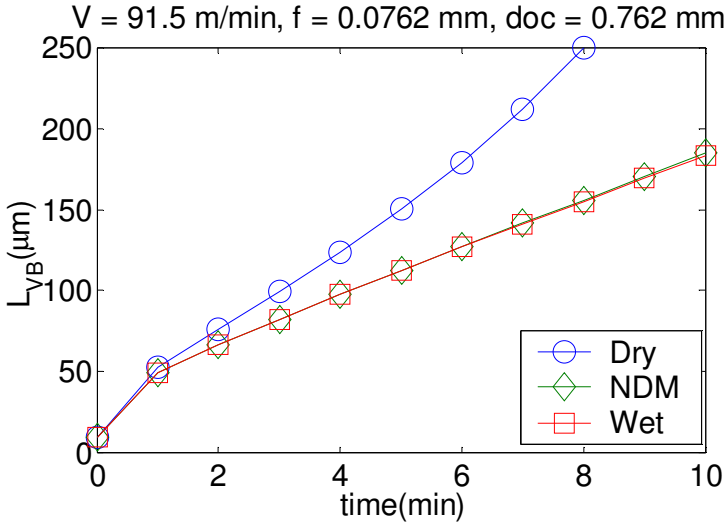

Figure 7-5: Trends of tool flank wear progressions.

The tool wear progression curves under NDM in Figure 7-6 show accelerated wear for high cutting speeds such as 183 m/min and 228.75 m/min, while the lower cutting speeds (91.5 and 137.25 m/min) see wear progressions within the uniform wear rate region after cutting for 5 minutes. Figure 7-7 shows magnitudes of the tool flank wear after cutting for 4 minutes under different lubrication circumstances. It is observed that the wear land expands quickly for dry machining. The values of the wear land length are similar for NDM and flood cutting within the cutting speed of 91.5 - 183 m/min followed by a noticeably higher wear rate at 228.75 m/min under NDM. The effects of feed and depth of cut on tool flank wear rate are also calculated, but rather low

sensitivities are concluded for dry, NDM, and flood conditions.

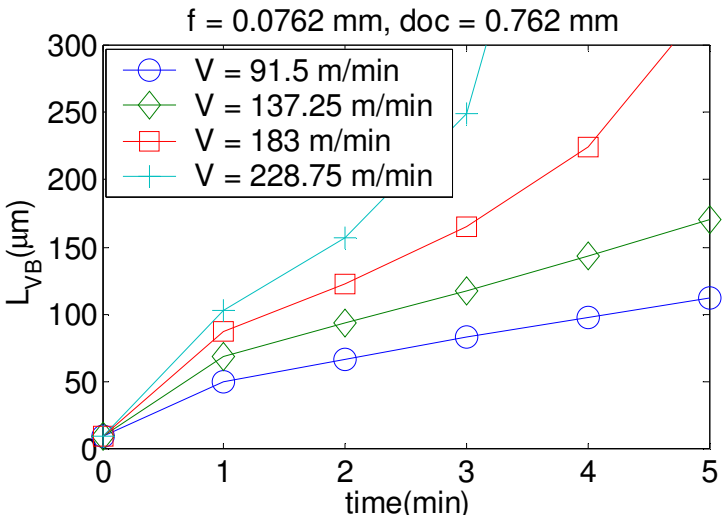

Figure 7-6: Effect of cutting speed on tool flank wear land length for near dry machining.

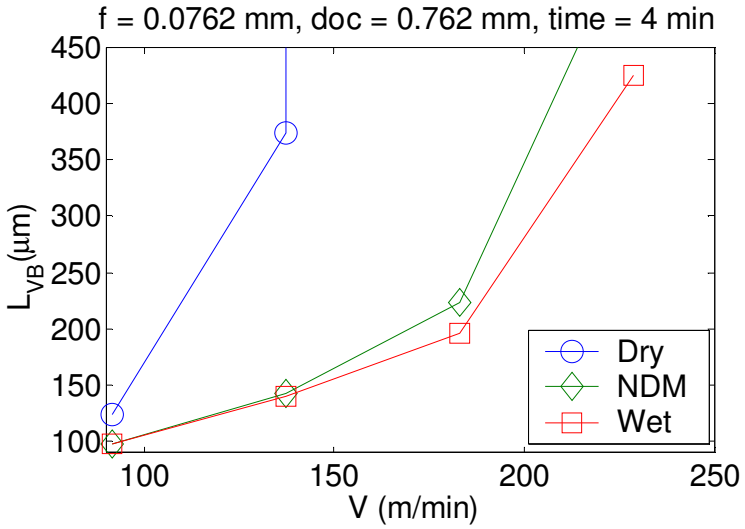

Figure 7-7: Effect of cutting speed on tool flank wear land

7.3.4 Power consumption

The power consumption is calculated as the product of the cutting force - obtained by the equivalent cutting edge model - and cutting speed. In Figure 7-8, since the cutting conditions for dry, NDM, and flood machining are the same, the power consumption is governed by cutting forces. Figure 7-9 shows that the power consumed decreases with higher feed for the same material removal rate. This tendency is understood by the size effect in that a smaller undeformed chip leads to a higher specific cutting energy which gives higher cutting force and thus power consumption.

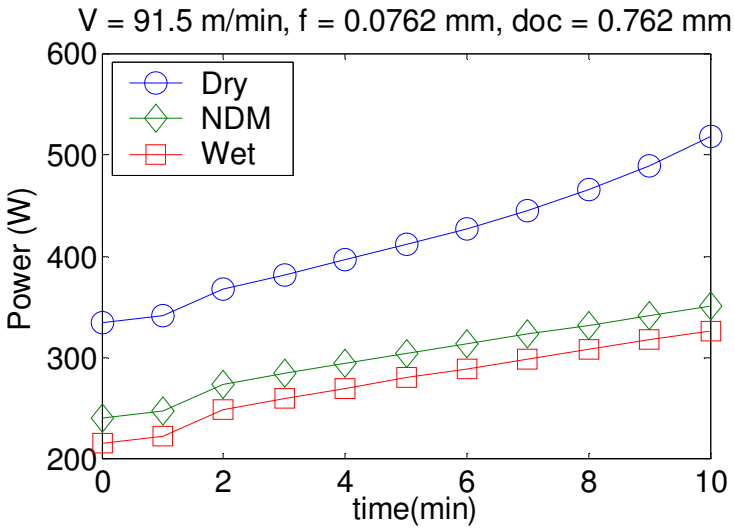

Figure 7-8: Trends of power consumption

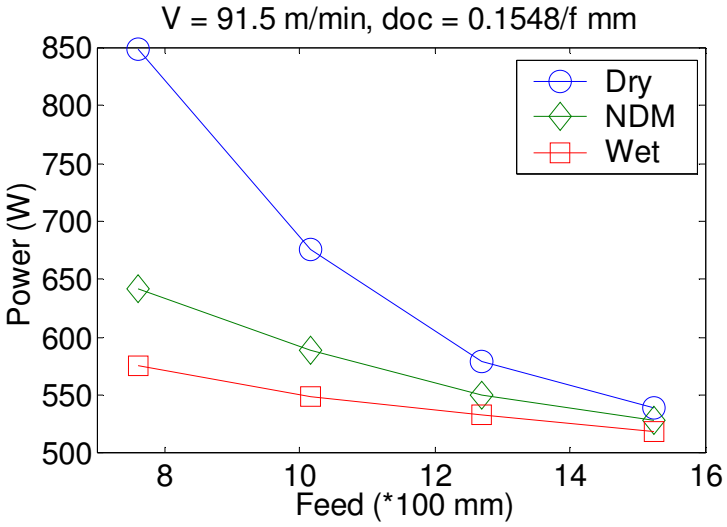

Figure 7-9: The effect of undeformed chip cross section on power consumption

7.3.5 Aerosol generation rate

The aerosol generation rate is proportional to the oil flow rate, as shown in Figure 7-10. For a NDM oil flow rate of 12.5 ml/hr and that for flood of 1.875 liter/min, the aerosol generation rates under NDM and flood cooling at various speeds are given in Figure 7-11. Although the flood cooling uses much more fluids, it generates a lower level of cutting fluid aerosol. This can be explained by the aerosol generation mechanisms in that aerosol generation is governed not only by fluid flow rate, but more importantly by the volumetric proportion of mist atomization. In NDM, the oil is delivered to the cutting zone in the form of mist flow with a large portion going through the runaway aerosol mechanism, as described in Chapter 6, with a high rate of aerosol generation. On the

other hand, in flood cooling the cutting fluid is delivered to cutting zone in the liquid form with a weaker spin-off atomization mechanism [22].

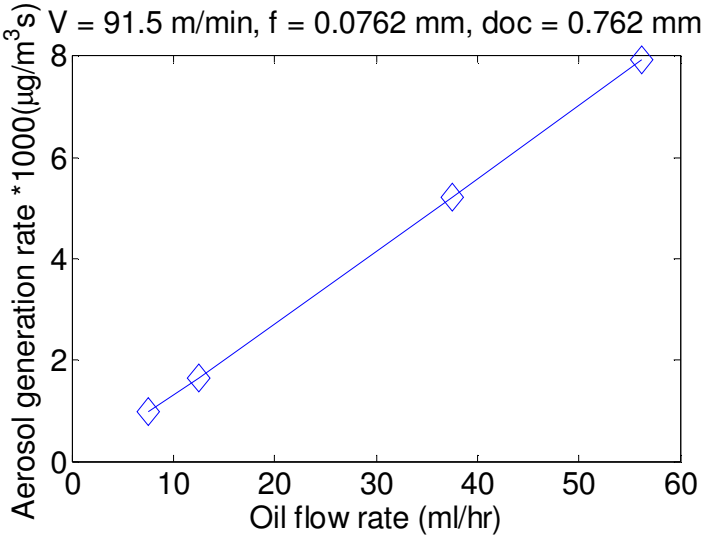

Figure 7-10: Predicted aerosol generation rate under various flow rates for NDM.

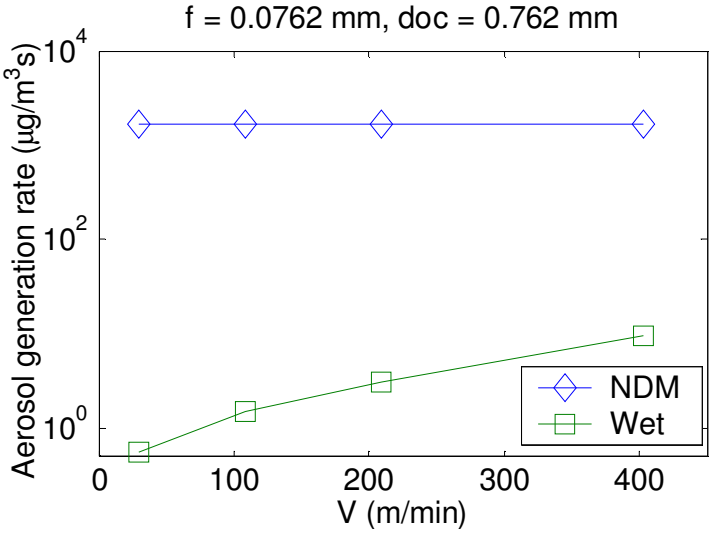

Figure 7-11: The effect of cutting speed on aerosol generation rate

7.4 Conclusions

Physics-based predictive models for near dry machining are developed to quantitatively profile the process performance and environmental measures in the context of cutting temperature, cutting force/power, tool wear, and cutting fluid aerosol generation. These attributes in NDM are benchmarked with respect to dry and flood cooling cuttings.

It is found that the application of NDM can effectively reduce the tangential cutting force, especially at low cutting speeds. The NDM shows a strong influence on the cutting temperature over a wide range of speeds, and it also lends itself to a lower cutting tool wear rate as compared to completely dry machining. However, as compared to flood cooling, NDM is expected to generate more cutting fluid aerosol due to the high oil flow velocity associated with mist application. According to the selected cutting conditions in this chapter, the predicted tangential, feed and radial cutting forces under near dry lubrication are reduced as high as 32%, 39% and 36% respectively compared with those in dry cutting but the cutting forces are higher than those in wet cutting by 10%, 18% and 15% respectively under the same cutting conditions. For the cutting temperature, tool wear land length and power consumption comparisons under the selected cutting conditions in this chapter, the predicted values are reduced by 29%, 60% and 32%

respectively compared with those in dry cutting but these values are higher than those in wet cutting by 11%, 1% and 10% respectively under the same cutting conditions. Based on the predicted values, with the appropriate cutting conditions, the tool performance for near dry machining is much better than that for dry cutting and only slightly inferior to that for wet cutting. However, the air quality for near dry machining with 12.5 ml/hr oil flow rate is 100 times worse than that for wet cutting due to different aerosol generation mechanisms. If the oil used in the near dry machining is reduced by 100 times (down to 0.125ml/hr) and the tool performance does not change much, the air quality is comparable to that for wet cutting.

Generally, NDM outperforms dry machining and is as good as flood cooling in all ways except mist generation. The cost for coolant used in NDM is much less than that in conventional flood cooling. The capability profiling results from this study can support further NDM process planning and optimization on quantitative scales.

CHAPTER 8

MODELING OF TOOL FLANK WEAR IN TURNING UNDER FLOOD COOLING

8.1 Introduction

Although the cost for using cutting fluids is approximately 7-17% of the total cost in machining processes [1], there is still a demand to use them for reducing tool wear, thereby extending the tool life. In addition, it helps to improve the surface finish and part tolerances as well as to facilitate chip flushing [75]. Therefore, the use of cutting fluid has often been favored in the interest of product quality and process productivity.

The effects of cutting fluids on machining process performance have been actively investigated for years. It has been shown that tool life and part finish can benefit from flood application of cutting fluid in certain situations relative to dry cutting [43, 76, 77]. The effects of fluid chemical composition on the machining performances, such as tool life, finish, and cutting power consumption, were also investigated [75, 78]. On this

topic, most of the research has been experimentally driven with only a few theoretical studies reported. Merchant [79] first suggested that the cutting fluid increases the shear angle and lowers the cutting forces through the reduction of friction coefficient between the chip and the tool rake face. DeChiffre [80] proposed that the fluid's lubricating action results in the reduction of the contact length, and this theory helps to explain the reduction of cutting forces and the extension of tool life. Smith [81] presented a theoretical model on chip formation and contact length under flood cooling based on a pre-described chip formation geometry. The cooling effect of the cutting fluid has been researched by finite element method [37] with chip shape and work rate as inputs to examine the effect of cutting fluids on tool temperatures.

The objective of this chapter is to develop a set of predictive models for the cutting forces, the cutting temperature, and the tool flank wear progressions under flood cooling situation. First, the friction angle describing the ratio of tangential to normal forces at the tool-chip interface is calculated based on the boundary lubrication model presented by Kato *et. al.* [51] to account for partial fluid penetration into the cutting zone. The resulting friction angle is then used in Oxley's model for considering the lubricating effect on the contact stress. Subsequently, the cooling effect of the cutting fluid is calculated by the moving heat source method [82] to estimate the cutting temperature.

The tool flank wear progressions are calculated based on the three primary wear mechanisms: abrasion, adhesion, and diffusion with contact stresses and temperatures obtained above. The built-up formation on the cutting tool is included in this study based on a dynamic strain aging analysis to address the observation of built-up edge in most of the flood cooling tests. For validation, the predicted cutting forces, cutting temperatures and tool lives are compared to experimental data for cutting AISI 1045 with uncoated carbide inserts under overhead jet cooling.

8.2 Modeling of Cutting Forces

8.2.1 Friction coefficient in overhead jet cooling based on boundary lubrication theory

The effect of cutting fluids on cutting forces from the view of lubricating in machining is discussed in this section. A major effect of cutting fluid is lubrication through the change of friction coefficient at the tool-chip interface. The cutting force behavior in this lubrication condition cannot be accurately described by a hydrodynamic lubrication model since it is not easy for fluid to penetrate into the cutting zone [43]. A cutting fluid film cannot be fully established even though abundant cutting fluid is applied. Instead, the boundary lubrication theory is a more proper explanation of the lubricating effect observed under flood cooling condition. The details to estimate the

cutting forces with lubricating effect are described in Chapter 4.

8.2.2 Modeling of cutting temperatures

In this section, the estimation of cutting temperatures under overhead jet cooling is performed considering three heat sources/losses - the primary heat source due to shear deformation, the secondary heat source due to friction, and the heat loss due to flood cooling, as shown in Figure 8-1. The segment AH represents the primary heat source generated by the shear deformation. AE represents the secondary heat source generated by the friction between the tool and the chip. DE, GH, and HI are the assumed coolant affected areas. The boundary EF is usually considered as an area affected by cooling [36] but it is ignored in this study because the movement of the chip away from the tool tip results in little influence of cooling on the tool temperature [37] (although it may have some effect on the chip temperature). The details about temperature changes based on the stationary heat source model or the moving-band heat source model were discussed in Chapter 3. The temperature distribution on the tool-chip interface is then estimated herein by the superposition of temperature changes due to different heat sources and heat losses due to overhead jet cooling.

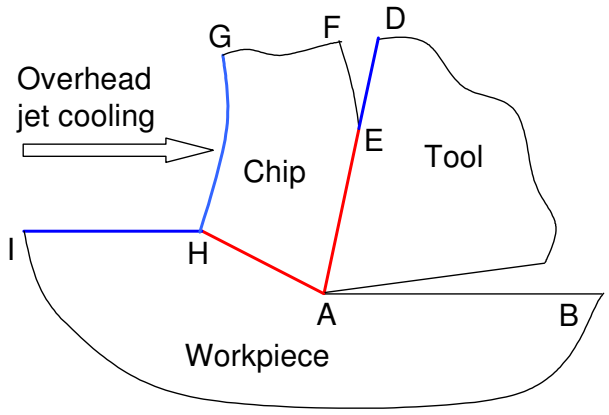

Figure 8-1: Heat sources and heat losses for the 2D model under overhead jet cooling

The heat loss intensity is calculated according to forced convection model as:

$$q_{hl} = \bar{h}(T - T_0) \tag{8-1}$$

where T can be the temperatures on the surfaces of DE, GH, and HI. The heat transfer coefficient $\bar{h}$ is estimated by a correlation equation for the local Nusselt number for the heat transfer from a flat surface to an oblique impinging liquid jet [36] while the segment GH can be approximated by a straight line:

$$Nu = \frac{\bar{h}L_{eff}}{K_{fluid}} = 1.122A\,\mathrm{Pr}^{1/3}\,\mathrm{Re}^{0.7}\,e^{-(B+C\cos\phi)(r/D_j)^m} \tag{8-2}$$

The temperature rise on the tool-chip interface is considered the same both in the chip and in the tool. The heat partition factors are solved based upon this assumption. With a sharp tool, the temperature distributions in the tool, in the chip and in the workpiece are calculated from the heat sources and/or heat losses with solved heat

partitions. Similarly, in the case of a worn tool, the rubbing heat source between the tool and the workpiece is also considered. The temperature distribution on the tool-workpiece interface should be the same in the tool and in the workpiece when the tool is worn. The heat partition factors between the tool-chip and the tool-workpiece interfaces are solved simultaneously by assuming equal temperatures on the interfaces. The temperature distributions for worn tools are calculated from the heat sources and/or heat losses with solved heat partition factors. The details about solving the temperature distributions in the tool were discussed in Chapter 3.

8.3 Modeling of Tool Flank Wear

8.3.1 Tool flank wear models

The volumetric loss of cutting tool resulting from the principal wear mechanisms of abrasion, adhesion, and diffusion is considered in this study. The important factors related to this model are contact stresses and temperatures that are estimated from the cutting force model and the cutting temperature model described earlier. Abrasive wear involves the loss of material when the tool flank and workpiece surfaces slide against each other with hard particles. Adhesive wear happens when the asperity junctions between the contact surfaces are torn off, as the tool and the workpiece slide against each

other. Diffusive wear plays an important role in the wear process due to the tool material diffusion across the tool-workpiece interface when the interface temperatures become very high. These primary wear mechanisms are calculated according to the model established in Chapter 5. The equation describing the tool flank wear rate is

$$\frac{dL_{VB}}{dt} = \frac{\cot\gamma - \tan\alpha}{L_{VB}} \left\{ K_{abrasion} K \left(\frac{1}{H_t} \right) V_c L_{VB} \sigma + K_{adhesion} e^{aT} V_c \sigma + K_{diffusion} \sqrt{V_c L_{VB}} e^{\frac{-K_Q}{T+273}} \right\} \tag{8-3}$$

8.3.2 Built-up edge formation

As discussed in Chapter 5, for cutting steels of carbon content of 0.45 %, it has been shown that the built-up edge (BUE) formation is closely related to the dynamic strain aging. By observing the BUE formation in the machining tests, it was proposed that:

1. if $T_{\text{mod}} > 550K$, there would be no BUE but for lower T_{mod}, there will be;

2. even if $T_{\text{mod}} < 550K$ there will be no BUE if $T_{\text{int}} > 1000K$.

where T_{int} is the average tool-chip interface temperature and T_{mod}, the modified temperature in Oxley's machining theory [39].

The BUE deposits on the tool surface and tends to protect the tool from direct

rubbing and abrasive wear with the workpiece, thereby extending the tool life. Therefore, if the cutting process parameters meet the above criteria and BUE is anticipated, the model assumes that the abrasive wear does not participate in the tool wear mechanisms.

8.4 Experimental Calibration and Validation of Predictive Models

8.4.1 Turning experiment set up

The predictive models of cutting force, cutting temperature, and tool flank wear progression are calibrated and validated by comparing to the experimental results of cutting AISI 1045 with uncoated carbide tool inserts (Valenite DPMT-2A) on a horizontal lathe (CMS-GT27) under the conditions shown in Table 3-1 in Chapter 3. The overhead jet cooling arrangement is shown in Figure 8-1. The carbide tool insert has 0° rake angle, 11° clearance angle, 6° inclination angle, and the thermal conductivity of $84.02 W/mK$ [45]. The workpiece (AISI 1045) has the thermal conductivity of 50.8 W/mK and the thermal diffusivity of $0.134\times10^{-4}\ m^2/s$ [46]. The flank wear land length is recorded with a Nikon microscope MICROPHOT-FXL before the cutting forces are measured by a tool-post dynamometer (Kistler model 9257B). At the same time, the cutting temperatures are measured with an embedded thermocouple (Omega K-type) located under the tool insert. The cutting conditions are selected in the ranges of cutting

speed = 45.75 - 137.25 m/min, feed = 0.0508 - 0.1016 mm/rev and depth of cut = 0.508 - 1.016 mm according to a factorial design of experiment [42]. The workpiece is 31.75mm in diameter and 76.2 mm long. Each cut takes away 50.8 mm length of material. The shortest cutting time in the tests is about 20 seconds (the 9th test) which is long enough to reach the steady state of the cutting temperature measurement.

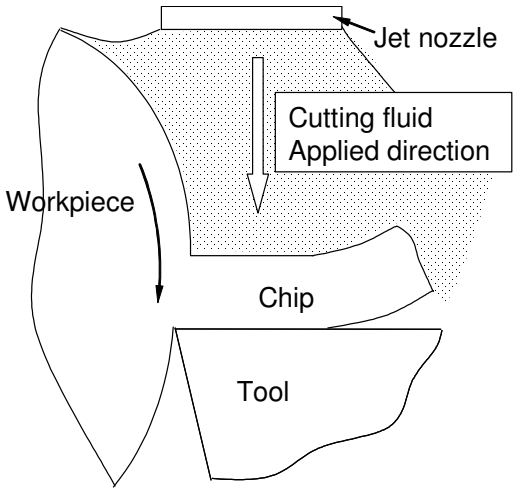

Figure 8-2: Schematic of overhead jet cooling

The fluid chosen is a semi-synthetic cutting fluid (Valenite ValCool Turntech Blue) with concentration of 1:20 as recommended. In view of its low concentration ratio, the material properties of the cutting fluid are approximated by those of water.

8.4.2 Model calibration

To establish the models for cutting forces, cutting temperatures and tool wear progressions, several parameters used in boundary lubrication for estimate cutting forces have to be determined. The process to estimate the boundary lubrication parameters is the same as that presented in Chapter 4. The estimated parameters for predicting the friction coefficient in turning under flood cooling are summarized in Table 8-1

Table 8-1: Parameters in boundary lubrication calculation

Parameter	t_b (μm)	C_2	$H_{\max}$ (μm)	R (μm)	D	z $(1/mm)$
Representative value	0.4	0.5	5	20	1.5	100

The coefficients in Equation (8-3) are determined based on experimental data under dry cutting as recorded with a microscope. On the other hand, the predicted tool wear rates are calculated according to the cutting forces and the cutting temperatures measured in machining. Then, the coefficients in tool wear rate model are determined by minimizing the least square errors between experimental tool wear rates and predicted tool wear rates according to Equation (8-3) at different times as tool wear progresses. The

measured wear rates of the 6th cutting condition are used in calibrating these coefficients. With the calibrated coefficients, the tool wear rate model becomes:

$$\frac{dL_{VB}}{dt} = \frac{\cot\gamma - \tan\alpha}{L_{VB}} \left\{ 7.394\times10^{-7} K\left(\frac{1}{H_t}\right) V_c L_{VB}\sigma + 5.147\times10^{-16} e^{7.456\times10^{-4}T} V_c \sigma + 1.29\times10^{5} \sqrt{V_c L_{VB}}\, e^{\frac{-20570}{T+273}} \right\} \quad (8\text{-}4)$$

8.5 Model Validation Results and Discussion

The model validation is made on the basis of comparing forces in the axial, radial, and tangential directions for sharp tools. The results are shown in Figure 8-3. The effective fluid film thickness (t_b) is determined to be $0.4\mu m$ by comparing the predicted and measured cutting forces in the 7th case. This is why the results of the 7th case show a better agreement between predictions and measurements. It is observed in the figure that the predicted cutting forces are larger than the experimental data in most cases. The over-estimation may be a result of the tendency of BUE formation under overhead jet cooling conditions to change the effective tool geometry which leads to the deviations of force predictions from the measured data. The model provides an average prediction error of 16% in the tangential cutting force directions, 20% in the axial directions, and 24% in the radial directions within the experimental test condition range; although in some cases,

the predicted values are close to the measurement by less than 5% difference.

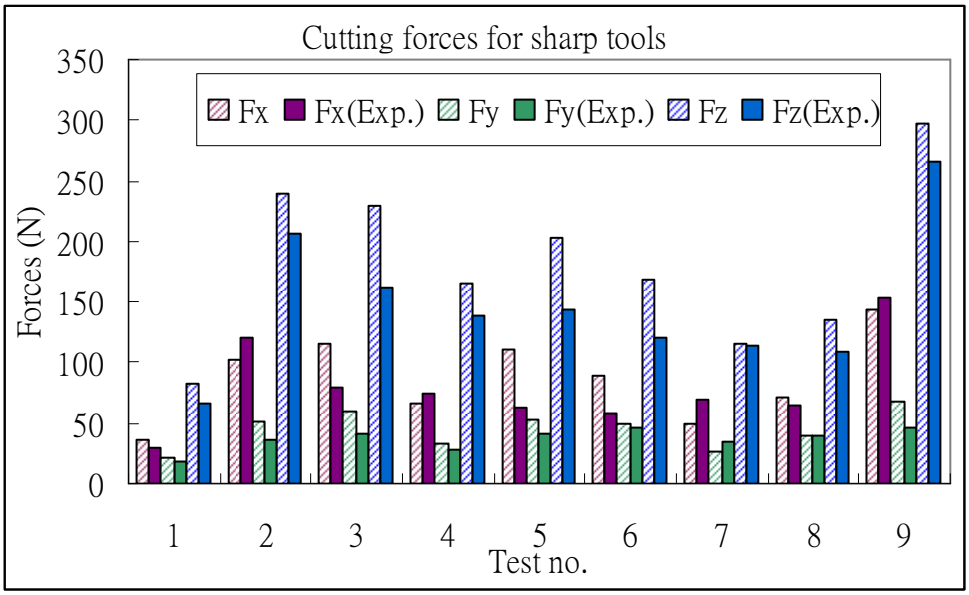

Figure 8-3: Comparisons of axial force (Fx), radial force (Fy) and tangential force (Fz) with a sharp tool between model predictions and experimental measurements

The model-predicted temperatures compared to measurements under various cutting conditions are shown in Figure 8-4. Because the embedded thermocouple is exposed to the cutting fluid, the measured temperature was comparably lower relative to the measured temperatures in dry cutting. The maximum prediction error is 14.7% in case 4.

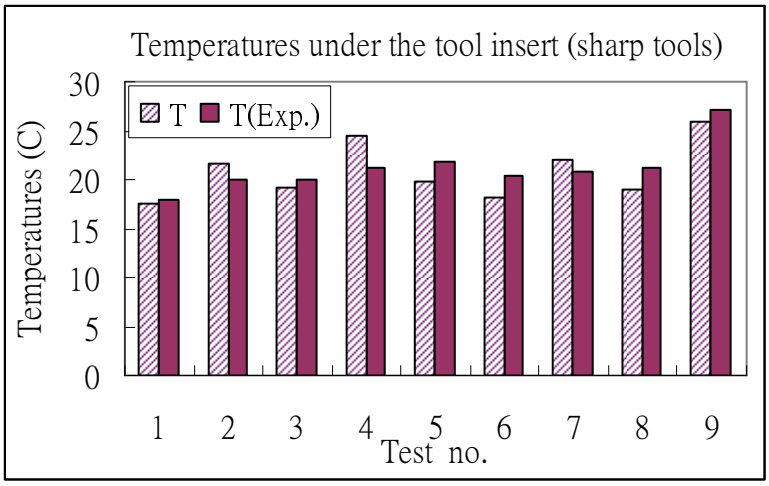

Figure 8-4: Temperature comparison between model-prediction and measurement with a sharp tool

The comparison of model predicted and measured tool wear progression is shown in Figure 8-5. The predicted values show good agreement with the experimental data in cases 4, 5, 6, 7, and 9. In cases 2 and 3, the predicted tool wear rate at the beginning is much higher than measurements. The over-estimation at the beginning of machining tests causes considerable difference between calculation and measurements although the tool wear rate is close for most of the time in the machining tests. The jump of the tool wear progression at the end of the machining test in case 4 indicates the sudden loss of the tool material due to chipping which is not included in the wear mechanisms in this study. According to the BUE formation criteria, the BUE would happen for cases 1, 2, 3, 4, and 7. BUE also physically occur at the beginning of cases 5 and 6 but it is not expected by

the model, which leads to a deviation from the prediction. Nevertheless, the solid lines have a close slope with respect to the experimental data at the steady state (after the BUE disappears) in these cases, suggesting that the proposed model still describes the wear process well in cases 5 and 6 if there was no BUE.

Compared with the results for dry cutting presented in Chapter 5, the lubricating and cooling effects due to overhead jet cooling in machining tests result in longer tool lives under flood cooling relative to dry situations. The existence of BUE also helps to explain the different tool lives in wet cutting and dry cutting. As observed in the cases 3 and 7, BUE stays for a longer time under flood cooling conditions, which reduces the abrasive wear contribution in these cases. Therefore, longer tool lives for wet cutting were observed in both experiments and calculations.

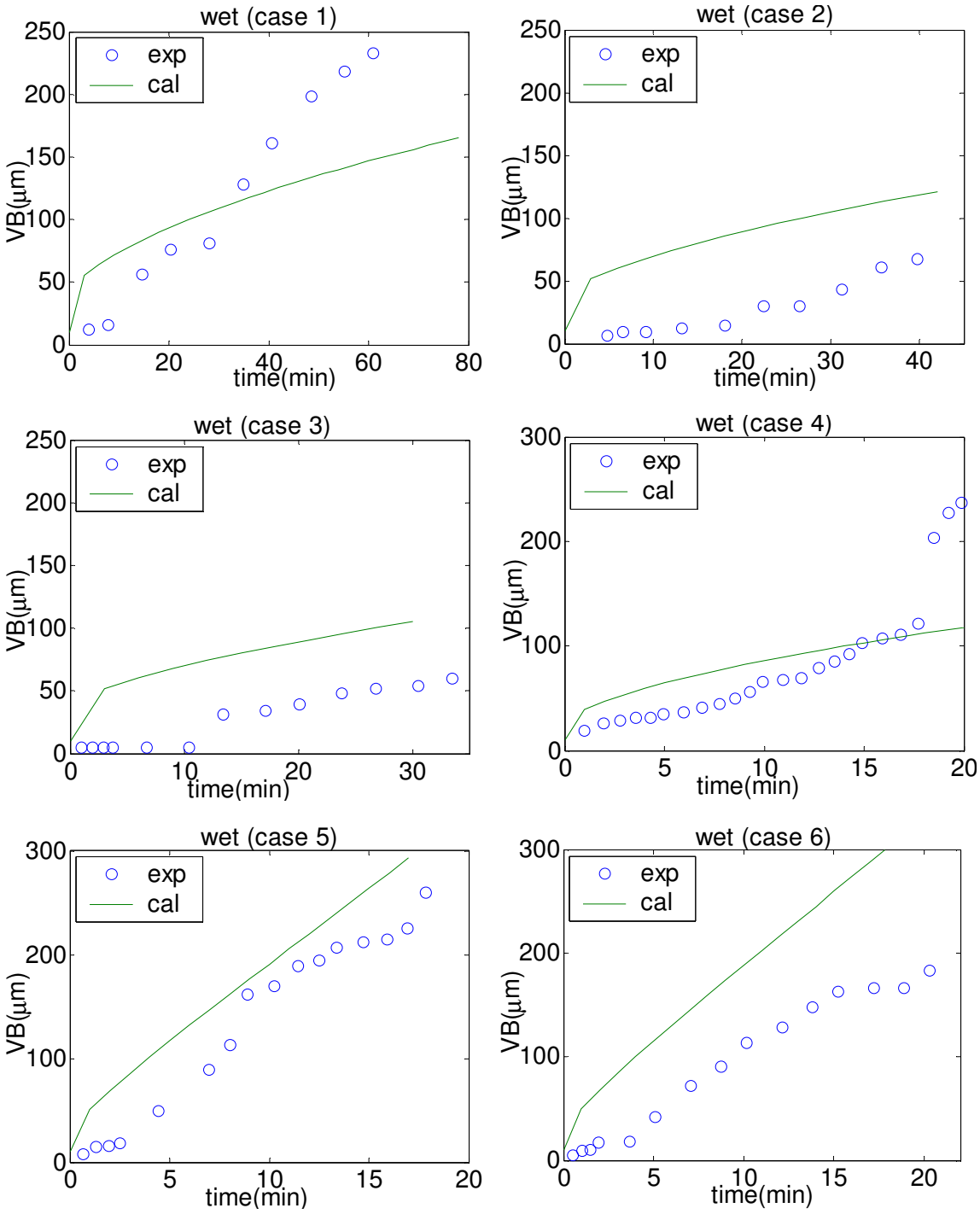

Figure 8-5: Comparisons of tool flank wear progressions under overhead jet cooling situations

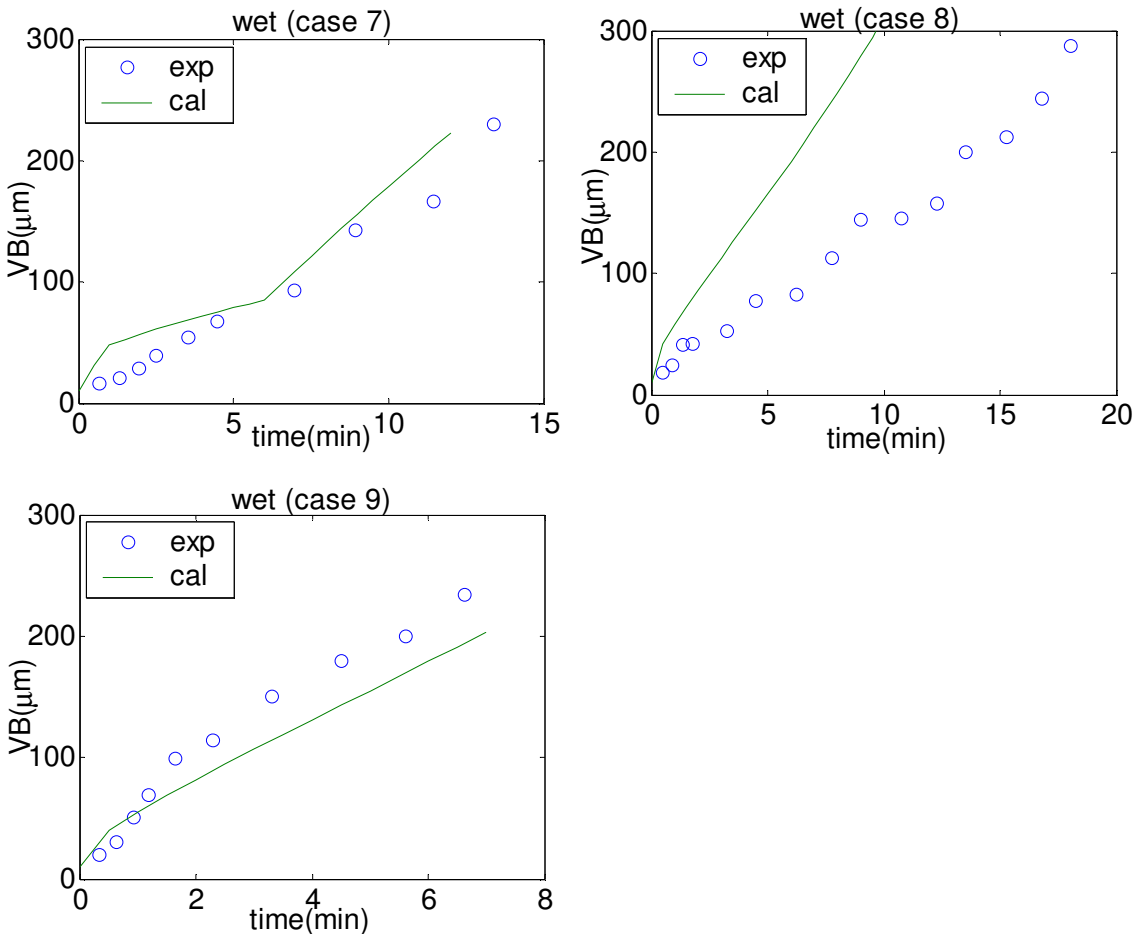

Figure 8-5 continued: Comparisons of tool flank wear progressions under overhead jet cooling situations

It is also noted that in the machining tests the tool flank wears are not uniform in most cases for both dry and wet cutting. The equivalent tool flank wear length used to describe a non-uniform tool wear is the average of five randomly picked flank wear lengths. It is possible to under-estimate the effective wear land lengths when the model only considers a uniform tool flank wear. Moreover, the predicted wear land length is

used subsequently to predict cutting forces and cutting temperatures. Therefore, the predicted error of tool life would accumulate and propagate.

8.6 Conclusion

Predictive models for cutting forces, cutting temperatures, and tool flank wear under flood cooling conditions are presented. The cutting force model is developed by incorporating the considerations of lubricating and cooling effects by flood cooling in the modification of the Oxley's model. The cutting temperature is obtained by modeling the primary heat source due to shear deformation, the secondary heat source due to friction, and the heat loss due to flood cooling based on a moving or stationary heat source in the tool. The thermal-mechanical responses of abrasion, adhesion, and diffusion wear mechanisms are considered for the estimation of tool flank wear rate as functions of material properties, tool geometry, and cutting conditions. The BUE formation is also formulated in the tool flank wear model based on a dynamic strain aging relationship. No measured cutting forces or measured cutting temperature information are required for the prediction of tool wear rate using the models.

CHAPTER 9

CONTRIBUTIONS AND RECOMMENDATIONS

9.1 Contributions

The main contribution of this dissertation is to establish a quantitative methodology to implement near dry lubrication in turning process to control both tool wear behavior and shop floor air quality. A set of analytical models are developed to predict cutting temperatures, cutting forces, tool wear progressions and aerosol generation rate in near dry turning.

9.1.1 Cutting temperature model based on moving heat source method

A model to address the effect of the oil mist on the cutting temperature in near dry turning is presented. This temperature model is developed based on heat source and heat sink mechanisms for near dry machining. With cutting forces and the material properties as inputs, the average tool-chip interface temperature and the average tool-workpiece temperature are obtained. The cooling effect in near dry situations is modeled as heat

losses on the tool flank face and the workpiece surface below the tool. The quantity of the heat loss due to oil mist is estimated by the average heat transfer coefficient based on the Nusselt number

9.1.2 Cutting force model based on both lubricating and cooling effect

A force modeling is presented for estimating the cutting forces in near dry machining based on the Oxley's machining theory and the Waldorf's worn tool model. Lubricating effect and cooling effect for near dry machining are considered in the proposed model. For worn tool cutting force predictions, the total cutting forces are obtained by summing up the predicted forces without any tool wear and the forces due to the flank wear.

9.1.3 Tool wear model based on contact stresses and temperatures

The methodology for tool flank wear modeling in near dry turning is presented. This study integrates the cutting force model and the temperature model with the tool flank wear mechanisms. Three wear mechanisms are considered: abrasion, adhesion, and diffusion. The BUE formation is also formulated in the tool flank wear model based on a dynamic strain aging relationship. The tool wear progression is estimated based on material properties, tool geometry, and cutting conditions as well as the predicted contact

stress and the predicted cutting temperature. No measured cutting forces or measured cutting temperature information is required for predicting the tool wear rate.

9.1.4 Cutting fluid aerosol generation model based on the characteristics of near dry lubrication

To address the issue of the environmental concerns of cutting fluids in near dry machining, an analytical model to predict the aerosol generation rate and mean aerosol size distribution is presented. This study focuses on the turning process with air-fluid mixture applied to the insert flank face. Two primary aerosol formation mechanisms are considered: aerosol runaway and evaporation. The resulting model can be also utilized to incorporate with the tool performance evaluation in order to achieve the requirements of air quality on the machine shop floor and cost in machining processes.

9.1.5 Model-based comparison of tool performance and air quality among dry machining, near dry machining, and flood-cooled machining

Based on the predictive models, the comparison of tool performance and air quality among dry machining, near dry machining, and flood-cooled machining is presented. It is found that near dry machining outperforms dry machining and is as good as flood cooling in all ways except mist generation when cutting medium carbon steel

with the uncoated carbide tool. The results from this model-based comparison show the potential of the established models for further NDM process planning and optimization on quantitative scales.

9.2 Recommendations

This study fills a void in near dry machining research by developing analytical models that predict tool life and cutting fluid aerosol generation. This is important because the established models can serve as a basis for machining process planning under near dry lubrication. There is also a potential to extend the developed methodology to other research areas, such as milling, grinding, drilling and so on. However, the analytical modeling always targets at simple, accurate and fast way to find the answers. It is important to continue developing predictive capabilities in all areas of near dry machining. The recommendations for the future near dry machining search are presented below.

9.2.1 Effective film thickness modeling

The effective film thickness in force model for considering the lubricating effect is a simplification of the real problem where the constant film thickness for the same air-cutting-fluid mixture application is assumed. In addition, the value of the effective

film thickness is calibrated by machining tests, not directly from the calculations. The application of this value in near dry turning is only appropriate for the same materials and cutting conditions selected in this study. There is a need to establish a physical model to describe the effective oil film behavior under high contact stress and high rotational speed in turning processes. The effective film thickness should be related to the oil flow rate, applied aerosol droplet sizes and cutting parameters.

9.2.2 Built-up edge formation

The BUE formation model presented in this dissertation is adapted from the work of Hastings *et. al.* [66]. It is found that the model was not capable of accurately predicting the BUE formation due to the different material used in this study. The previous semi-empirical formula is established based on the observations cutting force measurement. It is recommended that the BUE formation model could be developed from the view of material properties. In this way, the BUE formation model could be extensively applied for all metals.

9.2.3 Surface roughness model

The surface finish is an important measurement for product values. Much research showed that the introduction of near dry machining has the potential to improve the

product surface finish [1-12, 15, 17]. Nevertheless, no predictive models were presented. The analytical model could be developed based on the existing surface roughness models while accounting for the partial load carried by the near dry lubrication which would reduced the contact stresses between the tool and the worpiece. The different BUE formation behavior in dry and near dry cutting should be also considered because the BUE formation related to near dry lubrication is another important factor for surface finish.

9.2.4 Flow stress data for the workpiece material

The constitutive model for the workpiece presented in this study is only valid for medium carbon steels [39]. This material model limits the applications of the models developed in this dissertation. A full survey of material behavior in machining processes involving high stresses and high temperatures is necessary.

9.2.5 Air-cutting-fluid mixture application method

The in-tool-hole configuration is adopted in this study. The lubricant is applied to the tool flank face. Other application methods, for example, Venturi tube, tool rake face application and chip backside application, can be further investigated in the future. The best solution of application methods to control tool wear and air quality could be offered

through studying those configurations.

REFERENCES

1. Klocke, F. and Eisenblaetter, G., 1997, "Dry Cutting," CIRP Annals - Manufacturing Technology, **46**(2), pp. 519-526.

2. Heisel, U., Lutz, M., Spath, D., and Wassmer, R., 1994, "Application of Minimum Quantity Cooling Lubrication Technology in Cutting Process," *Production Engineering*, **II/1**, pp. 49-54.

3. Machado, A.R. and Wallbank, J., 1997, "Effect of Extremely Low Lubricant Volumes in Machining," Wear, **210**(1-2), pp. 76-82.

4. Rahman, M., Senthil Kumar, A., and Salam, M.U., 2002, "Experimental Evaluation on the Effect of Minimal Quantities of Lubricant in Milling," International Journal of Machine Tools and Manufacture, **42**(5), pp. 539-547.

5. Brockhoff, T. and Walter, A., 1998, "Fluid Minimization in Cutting and Grinding," Abrasives, pp. 38-42.

6. Braga, D.U., Diniz, A.E., Miranda, G.W.A., and Coppini, N.L., 2002, "Using a Minimum Quantity of Lubricant (MQL) and a Diamond Coated Tool in the Drilling of Aluminum-Silicon Alloys," Journal of Materials Processing Technology, **122**(1), pp. 127-138.

7. Varadarajan, A.S., Philip, P.K., and Ramamoorthy, B., 2002, "Investigations on Hard Turning with Minimal Cutting Fluid Application (HTMF) and Its Comparison with Dry and Wet Turning," International Journal of Machine Tools and Manufacture, **42**(2), pp. 193-200.

8. Sasahara, H., Kawasaki, M., and Tsutsumi, M., 2003, "Helical Feed Milling with MQL for Boring of Aluminum Alloy," Nippon Kikai Gakkai Ronbunshu, C Hen/Transactions of the Japan Society of Mechanical Engineers, Part C, **69**(8), pp. 2156-2161.

9. Chen, D.C., Suzuki, Y., and Sakai, K., 2001, "A study of turning operation by

oil-water combined mist lubrication machining method," Key Engineering Materials, **202-203**, pp. 47-52.

10. Diniz, A.E., Ferreira, J.R., and Filho, F.T., 2003, "Influence of refrigeration/lubrication condition on SAE 52100 hardened steel turning at several cutting speeds," International Journal of Machine Tools and Manufacture, **43**(3), pp. 317-326.

11. Dhar, N.R., Islam, M.W., Islam, S., and Mithu, M.A.H., 2006, "The influence of minimum quantity of lubrication (MQL) on cutting temperature, chip and dimensional accuracy in turning AISI-1040 steel," Journal of Materials Processing Technology, **171**(1), pp. 93-99.

12. Rahman, M., Senthil Kumar, A., and Manzoor Ul, S., 2001, "Evaluation of minimal quantities of lubricant in end milling," International Journal of Advanced Manufacturing Technology, **18**(4), pp. 235-241.

13. Lopez De Lacalle, L.N., Angulo, C., Lamikiz, A., and Sanchez, J.A., 2006, "Experimental and Numerical Investigation of the Effect of Spray Cutting Fluids in High Speed Milling," Journal of Materials Processing Technology, **172**(1), pp. 11-15.

14. Kelly, J.F. and Cotterell, M.G., 2002, "Minimal Lubrication Machining of Aluminium Alloys," Journal of Materials Processing Technology, **120**(1-3), pp. 327-334.

15. Heinemann, R., Hinduja, S., Barrow, G., and Petuelli, G., 2006, "Effect of MQL on the Tool Life of Small Twist Drills in Deep-Hole Drilling," International Journal of Machine Tools and Manufacture, **46**(1), pp. 1-6.

16. Hafenbraedl, D. and Malkin, S., 2000, "Environmentally-Conscious Minimum Quantity Lubrication (MQL) for Internal Cylindrical Grinding," *NAMRC XXVIII*, Lexington, Kuntucky.

17. Brinksmeier, E., Walter, A., and Brockhoff, T., 1997, "Minimum Quantity Lubrication in Grinding," *2nd International Machining & Grinding Conference*, Society of Manufacturing Engineers, Dearborn, Michigan, pp. MR97-230.

18. Bennett, E.O. and Bennett, D.L., 1987, "Minimizing Human Exposure to

Chemicals in Metalworking Fluids," Lubrication Engineering, **43**(3), pp. 167-175.

19. NIOSH, 1998, "What You Need to Know about Occupational Exposure to Metalworking Fluids," DHHS (NIOSH) Publication No. 98-116, National Institute for Occupational Safty and Health (NIOSH), Cincinnnati, OH.

20. Thornburg, J. and Leith, D., 2000, "Mist Generation during Metal Machining," Journal of Tribology, Transactions of the ASME, **122**(3), pp. 544-549.

21. Yue, Y., Sutherland, J.W., and Olson, W.W., 1996, "Cutting Fluid Mist Formation in Machining via Atomization Mechanisms," *Design for Manufacturing and Assembly (ASME)*, **89**, ASME, Atlanta, GA, USA, pp. 37-46.

22. Bell, D.D., Chou, J., Nowag, L., and Liang, S.Y., 1999, "Modeling of the Environmental Effect of Cutting Fluid," Tribology Transactions, **42**(1), pp. 168-173.

23. Chen, Z., Wong, K., Li, W., Stephenson, D.A., and Liang, S.Y., 1999, "Cutting fluid aerosol generation due to spin-off in turning operation: Analysis for environmentally conscious machining," American Society of Mechanical Engineers, Manufacturing Engineering Division, MED, **10**, pp. 285-291.

24. Atmadi, A., Stephenson, D.A., and Liang, S.Y., 2001, "Cutting Fluid Aerosol from Splash in Turning: Analysis for Environmentally Conscious Machining," International Journal of Advanced Manufacturing Technology, **17**(4), pp. 238-243.

25. Taylor, F.W., 1906, "On the art of cutting metals," Proceedings of the American Society of Mechanical Engineers, **28**(3).

26. Jaeger, J.C., 1943, "Moving sources of heat and the temperature at sliding contacts," Journal and Proceedings of the Royal Society of New South Wales, **76**, pp. 203-224.

27. Komanduri, R. and Hou, Z.B., 2000, "Thermal Modeling of the Metal Cutting Process Part I - Temperature Rise Distribution due to Shear Plane Heat Source," International Journal of Mechanical Sciences, **42**(9), pp. 1715-1752.

28. Komanduri, R. and Hou, Z.B., 2001, "Thermal Modeling of the Metal Cutting Process - Part II: Temperature Rise Distribution due to Frictional Heat Source at

the Tool-Chip Interface," International Journal of Mechanical Sciences, **43**(1), pp. 57-88.

29. Komanduri, R. and Hou, Z.B., 2001, "Thermal Modeling of the Metal Cutting Process - Part III: Temperature Rise Distribution due to the Combined Effects of Shear Plane Heat Source and the Tool-Chip Interface Frictional Heat Source," International Journal of Mechanical Sciences, **43**(1), pp. 89-107.

30. Huang, Y. and Liang, S.Y., 2003, "Modelling of the cutting temperature distribution under the tool flank wear effect," Proceedings of the Institution of Mechanical Engineers, Part C: Journal of Mechanical Engineering Science, **217**(11), pp. 1195-1208.

31. Hahn, R.S., 1951, "On the Temperature Developed at the Shear Plane in the Metal Cutting Process," *Proceedings of First U.S. National Congress of Applied Mechanics*, pp. 661-666.

32. Trigger, K.J. and Chao, B.T., 1951, "Analytical Evaluation of Metal-Cutting Temperatures," American Society of Mechanical Engineers -- Transactions, **73**(1), pp. 57-60.

33. Chao, B.T. and Trigger, K.J., 1955, "Temperature Distribution at Tool-ChipInterface in Metal Cutting," American Society of Mechanical Engineers -- Transactions, **77**(7), pp. 1107-1121.

34. Loewen, E.G. and Shaw, M.C., 1954, "On Analysis of Cutting-Tool Temperatures," American Society of Mechanical Engineers -- Transactions, **76**(2), pp. 217-225.

35. Carslaw, H.S., 1959, *Conduction of Heat in Solids*. 2nd ed, Oxford, Clarendon Press.

36. Li, X., 1995, "Effect of Coolant Flow Rate on Cooling in Machining," *Proceedings of the NAMRC XXIII Conference*, SME, Houghton, MI, USA, pp. 109-114.

37. Childs, T.H.C., Maekawa, K., and Maulik, P., 1988, "Effects of coolant on temperature distribution in metal machining," Materials Science and Technology, **4**(11), pp. 1006-1019.

38. Dhar, N.R., Paul, S., and Chattopadhyay, A.B., 2002, "Role of Cryogenic Cooling on Cutting Temperature in Turning Steel," Journal of Manufacturing Science and Engineering, Transactions of the ASME, **124**(1), pp. 146-154.

39. Oxley, P.L.B., 1989, *The Mechanics of Machining : An Analytical Approach to Assessing Machinability*, E. Horwood New York.

40. Kreith, F. and Bohn, M.S., 1993, *Principles of Heat Transfer*. 5th ed, PWS Pub. Co., Boston ; London.

41. Munson, B.R., Young, D.F., and Okiishi, T.H., 2002, *Fundamentals of Fluid Mechanics*. 4th ed, Wiley, New York.

42. Wu, C.-F. and Hamada, M., 2000, *Experiments : Planning, Analysis, and Parameter Design Optimization*, J. Wiley, New York.

43. Shaw, M.C., 1996, *Metal Cutting Principles*, Oxford University Press, New York.

44. Merchant, M.E., 1945, "Mechanics of the metal cutting process. II. Plasticity conditions in orthogonal cutting," Journal of Applied Physics, **16**, pp. 318-324.

45. Shackelford, J.F., Alexander, W., and Park, J.S., 1994, *CRC Materials Science and Engineering Handbook*. 2nd ed, CRC Press, Boca Raton.

46. 1992, *ASM Handbook*, ASM International, Materials Park, Ohio.

47. Liang, S.Y. and Sutherland, J.W., 2002, "Research Status of MQL in Machining," *Proceedings of the First International Workshop on High Performance Cutting*, Paris, pp. 39-49.

48. Boothroyd, G. and Knight, W.A., 1989, *Fundamentals of machining and machine tools*. 2nd ed, M. Dekker, New York.

49. Waldorf, D.J., 1996, "Shearing, Ploughing and Wear in Orthogonal Machining," Ph.D. thesis, Mechanical engineering, University of Illinois at Urbana-Champaign, Urbana-Champaign.

50. Smithey, D.W., Kapoor, S.G., and DeVor, R.E., 2001, "A new mechanistic model for predicting worn tool cutting forces," Machining Science and Technology, **5**(1), pp. 23-42.

51. Kato, S., Marui, E., and Hashimoto, M., 1998, "Fundamental study on normal load dependency of friction characteristics in boundary lubrication," Tribology Transactions, **41**(3), pp. 341-349.

52. Moore, D.F., 1975, *Principles and Applications of Tribology*. 1st ed, Pergamon Press, Oxford, New York.

53. Arsecularatne, J.A. and Mathew, P., 2000, "Oxley modeling approach, its applications and future directions," Machining Science and Technology, **4**(3), pp. 363-397.

54. Arsecularatne, J.A., Mathew, P., and Oxley, P.L.B., 1995, "Prediction of chip flow direction and cutting forces in oblique machining with nose radius tools," Proceedings of the Institution of Mechanical Engineers, Part B: Journal of Engineering Manufacture, **209**(B4), pp. 305-315.

55. Stabler, G.V., 1951, "The Fundamental Geometry of Cutting Tools," *Proceedings of the Institution of Mechanical Engineers*, **165**, pp. 14-26.

56. Williams, J.A., 1994, *Engineering Tribology*, Oxford University Press, Oxford ; New York.

57. Rabinowicz, E., Dunn, L.A., and Russell, P.G., 1961, "Study of abrasive wear under three-body conditions," Wear-Usure-Verschleiss, **4**(5), pp. 345-355.

58. Kramer, B.M. and Judd, P.K., 1985, "Computational Design of Wear Coatings," **3**, Los Angeles, CA, USA, pp. 2439-44.

59. Kannatey-Asibu, E., Jr., 1985, "Transport-Diffusion Equation in Metal Cutting and Its Application to Analysis of The Rate of Flank Wear," Journal of Engineering for Industry, Transactions ASME, **107**(1), pp. 81-89.

60. Loladze, T.N., 1981, "Of the Theory of Diffusion Wear," CIRP Annals - Manufacturing Technology, **30**(1), pp. 71-76.

61. Kwon, P., 2000, "Predictive Models for Flank Wear on Coated Inserts," Journal of Tribology, Transactions of the ASME, **122**(1), pp. 340-347.

62. Huang, Y. and Liang, S.Y., 2004, "Modeling of CBN Tool Flank Wear Progression

in Finish Hard Turning," Journal of Manufacturing Science and Engineering, Transactions of the ASME, **126**(1), pp. 98-106.

63. Rabinowicz, E., 1979, "Wear Equation for Erosion of Metals by Abrasive Particles," pp. 38.1-38.5.

64. Rabinowicz, E., 1977, "Abrasive Wear Resistance as a Material Test," **33**(7), pp. 378-381.

65. Young, H.T., Mathew, P., and Oxley, P.L.B., 1987, "Allowing for Nose Radius Effects in Predicting the Chip Flow Direction and Cutting Forces in Bar Turning," Proceedings of the Institution of Mechanical Engineers, Part C: Mechanical Engineering Science, **201**(3), pp. 213-226.

66. Hastings, W.F., Mathew, P., and Oxley, P.L., 1980, "Machining Theory for Predicting Chip Geometry, Cutting Forces etc. from Work Material Properties and Cutting Conditions," **371**(1747), pp. 569-587.

67. Arsecularatne, J.A., Fowle, R.F., Mathew, P., and Oxley, P.L.B., 1996, "Prediction of cutting forces and built-up edge formation conditions in machining with oblique nose radius tools," Proceedings of the Institution of Mechanical Engineers, Part B: Journal of Engineering Manufacture, **210**(B5), pp. 457-469.

68. Chen, Z., 2001, "Cutting Fluid Aerosol Generation and Dissipation in Machining Process: Analysis for Environmental Consciousness," Ph.D. thesis, School of Mechanical Engineering, Georgia Institute of Technology, Atlanta.

69. Lefebvre, A.H., 1989, *Atomization and Sprays*, Hemisphere Pub. Corp., New York.

70. Weber, R., Boysan, F., Swithenbank, J., Bolado, R., and Yule, A., 1985, "Spray Combustion of Small and Large Droplets of Heavy Fuel Oil," Inst of Energy, London, England, pp. 11-113.

71. Plesniak, M.W., Sojka, P.E., and Singh, A.K., 2004, "Transfer Efficiency for Airless Painting Systems," JCT Research, **1**(2), pp. 137-145.

72. Prasad, K.S.L., 1982, "Spray Characterization of Air Blast Atomizers," *Reports and proceedings of the Second International Conference on Liquid Atomization*

and Spray Systems, Madison, Wisconsin, pp. 123-130.

73. Jones, F.E., 1992, *Evaporation of Water : with Emphasis on Applications and Measurements*, Lewis Publishers, Chelsea, Mich.

74. Weinert, K., Inasaki, I., Sutherland, J.W., and Wakabayashi, T., 2004, "Dry machining and minimum quantity lubrication," CIRP Annals - Manufacturing Technology, **53**(2), pp. 511-537.

75. De Chiffre, L. and Belluco, W., 2002, "Investigations of cutting fluid performance using different machining operations," Lubrication Engineering, **58**(10), pp. 22-29.

76. De Chiffre, L., 1978, "Testing the Overall Performance of Cutting Fluids," Lubrication Engineering, **34**(5), pp. 244-251.

77. Avila, R.F. and Abrao, A.M., 2001, "The effect of cutting fluids on the machining of hardened AISI 4340 steel," Journal of Materials Processing Technology, **119**(1-3), pp. 21-26.

78. Upton, D.P., 2000, "Optimization of cutting fluid performance," International Journal of Production Research, **38**(5), pp. 1219-23.

79. Merchant, M.E., 1950, "Fundamentals of cutting fluid action," Lubrication Engineering, **6**(4), pp. 163-167.

80. De Chiffre, L., 1980, "Lubrication in Cutting - Critical Review and Experiments with Restricted Contact Tool," ASLE Transactions, **24**(3), pp. 340-344.

81. Smith, T., Naerheim, Y., and Lan, M.S., 1988, "Theoretical analysis of cutting fluid interaction in machining," Tribology International, **21**(5), pp. 239-247.

82. Huang, Y., 2002, "Predictive Modeling of Tool Wear Rate with Application to CBN Hard Turning," Ph.D thesis, School of Mechanical Engineering, Georgia Institute of Technology, Atlanta.